Cellular Metabolism Contributes To Therapeutic Responses in BRAF-Mutated Melanomas

By

Keisha Nicole Hardeman

Dissertation
Submitted to the Faculty of the
Graduate School of Vanderbilt University
in partial fulfillment of the requirements
for the degree of

DOCTOR OF PHILOSOPHY
in

Cancer Biology
May, 2017
Nashville, Tennessee

Approved By:

Christopher Chad Quarles, Ph.D.

Jamey D. Young, Ph.D

Kimberly B. Dahlman, Ph.D.

Vito Quaranta, M.D.

J. Ann Richmond, Ph.D. (Chair)

Joshua P. Fessel, M.D., Ph.D. (Thesis Advisor)

In memory of my father, Charles Hardeman, Sr. (July 31, 1946---January 31, 2011)

And, to my ancestors who endured and persevered our world's most difficult circumstances, kept their faith, purpose, and dignity, and passed to me that seed of stubbornness and persistence.

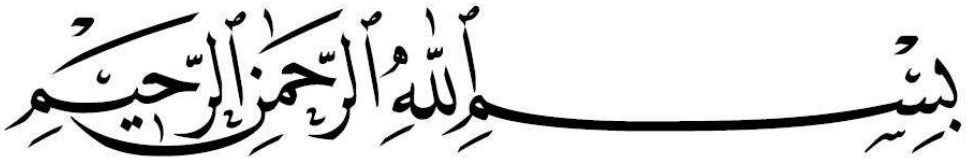

"In the name of God, the Most Gracious, the Most Merciful"

ACKNOWLEDGEMENTS

I have benefitted from many teachers, educators, and instructors; family and friends; and other scientists who saw something in me worthy of encouragement and advocacy. The culmination of finishing this thesis is my meager attempt at paying tuition for all those years of instruction and nurturing guidance, and I will attempt to concentrate my gratitude to those whose help put me on the path to completing this dissertation—directly or indirectly. All who know of me, appreciate I am a different type of *quirky* person; thus, my acknowledgements will reflect that.

"Setting goals is the first step to turning the invisible into the visible," Tony Robbins

I have dreamed of being a scientist since I was little girl, and although I have set goals towards that dream, none of the achievements would be possible without the unwavering support of several agencies. I would like to thank the funding agencies that supported this work, particularly the National Institutes of Health and the various internal funding mechanisms of Vanderbilt that helped with other expenses. Appreciation must be given for the support from administrators and faculty in the Cancer Biology Department and the Interdisciplinary Graduate Program (IGP). Additionally, I would like to thank the directors and preceptors of the Initiative for Maximizing Student Diversity (IMSD) Training Program: Drs. Linda Sealy and Roger Chalkley. Furthermore, the Biomedical Research and Education Training (BRET) Office has been outstanding in its assistance of my development as a trainee through its various programming, such as the ASPIRE program.

The people at Vanderbilt have made this institution truly exceptional, and I am honored to have received such guidance and mentorship. I would like to thank my Committee members—Drs. Chad Quarles, Jamey Young, Kim Dahlman, Vito Quaranta, Ann Richmond, and Josh Fessel—

for their expertise and support in my project and overall career goals. They have provided helpful critiques, generous advice, and the gift of scientific rigor. In particular, this project blossomed through the expertise of Jamey Young, who has been invested in my progress and success since the early days through the Co-Sponsorship of the F31. Also, many thanks and gratitude is owed to Ann Richmond for helping regenerate this project (and my progress as a graduate student) during one of the most critical points in the project.

"Your skin must be sensitive enough for the lightest kiss and thick enough to ward off the sneers. If you are going to spit in the eye of the world, make sure your back is to the wind.," Gloria Anzaldua

"You can never leave footprints that last if you are always walking on tip-toe," Nobel Peace Prize Laureate Leymah Gbowee

I was blessed with supportive colleagues, lab-mates and friends here at Vanderbilt who helped make the time enjoyable, provided camaraderie and encouragement, and were patient and kind. For my friends and colleagues: I hope that they continue to carve out a place in this world and set ablaze any obstruction hindering that endeavor. Hopefully—those naysayers who complain that something can not be done or is impossible—will get out of the way of my friends and colleagues who are ready to attain and accomplish the formerly impervious. I especially want to thank my best friend, co-author, and lab-mate: Bishal Paudel.

"Like farmers we need to learn that we can not sow and reap the same day," Akua Wood

My family can trace our ancestry back many generations to farmers, sharecroppers and slaves. A hard-working, industrious spirit must have been passed to my family, and through their support I

have been able to reap a harvest. I would like to thank my family for their understanding and support given to me in graduate school. Particularly I want to thank my big brother, Charles, for providing the first example of resolve and focus for me to look up to. Additionally, both my parents sacrificed and provided opportunities for me to thrive, and I am still heavy-hearted that my father is not alive to see my thesis completion.

"When a flower doesn't bloom you fix the environment in which it grows, not the flower," Alexander Den Heijier

I was fortunate to be encouraged very early on by Karen Pohlmeier to pursue scientific research and work in an academic lab. I have had substantial guidance and encouragement from my career mentors: Mary Jean Sparks, Elizabeth Heitman, and Michael Laposata. Moreover, my secondary dissertation advisor, Vito Quaranta, provided the most benevolent support, expertise, and resources that were crucial to the completion of this project.

Finally, I apparently lucked out in having the kindest, most selfless advisor any graduate student could hope for. I am immensely thankful for having Joshua Fessel as my primary thesis advisor. His unbreakable confidence in me during the darkest, bleakest hours was a gift I am forever indebted.

"Black is maple brass coffee iron mahogany copper cocoa bronze ebony chocolate," George Elliott Clarke, Canada's parliamentary poet laureate

As I write and prepare this thesis, the world and current state of affairs is troubling. Science is not always objective and is actually steeped in politics: the domain of what constitutes important science is shaped and regulated by what the prevailing societal and geographical pressures

dictate as worthwhile to human culture, experience and condition.

The irony is not lost upon me that this work is about cancer arising from melanocytes, which are characterized by the pigment melanin. This pigment has been used to put human beings on a spectrum of valuation and worth, and the more of this pigment one had in their skin, the worse they were treated by the medical enterprise. Indeed, studies have shown that there exists no other group that mistrusts the medical research enterprise more than Black Americans. And rightfully so: Black Americans' mistreatment goes far beyond the Tuskegee Syphilis Study, and includes a harrowing list of exploitation and experimentation without goals of therapeutic benefit, from the moment slave ships reached America. Thus, my final acknowledgement is to the countless black and brown bodies whose very fibers of being and personhood were devalued for the sake of science. Our history books have never acknowledged their pains, stolen livelihoods, nor tormented souls. I strive to be a conscious, decolonized scientist and I will never forget that my ancestors provided "clinical material" for southern medical practitioners to exploit.

#BlackLivesMatter #BlackExcellence #BlackGirlMagic

PREFACE

Melanoma—a skin cancer arising from melanocytes—has been mentioned in medical texts dating back to Hippocrates in the 5th Century B.C. Although progress has been made in the field of melanoma biology, unfortunately, the overall death rates per 100,000 have remained relatively stable since 1975. Particularly, about half of melanoma patient tumors harbor an oncogenic mutation in the BRAF kinase and successfully achieving even, durable responses for patients remain a challenge.

In many cases, dysregulated cellular metabolism broadly affects therapy response by influencing compensatory signaling and expanding proliferation. Given many BRAF-mutated melanoma patients experience disease progression with targeted BRAF inhibitors, I hypothesized that therapeutic response is related to tumor metabolic phenotype, and that altering tumor metabolism could change therapeutic outcome. The work described in this dissertation addresses heterogeneous responses to targeted therapies in cell line models with respect to the tumor cell metabolism.

This dissertation attempts to discern the relationship of altered tumor cell metabolism and drug resistance, and the chapters are arranged to emphasize a linear course of response variability and assay development, glycolytic biology in relation to BRAF inhibition, and finer inspection of variability within a tumor. These findings help resolve discordant reports in the literature and link a targetable metabolic phenotype to cellular proliferation. Additionally, this work brings insight regarding the phenotypic roles of glycolysis and oxidative phosphorylation in BRAF-mutated melanomas.

TABLE OF CONTENTS

LIST OF TABLES

LIST OF FIGURES

LIST OF PUBLICATIONS

Hardeman KN, Peng C, Paudel BB, Meyer CT, et al. (2017). "Dependence On Glycolysis Sensitizes BRAF-mutated Melanoma For Increased Response To BRAF Inhibition." *Scientific Reports* 7; 42604.

Harris LA, Frick PL, Garbett SP, **Hardeman KN**, et al. (2016). "An Unbiased Metric Of Antiproliferative Drug Effect *In Vitro*." *Nature Methods* 13, 497-500.

Paudel BB, Harris LA, **Hardeman KN**, Abugable A, Lizama-Manibusan B, McLaughlin BA, Tyson DR, Fessel JP, and Quaranta V. "Dysfunctional Mitochondria Leads To A Non-quiescent Idling State In Drug Treated BRAF Mutated Melanoma Cells." (In Preparation)

Hardeman KN, Meyer CT, Tyson DR, Quaranta V, and Fessel JP. "Proliferation Responses and Drug Treatments: Basic Protocol of Generating Dose Response Metrics." (In Preparation)

LIST OF ABBREVIATIONS

α-KG	Alpha Ketoglutarate
2DG	2-deoxyglucose
AA	Activity Area
ABC	ATP-binding cassette
ACLY	ATP citrate lyase
ADP/ATP	Adenosine Diphosphate/Adenosine Triphosphate
AKT/PKB	v-Akt murine thymoma viral oncogene/Protein kinase B
ALL	Acute lymphoblastic leukemia
AMPK/pAMPK	Amp-Activated Protein Kinase
AUC	Area Under the Curve
BHI	Bioenergetics Health Index
BRAF	v-Raf murine sarcoma viral oncogene homolog B
cFP	Clonal Fractional Proliferation
CCLE	Cancer Cell Line Encyclopedia
CEFs	Chicken embryo fibroblasts
CK1α	Casein Kinase 1 alpha
COT	Cancer Osaka Thyroid
CTRPv2	Cancer Therapeutics Response Portal version 2.0
CRAF	v-Raf murine sarcoma viral oncogene homolog C
ddC	2', 3' dideoxycytidine
DIP	Drug-induced proliferation
DMEM	Dulbecco's Modified Essential Medium
DMSO	Dimethyl Sulfoxide
DNA	Deoxyribonucleic acid

Drp1	Dystrophin-related protein 1
EC50	Effective concentration (half-maximal)
ECAR	Extracellular acidification rate
EGFR	Epidermal growth factor receptor
Emax	Effect (maximum)
ERK	Extracellular Regulated MAP Kinase
ETC	Electron transport chain
FAD	Flavin adenine dinucleotide
FBS	Fetal Bovine Serum
FCCP	Carbonilcyanide *p*-triflouromethoxyphenylhydrazone
FDA	Food and Drug Administration
FUCCI	Fluorescent ubiquitin-dependent cell cycle indicator
GDSC	Genomics of Drug Sensitivity in Cancer
GLUD2	Glutamate dehydrogenase 2
GLUT1/4	Glucose Transporter 1 or 4
GOT2	Glutamic-oxaloacetic transaminase 2
GSTP1	Glutathione S-transferase pi 1
GTP	Guanosine triphosphate
H2BmRFP	Histone 2B monomeric red fluorescent protein
hESCs	human embryonic stem cells
HEM DEL	Hemizygous deletion
HER2	v-Erb-B2 Avian erythroblastic leukemia viral oncogene homolog 2
HIF1α	Hypoxia-inducible factor 1 alpha
HIV	Human immunodeficiency virus
HK	Hexokinase
HOMOZ	Homozygous

HPLC	High-pressure liquid chromatography
HTS	High-throughput screening
IC50	Inhibitory concentration (half-maximal)
IDH1	Isocitrate dehydrogenase 1
IGFR1	Insulin Growth Factor Receptor 1
KC	Keratinocyte Carcinoma
L2HG	L-2-hydroxyglutarate
LDH	Lactate dehydrogenase
LKB1	Liver Kinase B1
MALD-TOF	Matrix assisted laser desorption ionization time-of-flight
MAPK	Mitogen Activated Protein Kinase
MEK	Mitogen Activated Protein Kinase Kinase 1
MITF	Microphthalmia-associated transcription factor
MiDAS	Mitochondrial dysfunction-associated senescence
mtDNA	Mitochondrial DNA
MU	Mutated
MYC	v-avian myelocytomatosis viral oncogene homolog
NAC	N-acetylcysteine
NAD	Nicotinamide adenine dinucleotide
NF1	Neurofibromin 1
NRAS	Neuroblastoma RAS viral oncogene homolog
NSCs	Neuronal stem cells
OCR	Oxygen consumption rate
PCA	Principal Component Analysis
PDGF	Platelet derived growth factor
PDX	Patient Derived Xenograft
PI3K	Phosphoinositide-3-Kinase

PGC1α	Peroxisome proliferator-activated receptor γ Co-activator 1α
PKB/AKT	Protein Kinase B/ v-akt murine thymoma oncogene
PKM2	Pyruvate kinase M2 isoform
PP	Pyrvinium pamoate
PTEN	Phosphatase and tensin homolog
RAF	v-Raf murine sarcoma viral oncogene
RAS	Rat sarcoma viral oncogene
ROS	reactive oxygen species
RTK	Receptor tyrosine kinase
RT-PCR	Reverse transcription-polymerase chain reaction
Rho0	Rho-or ρ0
RPMI-1640	Roswell Park Memorial Institute 1640
SD	Standard deviation
SILAC	Stable isotope labeling with amino acids
Ski	v-Ski Avian sarcoma viral oncogene homolog
SLC25A1	Solute carrier family 25, Member 1
SLC25A13	Solute carrier family 25, Member 13
TCA	Tricarboxylic acid
TCGA	The Cancer Genome Atlas
UV	Ultraviolet
WNT5A	Wingless-Type MMTV Integration Site Family, Member 5A
WT	Wild type

CHAPTER I

INTRODUCTION

Melanoma Incidence, Prevalence, and Classification:

Incidence and Prevalence

Skin cancer is the most common cancer diagnosed in the US, although the true number of cases is difficult to estimate because the vast majority of skin cancers—basal and squamous cell carcinomas—are generally not reported in the national cancer registries because they are rarely fatal and considered curable (American Cancer Society, *Cancer Facts & Figures 2017*). These non-melanoma skin cancers, also collectively called Keratinocyte Carcinoma or KC, were estimated to affect 3.3 million people in 2012 and comprise 5.4 million cases (this figure includes persons with multiple cases of KC, which is common) (American Cancer Society, *Cancer Facts & Figures 2017*). Contrastingly, melanoma skin cancer, originating from melanocytes, constitutes approximately 1% of skin cancer cases but accounts for the majority of skin cancer deaths. The estimated number of new cases for the year of 2017 is 87,110 and the estimated number of deaths is 9,730 for that same year (American Cancer Society, *Cancer Facts & Figures 2017*). In the state of Tennessee, an estimated 1,840 new cases and 250 deaths will occur for the year 2017 (American Cancer Society, *Cancer Facts & Figures 2017*). Past data ranks the state of Tennessee at number 29 for age-adjusted death rates, but some neighboring states rank very high, like the state of Kentucky at number 6 (Howlader, Noone, et al., 2016). Melanoma has been mentioned in medical texts dating back to Hippocrates in the 5th Century B.C. (Rebecca, Sondak, and Smalley, 2012) and has been found in Inca mummies of Peru dating

back nearly 2,400 years (Urteaga and Pack, 1966). Incidence trends have continued to rise over the years, probably due to better detection methods, and changes in the population's cancer risk factors—particularly older age and lifespan. Major risk factors include numerous (50+) moles, exposure to sun or UV radiation or tanning, family history of melanoma or other skin cancers, suppressed immune system, or increased sun sensitivity (excessive sunburns, blonde or red hair color) (American Cancer Society, *Cancer Facts & Figures 2017*). Melanoma continues to have a strong prevalence in both genders, and the projected percent new cases of melanoma for the year 2017 are 6% and 4% for men and women, respectively (American Cancer Society, *Cancer Facts & Figures 2017*). Broken down by stage at diagnosis, the 5-year survival rate across all races is 98% in the localized stage, but drops to 62% and 16% if regional or distant metastases, respectively, are present (Siegel, Ma, et al., 2014). Unfortunately, the overall death rates per 100,000 have remained relatively stable since 1975 (Howlader, Noone, et al., 2016).

Classification and Molecular Landscape

Melanoma has been historically managed surgically ever since the 1850s, particularly once surgical anesthesia became available and publications of surgical excision case reports appeared regularly in *The Lancet* (Rebecca, Sondak, and Smalley, 2012). In 1967, Wallace Clark published a scale to standardize and assess melanoma prognosis based upon histology: the extent of invasion into the epidermis and subcutaneous skin layers of dermis and fat (Clark, From, et al., 1969). This system of Clark levels (I-V, for melanoma *in situ*) would help guide surgical treatment and staging of melanoma for decades, and others like Alexander Breslow built upon this system to further demonstrate that tumor size and thickness played a considerable role in prognosis (Breslow, 1970). The mutational status and molecular landscape of melanoma has become of great importance in the last several years. Using multi-platform data (DNA, RNA,

and protein level) from one of the largest cohorts of clinically annotated patient samples ever collected, The Cancer Genome Atlas (TCGA) program cataloged the molecular landscape of melanoma and identified four genomic subtypes of melanoma: *NRAS*, *BRAF*, *NF1*, and Triple-WT (Akbani, Akdemir, et al., 2015). These molecular subtypes are important indicators of prognosis and therapeutic options for patients with melanoma, and are generally mutually exclusive (i.e., patients harboring a NRAS mutation do not have a co-existing BRAF mutation, etc.). Approximately 50-60% of melanomas have a mutation in the BRAF kinase, generally an amino acid change of valine to glutamic acid at the 600 position, $BRAF^{V600E}$ (Davies, Bignell, et al., 2002; Ribas, Flaherty, et al., 2011; Ascierto, Kirkwood, et al., 2012). The patients harboring this mutation generally benefit from treatment regimens with small, targeted inhibitors of mutated-BRAF, such as vemurafenib or dabrafenib (Chapman, Hauschild, et al., 2011; Sosman, Kim, et al., 2012). Frustratingly, however, the response across the patients is highly variable and heterogeneous, despite the patients all harboring the same oncogenic lesion. A common, powerful endpoint of large clinical trials is the percent change in the largest target lesion; vemurafenib treatment provides confirmed objective responses in 48% of treatment-naïve patients (Chapman, Hauschild, et al., 2011) and an overall response rate of 53% in the metastatic setting (Sosman, Kim, et al., 2012). Drug resistance to anti-BRAF therapy significantly contributes to patient deaths and investigating mechanisms of resistance is vital for broadening efficacy of anti-BRAF therapy. Thus, there remains a need to further examine mechanism of action and ultimate effect on cell behavior of anti-BRAF agents, and increase our understanding of the biochemical basis for resistance. Later in this chapter, mechanisms of resistance reported in the literature will be discussed in more detail. Ultimately, heterogeneous responses can also be found in the cell line models used to study BRAF-mutated melanomas and data-mining in the

Cancer Cell Line Encyclopedia (CCLE) online data bank revealed a variable response to BRAF inhibitor PLX4720—similar to that found in patients (Figure 1.1).

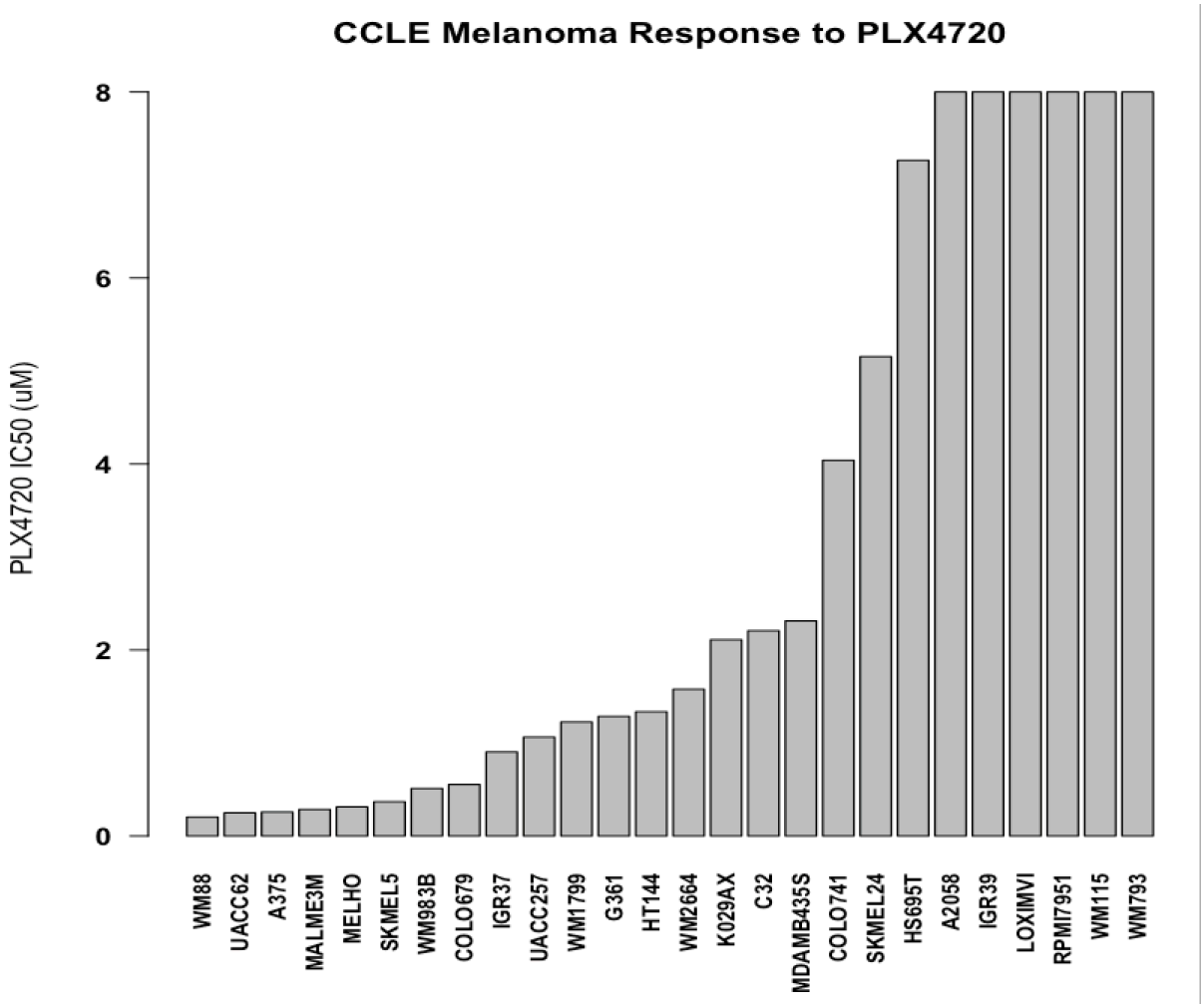

Figure 1.1: Heterogeneous Responses to BRAF Inhibition. Plot of IC50 response of BRAF-mutated melanoma cell lines in the CCLE. Cells were grown in either DMEM or RPMI1640 media, plated at ~250 per well in 1,536 well plates; an 8 point dose curve was generated using concentrations starting at 8 μM, with 3.16 fold dilutions down. After 72 or 84 hours, Promega's CellTiter-Glo (luciferase-based ATP assay) was used to count viable cells. All conditions were done with at least 2 replicates in the run; occasionally, some cell lines were run again/repeated. Due to the large nature of the repository and acquisition protocols, it is impossible to know which cell line/drug treatment combinations had which unique details (medium type, exact replicate numbers, plates runs, etc.)

Pathobiology of Mutated BRAF Kinase:

Importance of Mutation Status

The RAF oncogene was discovered more than 30 years ago and is an important integrator of signaling processes between receptor tyrosine kinases and downstream transcription factors (Rapp, Goldsborough, et al., 1983). The RAF homologues A, B, and C homo/hetero-dimerize and activate a cascade of signaling as part of the RAS-RAF-MEK-ERK axis. Thus, over-activation of the homologue BRAF in melanoma can cause downstream signaling that inappropriately regulates cell proliferation, protein synthesis, metabolism, and migration. The RAF kinases generally signal as dimers, however, the mutation V600E (or, less commonly, V600D) makes the BRAF kinase constitutively active and mutated BRAF will signal as a monomer.

The company Plexxikon marketed the first BRAF inhibitor, Zelboraf also known as vemurafenib or PLX4032. This compound, along with a research variant called PLX4720, is a heterocyclic, 7-aza-indole; PLX4032 differs in structure by the inclusion of 1 benzyl ring (compared to the PLX4720). The compounds also contain a difluoro-phenylsulfonamide structure that enriched and increased anti-BRAF activity (Tsai, Lee, et al., 2008). Targeted BRAFi has a favorable short-term response in most patients, as demonstrated by significant reductions in FDG uptake following just 2 weeks of treatment with vemurafenib (Bollag, Hirth, et al., 2010). Interestingly, an up-regulation in MEK activation and tumor insensitivity is found with BRAFi and WT normal BRAF kinase, mostly attributed to a transactivation of the BRAF (Halaban, Zhang, et al., 2010; and Poulikakos, Zhang, et al., 2010). In the presence of active Ras signaling, binding of these ATP-competitive drugs in one RAF molecule of a dimer will induce an allosteric change that transactivates the other RAF molecule. However, BRAF-mutated

melanomas have a sufficient low RAS activity that the potency of the ATP-competitive drugs is not tempered; thus, these inhibitors have select antitumor activity towards the melanoma cells and reduced clinical toxicity (Poulikakos and Rosen, 2011).

Acquired Resistance To Therapies

There have been several mechanisms of acquired resistance to BRAF targeted therapy described in the literature. Collectively, these findings can be grouped into two categories: MEK-dependent and MEK-independent pathway alterations. Figure 1.2 outlines many of the main mechanisms described, including $BRAF^{V600E}$ splice variants (Poulikakos, Persaud, et al., 2011), BRAF amplification (Shi, Moriceau, et al., 2012), BRAF kinase domain duplications (Kemper, Krijgsman, et al., 2016), mutations in MEK (Wagle, Van Allen, et al., 2014) and NRAS (Nazarin, Shi, et al., 2010), overexpression of COT (Johannessen, Boehm, et al., 2010), EGFR (Sun, Wang, et al., 2014), PDGFRb (Nazarin, Shi, et al., 2010) or CRAF (Montagut, Sharma, et al, 2008), and loss of negative regulators like NFI (Whittaker, Theurillat, et al., 2013). Amplification of the transcription factor MITF was reported by whole-exon sequencing of tumors treated with BRAF inhibitors (Van Allen, Wagle, et al., 2014) and Vergani et al. utilized MALDI-TOF to probe phosphotyrosine signaling and find cMET activation as a mediator of resistance (Vergani, Vallacchi, et al., 2011). Gatekeeper mutations in residues critical for ATP binding occurs frequently for other targeted therapies (for example, gefitinib against EGFR), but are virtually nonexistent in BRAF-mutated melanomas—despite the fact that gatekeeper mutations in the $BRAF^{V600E}$ kinase have been shown experimentally in cell lines to provide resistance to PLX4720 (Whittaker, Kirk, et al., 2010). Additionally, Keiran Smalley's group has demonstrated in cell line models that loss of PTEN will confer increased AKT signaling and

resistance to BRAF inhibition (Paraiso, Xiang, et al., 2011) and it has been correlated with increased brain metastases and decreased Overall Survival (OS) (Bucheit, Chen, et al., 2014). These data at a minimum highlight PTEN loss as a strong factor in regards to intrinsic resistance.

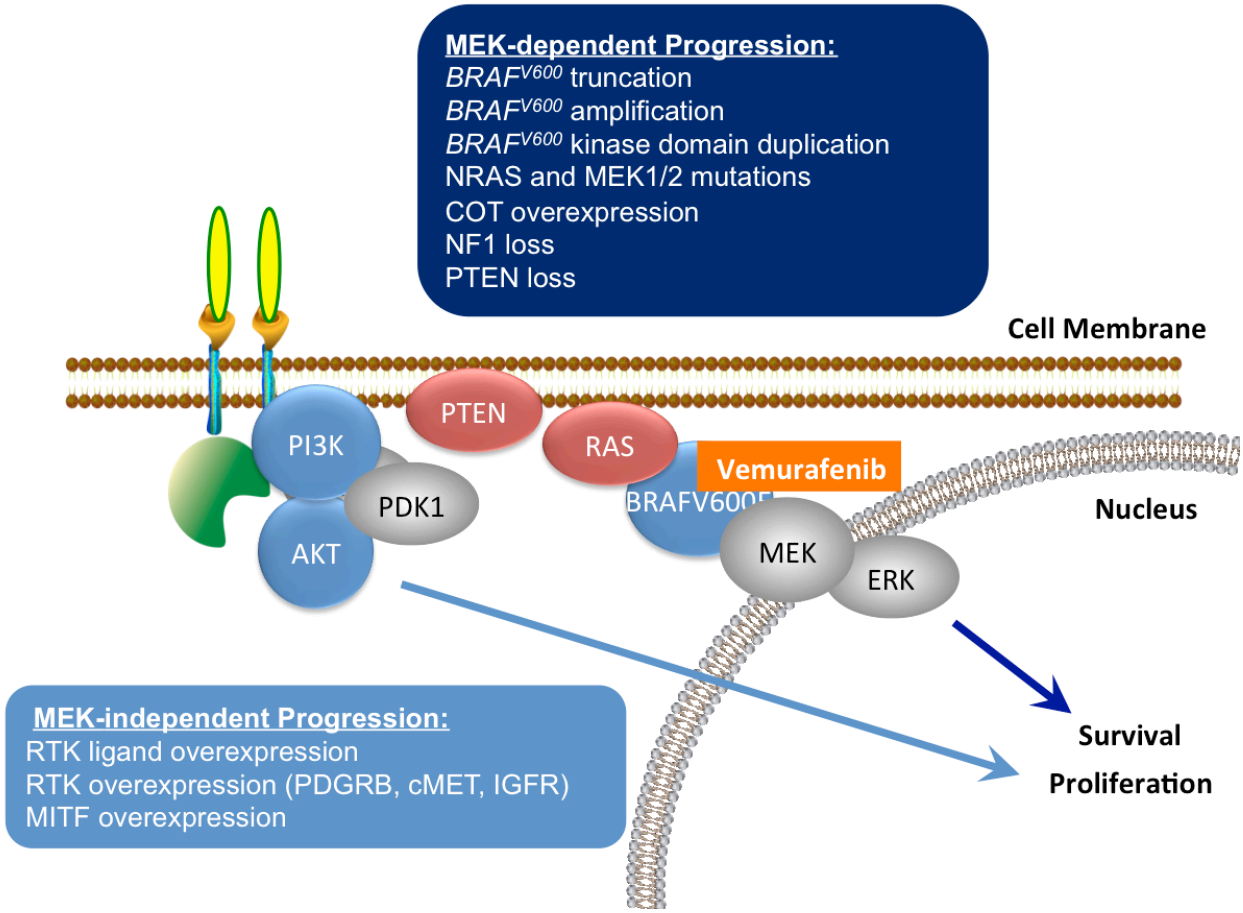

Figure 1.2: Mechanisms of Resistance to BRAF Inhibition. In resistant BRAF-mutant melanomas MEK-independent and MEK-dependent alterations have been described in the literature. Mechanisms have been identified and validated in patient samples/tissues, and shown in clinical models such as cell lines. Figure structure is adapted and modified from educational material provided courtesy of Dr. Jeffrey Sosman in 2013.

Most of what we know about resistance to BRAF inhibitors comes from patient tumors or cell lines with acquired resistance, i.e., continued proliferation, growth or metastasis while under BRAF inhibitor therapy. Rizos and co-authors extensively examined therapeutic resistance in patients that progressed on vemurafenib or dabrafenib therapy. All of the patients had a progressing lesion (primary or metastatic) that was macro-dissected and analyzed for known progression-associated alterations by RT-PCR (for known mutated alleles and splice variants), gene expression microarray analysis (for known MAPK pathway activation signatures) and immunohistochemistry (protein staining of IGFR, pAKT, and PDGFRβ) (Rizos, Menzies, et al., 2014). Frustratingly, only 22 of 38 tumors (that had matched treatment-naïve tissue) could be mapped back to a known mechanism of resistance previously described in the literature (Rizos, Menzies, et al., 2014). This large portion of unexplained resistance in approximately 42% of the tumor sampled after therapy failure highlights a major knowledge gap in the field. Others have commented on the dearth of knowledge regarding the cellular dynamics and biology leading up to observed BRAFi resistance (Smith, Brunton, et al., 2016) and this has fueled an explosion of research on non-genetic biology (such as cellular metabolism) in BRAF-mutated melanomas.

Cellular Metabolism:

Cellular metabolism is connected to an amazingly diverse set of biological processes including oogenesis (Sieber, Thomson, and Spradling, 2016), self-renewal of pluripotent stem cells (Zhang, Badur, et al., 2016), the cellular fate of immune T-cells (Buck, O'Sullivan, et al., 2016), the tumor vasculature (Wenes, Shang, et al., 2016), and even the organ-specific site of cancer metastases (Dupuy, Tabaries, et al., 2015). Furthermore, cellular differentiation and epigenetics can change cellular metabolism and bioenergetics. Birket and coauthors' elegantly

showed this in human embryonic stem cells (hESCs) and neuronal stem cells (NSCs): despite having similar relative distributions of ATP-consuming activities, the related secretion biology of hESCs accounts for a shift in not only global metabolism, but allocations of energetic demands (Birket, Orr, et al., 2010).

When oxygen is present and abundant, non-proliferating (usually differentiated) cells will catabolize glucose to pyruvate via glycolysis and then completely oxidize most of that pyruvate to CO_2 in the mitochondria—a process called oxidative phosphorylation. Otto Warburg, a German physiologist, noted more than 90 years ago that cancer cells catabolized most glucose to lactate, regardless of the abundance of oxygen. Termed the Warburg Effect, he postulated that the mitochondria of tumor cells must be damaged because it is inefficient to rely on aerobic glycolysis (which nets 2 ATP molecules per glucose) as opposed to oxidative phosphorylation (which nets about 36 ATP molecules) (Warburg, 1956).

The link between cancer and metabolism has been previously established; however, only recently has this reprogramming of metabolism or "deregulation of cellular energetics" been recognized as an emerging hallmark of cancer (Hanahan and Weinburg, 2011). Deregulated metabolism resonates with uncontrolled cellular proliferation: activating oncogenes have a propensity toward pushing cells into glycolytic metabolism, which supports fast proliferation (Vander Heiden, Cantley, and Thompson, 2009; DeBerardinis and Thompson, 2012). Fast proliferating cancer cells generally rely on aerobic glycolysis (the Warburg effect) despite the observation that the vast majority of glucose does not contribute to the biomass of cell; instead, the high glycolytic flux seems to be needed to provide energy and reducing equivalents, ATP and NAD+ respectively, and amino acids contribute the lions' share to cellular biomass (Hosios, Hecht, et al., 2016).

Historically, the field of cancer biology viewed Warburg's glycolytic metabolism as a separate metabolic upshift that occurred exclusively within a cancer cell with no other concurrent metabolic programs directing or regulating cellular processes. However, this dualist framework of pitting Warburg glycolysis against particularly oxidative phosphorylation is problematic and—to borrow David Nicholls' and Stuart Ferguson's terminology—"bioenergetically dubious". We now understand and appreciate that Warburg glycolysis and oxidative phosphorylation occur concurrently within a cell (Chi Dang, 2012) and, depending on the cellular context being studied, certain cancers may up regulate glycolysis, mitochondrial respiration or both. A perfect example of this phenomena is the *Ski* oncogene, and its bioenergetic effects as part of oncogenesis within a cell. The *Ski* oncogene is a transcriptional co-factor whose interactions mediate a wide range of transcriptional programs, including TGF-β signaling (Chen, Lin, et al., 2009). Although it had been shown to promote oncogenesis, it was curious that chicken embryo fibroblasts (CEFs) overexpressing Ski did not appear to produce extra lactate and acidify the cell culture media as expected due to presumed Warburg glycolysis (Ye, Lemieux, et al., 2011). The authors went on to demonstrate that the Ski oncogene increased mitochondrial respiration in nearly every part of the electron transport chain (ETC) analyzed by high-resolution respirometry; the increases in oxygen consumption across the oxygraph trace support activity increases in virtually all ETC complexes (Ye, Lemieux, et al., 2011).

The translational need for large-scale datasets has resulted in massive efforts to produce quality datasets that can be probed and analyzed across multiple platforms and biological processes. Large-scale profiling platforms were fundamental in the discovery of the best-studied examples of aberrant, metabolic re-wiring in cancer (Benjamin, Cravatt, and Nomura, 2012). Using stable isotope labeling of amino acids in cell culture (SILAC) as a large-scale proteomic platform, the

enzymatically-slow pyruvate kinase M2 isoform (PKM2) was found to shift metabolism of cancer cells to favor aerobic glycolysis and accumulate glycolytic intermediates for tumor growth (Christofk, Vander Heiden, et al., 2008). Similarly, large-scale metabolite profiling via metabolic flux analysis led to the finding that citrate born of the TCA cycle, which is then converted to Acetyl-CoA once exported to the cytosol, is the primary building block of lipids and fatty acids (DeBerardinis, Mancuso, et al., 2007). Metabolomic profiling also led to the discovery of the first oncometabolite via mutant isocitrate dehydrogenase 1 (IDH1): 2-hydroxyglutarate (Dang, White, et al., 2009). These examples are not cancer-specific in their origin, but more or less pathway and biochemistry centered. In cancer biology, large-scale genomics have taken prominence over phenotypic and functional platforms and this has probably limited the ability to find non-genetic sources of dysregulated metabolism driving cancer. Phenotype will likely precede the observance of genetic changes, therefore it is postulated that changes in cellular metabolism will be an early proximal marker for resistant phenotypes.

Metabolic Strategies That Influence Therapeutic Response:

Classic Routes of Tumor Drug Resistance Through Metabolism

Prevailing models of classic routes of tumor drug resistance have been historically linked to cellular metabolism. Zhao et al. summarize some of the major mechanisms of metabolic resistance to cancer agents (targeted or chemo-agents) in the broadest terms of accessibility for multiple cancer types. Figure 1.3 simplifies the mechanisms into 4 groups: 1) proliferation, 2) drug export, 3) pH regulation, and 4) signaling (Zhao, Butler, and Tan, 2013). Glycolytic intermediates generated by dysregulated cancer metabolism fuel expanded cellular growth and contribute to clinical resistance. The ATP generated by the glycolytic breakdown of glucose

fuels the active export of chemotherapeutic agents by the ABC transporters (which are ATP-dependent and consuming) and induces HIF1α expression. Export of the glycolytic end product, lactate and expression of carbonic anhydrases shift the pH ratio of the interior and exterior of the cell resulting in decreased passive transport of basic drugs. Signaling pathways activated by dysregulated metabolism also contribute to resistance, either via repressing pro-apoptotic signaling or activating compensatory pathways to circumvent drug-induced signal inhibition.

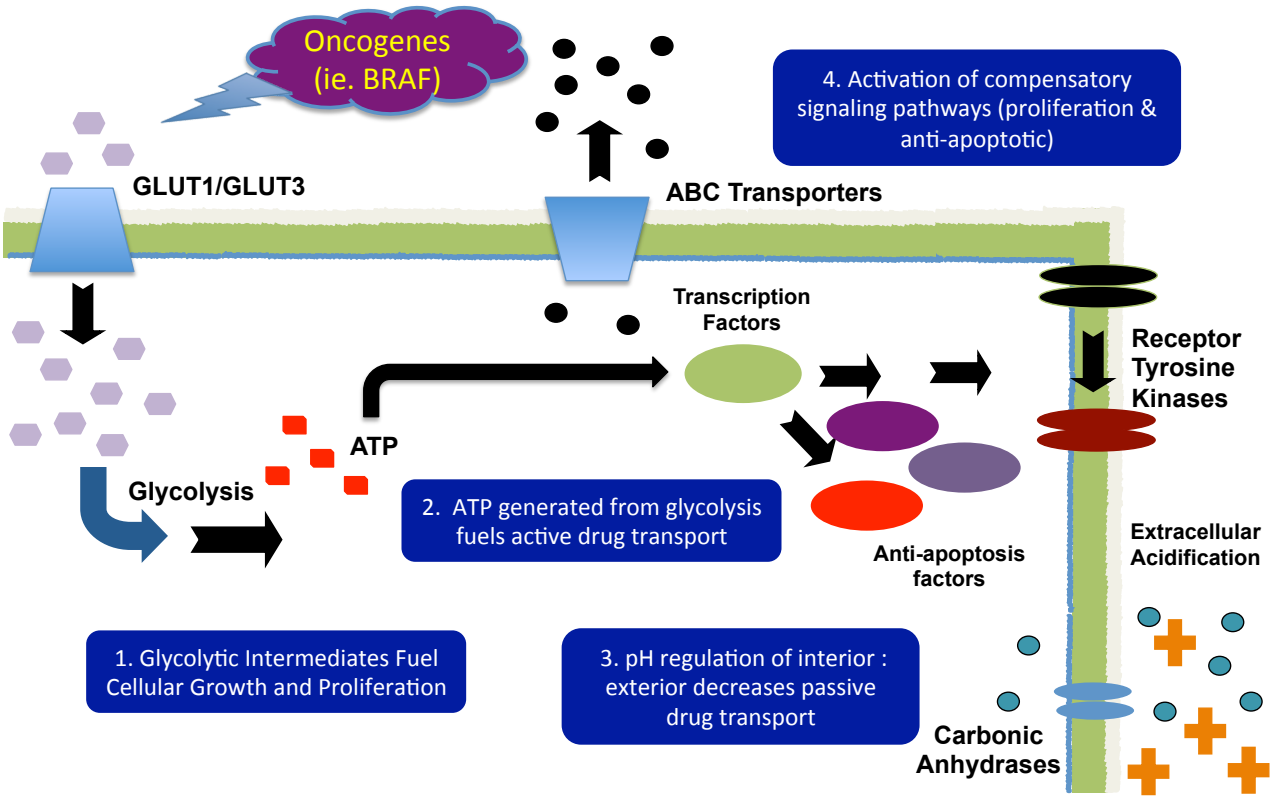

Figure 1.3: Dysregulated Metabolism Can Affect Therapy Response. Dysregulated metabolism affects chemo-resistance via multiple cellular pathways. (Re-imagined and adapted from Zhao, Butler, and Tan, 2013)

Cancer cells, in particular, exist in a "Metabolic Bubble" where stressors converge to present unique bioenergetics challenges. Traditionally, most cells must overcome three stress points: 1) biosynthetic stress (doubling mass for proliferation or macromolecule synthesis of

cytokines, factors, etc.); 2) reductive stress (maintaining NAD+ and FAD+ pools of reducing equivalents and cofactors for enzymatic reactions; and 3) energetic stress (ATP and GTP for normal cellular functions). The distribution of NAD+ within a cell is very disparate: the nucleus has NAD+ concentration around ~70 μM, where as the mitochondria has estimates > 250 μM (Canto, Menzies, and Auwerx, et al., 2015). NAD+/NADH cannot diffuse through cell membranes to different biological compartments, thus the cell must maintain reducing equivalent levels within each cellular compartment via transfer of metabolic substrates and enzymatic salvage reactions.

Metabolism in BRAF-mutated Melanomas:

MITF and PGC1α

Microphthalmia-associated transcription factor (MITF) has been under intense scrutiny in melanoma metabolism, due to the downstream signaling to Peroxisome proliferator-activated receptor Gamma Coactivator 1a (PGC1α) and subsequent mitochondrial biogenesis (Haq, Shoag, et al., 2013; and Vazquez, Lim, et al., 2013). Interestingly, Haq et al. demonstrated increased *in vitro* antitumor effect with the combination of PLX4720 and oligomycin, but the cell line used displayed an incredibly marked induction of PGC1α upon PLX4720 treatment—unlike any of the other cell lines in their panel (Haq, Shoag, et al., 2013). Additionally, there exists a discrepancy between therapeutic doses of BRAF inhibitors and responses in BRAF-mutated melanomas. When using PLX4720 at very low concentrations, MITF levels correlate with response, but at "IC50 doses" the correlation disappears (Calpaldo, Roller, et al., 2015). Thus, the level of MITF does not potentially explain non-responsive BRAF-mutated melanomas.

Presently, it is unknown whether BRAF-mutated melanomas all have constitutively high signaling across the MITF axis, if the signaling is fixed or permanent, or if there exists kinetic delays that render signaling defective for some melanomas. The interplay of transcription factors MITF and PGC1 and their role in mitochondrial biogenesis is a crucial topic in the field. Previously, the master metabolic regulator, AMP-activated Protein Kinase (AMPK), was thought to be a crucial component and effector of the MITF-PGC1a signaling axis. AMPK is a heterotrimeric protein with three subunits (α, β and γ); the γ subunit binds and senses AMP levels and helps to promote phosphorylation on the catalytic α subunit (Hardie, 2007). pAMPK regulates a p53-dependent cell cycle checkpoint for energetically unfavorable conditions (DeBerardinis, Lum, et al., 2008; Hardie, 2004). So, it is quite possible to imagine that pAMPK is mediating cancer cell survival in some insensitive BRAF-muted melanomas. However, BRAF-mutated melanomas have been shown to negatively regulate LKB1 through phosphorylation of S325 and S428 sites; $BRAFV^{600E}$ immuno-precipitates with AMPK. Zheng and colleagues showed ERK phosphorylates the LKB1, hindering its ability to activate the metabolic regulator AMPK (Zheng, Jeong, et al., 2009). This may be a mechanistic strategy for BRAF-mutated tumors to maintain and preserve strong MAPK pathway signaling: by negatively regulating LKB1, this could prevent AMPK from actively attenuating BRAF signaling through phosphorylation as shown in keratinocytes (Shen, Yuan, et al., 2013).

Current Field of Melanoma Metabolism

The global, cellular metabolism of melanoma was somewhat poorly understood and studied until a bevy of articles appeared approximately 5 years ago. Researchers found melanoma cells to be excellent models to study the transcription factor MITF and one of its best-known targets, PGC1a. Two back-to-back papers in the same issue of *Cancer Cell* demonstrate

the aberrant activation of PGC1a in a broad subset of melanoma cell lines (Vazquez, Lim, et al., 2013) and the relationship of mutated BRAF signaling and oxidative phosphorylation (Haq, Shoag, et al., 2013). In particular, Haq et al. suggested that mutated BRAF likely regulates a robust oxphos program via MITF and PGC1a signaling, and this oxphos phenotype is increased upon treatment with the BRAF inhibitor PLX4720 (Haq, Shoag, et al., 2013). Interestingly, other researchers have postulated that mutated BRAF signaling regulates a glycolysis program crucial to these cells (Hall, Meyle, et al., 2013; and Parmenter, Kleinschmidt, et al., 2014). In fact, Parmenter et al.'s work provides the best evidence that inhibitors targeting the mutated BRAF functionally target glycolysis: lactate production, GLUT1 and GLUT3 protein expression on cell membranes, and uptake of [^{3}H]2-Deoxy-Glucose (2DG) all are significantly higher in BRAF-mutated melanomas versus WT-BRAF (Parmenter, Kleinschmidt, et al., 2014). Amazingly, matched trios of BRAFV600 melanoma patient biopsies before treatment, during early treatment (less than 22 days) and after treatment failure/progression showed statistically significant dynamics of hexokinase-2 (HK2) expression decreasing upon treatment then increasing back up after resistance (Parmenter, Kleinschmidt, et al., 2014). This discordance in our understanding of melanoma cellular metabolism is further highlighted by recent data from Meenhard Herlyn's group: analysis of TCGA data revealed patients with the worst prognosis (overall survival) had tumor biopsies that highly expressed genes enriched in both glycolysis and oxidative phosphorylation (Zhang, Frederick, et al., 2016).

Summary and Purpose of Study:

Summary

Although considerable work has been done to investigate mechanisms of resistance in BRAF-mutated melanomas, the substantial portion of unexplained resistance to therapy (approximately 40%) amongst patients that progressed on targeted BRAFi therapy highlights a gap in our understanding of the biochemical basis of therapeutic resistance. As part of my project, I considered the possibility that the diversity of vemurafenib responses seen in patients was due to metabolic differences within their tumor cells, in spite of possessing the same driving oncogenic lesion of $BRAF^{V600E}$ or $^{-V600D}$. The purpose of this study is to test the hypothesis that oncogene addicted tumor cells, such as BRAF mutated melanomas, respond to targeted therapy based on intrinsic cellular metabolism, and to test whether that cellular metabolic state is clinically targetable with FDA-approved drugs. Several tasks were identified to help achieve that goal and move this thesis project forward: 1) curating *in vitro* melanoma cell line models that exhibit therapeutic response variability in regards to proliferation; 2) refining and employing an assay to measure proliferation dynamics and catch subtleties missed by typical end point assays; and 3) mapping and assessing global metabolism and potential substrate utilization as part of cellular bioenergetics. For this work I aimed to create a suite of high-throughput experiments that would allow me to ascertain the bioenergetic landscape by looking at the tumor cells' ability to proliferative under various metabolic stressors, and utilize substrates for glycolytic or oxidative phosphorylation processes. In the following chapters I show that we can overcome time-related biases and poor dynamical outputs of traditional IC50 assays (Chapter III), link glucose utilization with therapeutic response phenotypes (Chapter IV), suggest mitochondrial function and physiology as a biological indicator of response (Chapter V), and steer high-throughput

pipelines to find putative drug targets that may augment response in these cell line models (Chapter VI). Additionally, in Chapter VI, I present unpublished data that can help drive future experiments and research questions. Some of this data (like the reactive oxygen species (ROS) experiments) was completed early in the project in order to help eliminate and streamline the questions and project motivations. Other data (like the high-throughput screening (HTS) response data) are logical extensions of other completed manuscripts. At the time of writing this thesis, we are curating compounds for a targeted HTS of anti-retrovirals and other mitochondrial inhibitors; data on an interesting WNT inhibitor—pyrvinium pamoate—are shown in preliminary form.

Project Motivations

Although progress has been made in the field of melanoma biology, a finer understanding of the cellular metabolism is still needed. This is particularly highlighted again by the TCGA data presented by Zhang et al.: of the four subgroups ($Glyc^{Hi}/Ox^{Hi}$, $Glyc^{Hi}/Ox^{Low}$, $Glyc^{Low}/Ox^{Hi}$, $Glyc^{Low}/Ox^{Low}$) the best overall survival correlations had low Glycolysis gene signatures, but it is clear that only melanomas of a particular phenotype of glycolysis are super-sensitive and responsive to BRAF inhibition (Zhang, Frederick, et al., 2016). The metabolic activities of cancer cells make attractive targets of therapeutic intervention because they arise in concert with uncontrollable proliferation, oncogenic signaling, and therapeutic resistance. Thus, creating a thesis project that can add information about the unique metabolic biochemistry of BRAF-mutated melanomas is desirable. Several goals and motivations of this project include: 1) to examine BRAF inhibition's heterogeneous effect on tumor proliferation; 2) to discern the relationship of altered tumor cell metabolism and drug resistance, and possibly resolve some of the field's discordant findings about BRAF-mutated melanoma cellular metabolism; and 3)

obtain multi-parametric metabolic data that could possibly classify or cluster subtypes of sensitive or insensitive melanomas.

Research Questions

As stated earlier, the purpose of this study is to understand how BRAF-mutated melanomas respond to targeted therapy and manage to proliferate when deprived of the signaling induced by the oncogene those cell's are addicted to. The larger, overarching research question that this project entails is**: Can we manipulate the metabolism of BRAF-mutated melanomas and affect sensitivity or response to targeted therapies?** Imbedded within this larger framework of questions includes other smaller aims to 1) study and characterize the variability in melanoma cell line models more closely, and 2) query the relationship between a cell's metabolism and the cell's response (in regards to proliferation) to BRAF inhibition. This approach of targeting differential tumor metabolism represents a break from previous models constrained within the narrow scopes of upstream and downstream the RAS-RAF-MEK-ERK signaling axis. The metabolic phenotypes should be independently actionable—regardless of the driving mutations upstream. Based on the recent flurry of melanoma metabolism papers, tackling the problem of heterogeneous responses through the lens of tumor metabolism puts the concepts and approach of this application on the leading edge.

CHAPTER II

MATERIALS & METHODS

Reproduced and adapted from: Hardeman KN, Peng C, Paudel BB, Meyer CT, et al. (2017). "Dependence On Glycolysis Sensitizes BRAF-mutated Melanoma For Increased Response To BRAF Inhibition." *Scientific Reports* 7; 42604.

And: Harris LA, Frick PL, Garbett SP, Hardeman KN, et al. (2016). "An Unbiased Metric Of Antiproliferative Drug Effect *In Vitro*." *Nature Methods* 13, 497-500.

And: Paudel BB, Harris LA, Hardeman KN, et al. "Dysfunctional Mitochondria Leads To A Non-quiescent Idling State In Drug Treated BRAF Mutated Melanoma Cells." (In Preparation)

Reagents:

The BRAF inhibitor used in these studies, PLX4720 (catalog# S1152), was obtained from Selleckchem (Houston, TX) and solubilized in dimethyl sulfoxide (DMSO) at a stock concentration of 10 mM. BKM120 (Cat# S2247, Buparlisib) was obtained from Selleckchem (Houston, TX) and solubilized in DMSO at a stock concentration of 10 mM. Trametinib (Cat# T-8123) and BEZ235 (Cat# N-4288) were obtained from LC Laboratories (Woburn, MA) and solubilized in DMSO at stock concentrations of 1 mM. Cisplatin (Cat# 479306, cis-Diamineplatinum(II) dichlorine) was obtained from SigmaAldrich and solubilized in phosphate buffered saline (PBS) at a stock concentration of 12.5 mM. All drugs were aliquoted and stored

at -20°C until use except for cisplatin, which was stored at -80°C. Glycolysis Stress Test and Mitochondrial Stress Test kits were obtained from Seahorse Biosciences and used according to manufacturer instructions. Briefly, the components were mixed and constituted the day of the experiment, and utilized only once (the kits have reagents that are divided for single-use purposes). Ethidium bromide and uridine were obtained from Sigma.

Cell Culture:

Cell lines used throughout this thesis include BRAF-mutated melanoma cells (WM115, WM165, WM88, WM1799, WM793, WM2664, WM983B, SKMEL5, SKMEL28, A375, and A2058), BRAF-WT melanoma cells (MEWO), triple-negative breast cancer cells (MDA-MB-231), and HER2+ breast cancer cells (HCC1954). All melanoma cells were grown and cultured in Dulbecco's Modified Eagle Medium (DMEM) media containing 2 mM glutamine, 4.5 g/L glucose, 10% FBS and no sodium pyruvate (Gibco, catalog 11965-092), except where specified otherwise. The HCC1954 and MDA-MB-231 cells were grown in RPMI-1640 media with 2 mM glutamine, 2 g/L glucose, 10% FBS and no sodium pyruvate (Gibco, catalog 11875-093). Cells were split and seeded at ratios that allowed for splitting 1-2x per week. The cells were labeled lenti-virally with a fluorescent, nuclear tag (Histone 2B monomeric Red Fluorescent Protein, H2BmRFP from AddGene), flow sorted for H2BmRFP positivity (top 10-15% brightest), and kept as stocks annotated with "H2BmRFP"; if the cell line was labeled with the fluorescent ubiquitin-labeled cell cycle indicator FUCCI, then an additional annotation of "FUCCImAG-gem" was added as well. For proliferative experiments, the cells were plated the night before, then reagents/drugs were prepared in fresh media and added to the cells immediately before the start of the experiment the following day. For experiments involving nutrient deprivation (like glucose deprivation), cells were washed 1x with PBS then experimental

media was added onto the cells. For glucose deprivation, dialyzed FBS was added to DMEM medium to mitigate contribution of glucose from FBS. Dialyzed FBS+No glucose DMEM was titrated against the normal FBS+DMEM when preparing the drug dilutions for the experiments.

Rho0 Cell Generation:

Rho0 cell variants of BRAF-mutated cell lines WM164 and A2058 were generated using DMEM medium containing 4.5 g/L or 25 mM glucose, 2 mM glutamine, 1mM sodium pyruvate, 50 μg/ml uridine and 50 ng/ml ethidium bromide; cells were passaged at least 10x in this medium before using in experiments. PCR was used to confirm loss/reduction of mtDNA as a ratio of mtDNA to nuclearDNA (data not shown). These cells are classically referred to as rho0 or ρ0.

Measurement of Oxygen Consumption and Extracellular Acidification Rates:

Cells were plated in 96-well plates (Seahorse Biosciences, Bilerica, MA) at a density of 25-40,000 cells/well 24 hours before analysis on the Seahorse XF^e 96 extracellular flux analyzer. Mitochondrial oxygen consumption was quantified using the Mito Stress Test kit, and glycolytic rate quantified using the Glycolysis Stress Test kit, each according to manufacturer's instructions. Briefly, assay medium was un-buffered DMEM containing either 10 mM Glucose, 2 mM Glutamine, and 1 mM Sodium Pyruvate (Mito Stress Test) or none of the aforementioned (Glyco Stress Test). No FBS was used in assay medium.

Proliferation Assays:

The fluorescently labeled cells were counted under drug treatments using fluorescent microscopy. Cells were seeded into 96 well plates (1-5,000 cells per well) and drug treatments applied the following day, including DMSO or PBS control (all concentrations contained equal

percentage of DMSO or PBS solvent). Images were taken every 8-12 hours with sufficient image alignment (montaging) in order to capture about 25-100 cells per well/treatment (over the course of the experiment, cell counts typically exceed 1,000 in DMSO or low drug concentration wells). Direct measurements of cell counts were made using Cellavista software and Image J macros (please see Cell Counting Algorithms section in this Chapter). The images were filtered through these computer programs to track and label each cell, quantifying the number of cells in each time-stamped frame. Proliferation was plotted as log2 normalized growth, using the initial cell count from the first image frame for normalization.

Cell Counting Algorithms:

Image J macros are usually employed to directly count the cells. Raw microscopy images (usually in the highest, TIFF resolution format) are saved locally for the analysis. The macro identifies image files by 2 methods: 1) the file location or folder that is directed to "open," and 2) the string characters in the file name such as "-R0" +R+ "-C0" +C. By understanding the naming convention of the Cellavista microscope, we designed macros that can pick and group the individual image files of each well, putting all the subfield images together (montaging). Below is an example of a macro used. After the images are pulled and concatenated into an image stack, the median background is subtracted, I threshold the images for optimal pixel visualization, then a series of commands are run using built-in Image J functions. The ending output is a count of the particles (or nuclei) present.

Image J Macro Example:

```
//SKMel5 treated on 2 dimensions with varying glucose and PLX4720
//Have 7 time points taken, this plate is all SKMel5; washed 1x with PBS before drug addition
//3 x 5 montage, so total 15 in number=15; There was a total of 10 plates run with this group
```

```
//this for loop pulls all wells in loop

//for (R=row where to start; R< row to end at; same for column

for (R=2; R<8; R++) {

for (C=2; C<12; C++){

if (C < 10)

WellNumber = "-R0"+R+"-C0"+C;

else

WellNumber = "-R0"+R+"-C"+C;

time0 = "F:\\Keisha Hardeman\\hardemkn\\Melanoma\\March 2016\\20160325 SKMel5
GlucPLX\\1\\";

time1 = "F:\\Keisha Hardeman\\hardemkn\\Melanoma\\March 2016\\20160325 SKMel5
GlucPLX\\2\\";

time2 = "F:\\Keisha Hardeman\\hardemkn\\Melanoma\\March 2016\\20160325 SKMel5
GlucPLX\\3\\";

time3 = "F:\\Keisha Hardeman\\hardemkn\\Melanoma\\March 2016\\20160325 SKMel5
GlucPLX\\4\\";

time4 = "F:\\Keisha Hardeman\\hardemkn\\Melanoma\\March 2016\\20160325 SKMel5
GlucPLX\\5\\";

time5 = "F:\\Keisha Hardeman\\hardemkn\\Melanoma\\March 2016\\20160325 SKMel5
GlucPLX\\6\\";

time6 = "F:\\Keisha Hardeman\\hardemkn\\Melanoma\\March 2016\\20160325 SKMel5
GlucPLX\\7\\";

run("Image Sequence...", "open=[time0] number=15 starting=1 increment=1 scale=100
file=&WellNumber or=[] sort");

rename("stack");

run("Image Sequence...", "open=[time1] number=15 starting=1 increment=1 scale=100
file=&WellNumber or=[] sort");

rename("time1");

run("Concatenate...", "  title=[Concatenated Stacks] image1=[stack] image2=[time1] image3=[--
None --]");

run("Image Sequence...", "open=[time2] number=15 starting=1 increment=1 scale=100
file=&WellNumber or=[] sort");
```

```
rename("time2");

run("Concatenate...", "  title=[Concatenated Stacks] image1=[Concatenated Stacks]
image2=[time2] image3=[-- None --]");

run("Image Sequence...", "open=[time3] number=15 starting=1 increment=1 scale=100
file=&WellNumber or=[] sort");

rename("time3");

run("Concatenate...", "  title=[Concatenated Stacks] image1=[Concatenated Stacks]
image2=[time3] image3=[-- None --]");

run("Image Sequence...", "open=[time4] number=15 starting=1 increment=1 scale=100
file=&WellNumber or=[] sort");

rename("time4");

run("Concatenate...", "  title=[Concatenated Stacks] image1=[Concatenated Stacks]
image2=[time4] image3=[-- None --]");

run("Image Sequence...", "open=[time5] number=15 starting=1 increment=1 scale=100
file=&WellNumber or=[] sort");

rename("time5");

run("Concatenate...", "  title=[Concatenated Stacks] image1=[Concatenated Stacks]
image2=[time5] image3=[-- None --]");

run("Image Sequence...", "open=[time6] number=15 starting=1 increment=1 scale=100
file=&WellNumber or=[] sort");

rename("time6");

run("Concatenate...", "  title=[Concatenated Stacks] image1=[Concatenated Stacks]
image2=[time6] image3=[-- None --]");

run("Median...", "radius=2 stack");

run("Subtract Background...", "rolling=50 stack");

setThreshold(20, 255);

run("Convert to Mask", " ");

run("Watershed", "stack");

run("Analyze Particles...", "size=100-1500 circularity=0.60-1.00 show=Outlines exclude clear
include summarize stack");

while (nImages>0) {
```

```
        selectImage(nImages);
        close();
    }
}
}
```

The text is usually saved with basic text editors (ex: TextEdit on MAC processors) and the file name is annotated with the experiment date, and cell line name (and sometimes other pertinent information).

Clonal Fractional Proliferation Assay:

Clonal Fractional Proliferation (cFP) was done as previously described (Frick, Paudel, et al., 2015). Briefly, sub-confluent cells are seeded at low density (~10–20 cells per well) in 96-well culture imaging plates. Plates are kept in humidified and CO_2-controlled incubators for approximately one week with medium replacement every 3 days to allow single cells to expand into colonies of approximately 50 cells. Medium is then replaced with drug- or vehicle-containing medium and cells are imaged every ~8–12 hours until the end of the experiment, with drug replacement every three days. Images are processed as follows: raw images are sequentially organized into spatially registered montages and temporally assembled into image stacks. Cell counts per colonies were obtained using the freely available software called ImageJ (https://imagej.nih.gov/ij/), with a custom-written macro as described previously (Frick, Paudel, et al., 2015). This macro differs from the population-counting macros described in the prior section of this Chapter. Growth curves of single cell-derived colonies were plotted as described above.

Single Cell Derived Subclones:

SKMEL5 sublines were derived from single cells by serial dilution. Briefly, SKMEL5 cells were serially diluted and plated to less than 1 cell per well in 96-well imaging plates and imaged to identify wells containing a single cell. Cells were expanded in complete growth medium (in the absence of any inhibitors) and sequentially transferred to 48-, 24-, and 6-well plates until sufficient numbers of cells were available for cryopreservation of each subline. Sixteen such sublines were tested for their sensitivity to BRAF inhibitor (PLX4720) prior to cryopreservation (about 40+ sublines were produced from the entire assay, but most are not utilized in any experiments and have not been characterized).

Time-Lapse Single Cell Tracking:

For single-cell tracking, fluorescence images of nuclei were obtained as previously described (Quaranta, Tyson, et al., 2009). Briefly, images were acquired using a BD Pathway 855 in (spinning disk) confocal mode with a 20× (0.75NA) objective in a CO_2- and temperature-controlled environment every 20 min for 260 h from the time of first drug addition. Medium was replaced with freshly prepared drug every three days. Images from each well were organized into stacks of time series. Fluorescent nuclei were manually tracked across sequential images to obtain cell lifespans and resultant cell fates (death or division) as previously described (Tyson, Garbett, et al., 2012). “Birth time” denotes the time at which a mitotic event occurs, giving rise to two sister cells. “Lifetime” denotes the duration of single cell viability until they either died or underwent another mitosis. End of Experiment (EOE) represents the cells that were born in drug but did not exhibit any cell fate during the remaining observation time. A two-dimensional plot

of birth time (h) vs lifetime (h) shows the occurrence of differential cell fates in drug at the single-cell level.

Principal Component Analysis (PCA) and Liner Regressions:

Metabolic parameters were extracted for nine cell lines from two representative experiments, a glycolytic function experiment (Glyco Stress Test) and a mitochondria function experiment (Mito Stress Test) according to equations in supplemental table. Bioenergetic Health Index was calculated as previously described by Chacko, Kramer, et al. 2014. Correlation between metabolic parameter and IC50 was calculated using Pearson correlation. Before principal component analysis (PCA), each extracted parameter was Z-score normalized to minimize variation due to the different parameter scales. The first principal component was calculated using all possible combinations of parameters and each combination was correlated with the measured IC50 for nine cell lines in panel. All code for analysis is available in the public repository in GitHub:

https://github.com/hardemkn/Hardeman_et_al_2016

Statistical Analyses:

Data are presented as either an average of 3+ separate experiments or a representative example; error bars are means + or – SD and p values were obtained using unpaired t-test (Gaussian distribution assumed, two-tailed) done in Prism 7. Statistics for PCA and IC50 calculation are described in preceding sections. Estimates of DIP rate are determined within an experiment using the sum of cells across all technical replicates at a given time point and obtaining the slope of a linear model of log2(cell number) ~ time for time points greater than the observed delay. Minimum delay time is estimated by visual inspection of log-growth curves for the time at which

they become approximately linear. All data analysis was performed in R (version 3.2.1) and all raw data and additional R analysis code is freely available at github.com/QuLab-VU/DIP_rate_NatMeth2016.

Publicly available data sets

Drug-response data were obtained from the Genomics of Drug Sensitivity in Cancer (GDSC) project[4,9] website at ftp://ftp.sanger.ac.uk/pub/project/cancerrxgene/releases/release-5.0/gdsc_drug_sensitivity_raw_data_w5.zip and from the Cancer Cell Line Encyclopedia (CCLE)[6] website at http://www.broadinstitute.org/ccle/ in the data file CCLE_NP24.2009_Drug_data_2015.02.24.csv (user login required).

CHAPTER III

CELLULAR PROLIFERATION BIASES IN ONCOGENE-ADDICTED TUMORS: AN UNBIASED METRIC OF ANTIPROLIFERATIVE DRUG EFFECT *IN VITRO*

Adapted From: Harris LA, Frick PL, Garbett SP, Hardeman KN, et al. (2016). "An Unbiased Metric Of Antiproliferative Drug Effect *In Vitro*." *Nature Methods* 13, 497-500.

Abstract:

In vitro cell proliferation assays are widely used in pharmacology, molecular and cellular biology, and drug discovery. The gold standard metric is the number of viable cells remaining 72 h after drug addition. This is a "static" drug effect metric, since it is a single-time-point measurement. We found that dose–response curves constructed using "static," standard metrics of drug effect can result in erroneous and misleading values of drug-activity parameters, skewing data interpretation. This is because these metrics can suffer from time-dependent bias: i.e., the metric value varies with the time point chosen for experimental measurement. Using theoretical modeling and experimentation, we demonstrate these effects and possible inaccurate assessments of parameters such as drug potency and efficacy. To overcome this problem of bias, we propose using the slope of the proliferation response once it has linearized: a metric we call the drug-induced proliferation (DIP) rate. This DIP rate is essentially the slope of the line on a plot of cell population doublings (in log2 scale, on the y-axis) versus time (on the x-axis). My co-authors model mathematical, theoretical scenarios or treatments that could produce time-dependent biases in *in vitro* proliferation assays: (1) fast-proliferating cell line with a fast-acting drug, (2)

slow-proliferating cell line with a fast-acting drug, and (3) fast-proliferating cell line with a delayed-action drug.

My contribution to this manuscript is primarily in the 2nd half where cell line data is utilized to demonstrate the validity of the theoretical models and metrics. Under the section "Experimental Demonstration of Time-Dependent Biases" within this chapter, data I generated on two breast cancer cell lines (HCC1954 and MDAMB231) is used to experimentally demonstrate the scenarios of fast-proliferating cells treated with either fast-acting drugs (the metabolic inhibitors rotenone and phenformin) or slow-acting drugs (the tyrosine kinase inhibitors lapatinib and erlotinib). We generate dose–response curves from those data using the standard static effect metric and our novel DIP rate for various drug exposure times. Consistent with our theoretical results, the shape of the static-based dose–response curve strongly depended on the time point at which cell counts were taken: an illustration of time-dependent bias. These data make up the majority of Figure 3.5 of this chapter. Additionally, proliferative response data I collected using BRAF-mutated melanoma cell lines is included in the section title "Biases Found For Melanoma Cell Lines In Public Data Sets." Theoretically and in our hands we show that time-dependent biases can shape the metrics we obtained from proliferative assays; naturally, we wondered if these biases exist in public datasets. We extracted IC50 values from four BRAF-mutated melanoma cell lines (SKMEL5, A2058, A375, and WM115) that were shared in common within two large public data sets: the Cancer Cell Line Encyclopedia (CCLE) and the Genomics of Drug Sensitivity in Cancer (GDSC). Comparison-wise, our IC50 values corresponded closely to the value from at least one of the public data sets. Furthermore, in three cases the static- and DIP-rate-based IC50 values corresponded within an order of magnitude, however in one case (A375), they differed by nearly two orders of magnitude. This discrepancy

can be traced to a period of complex, nonlinear dynamics (brief regression followed by rebound) observed for this cell line between 24 h and 72 h post drug addition.

Introduction:

Evaluating antiproliferative drug activity on cells *in vitro* is a widespread practice in basic biomedical research (Zuber, McJunkin, et al., 2011; Berns, Hijmans, et al., 2004; Bonnans, and Werb, 2014) and drug discovery (Garnett, Edelman, et al., 2012; Wang, McLeod, et al., 2011; Barretina, Caponigra, et al., 2012). Typically, quantitative assessment relies on constructing dose–response curves (Stephenson, 1956). Briefly, a drug is added to a cell population over a range of concentrations, and the effect on the population is quantified with a metric of choice (Fallahi-Sichani, Monarnejad, et al., 2013). The de facto standard metric is the number of viable cells 72 h after drug addition (Garnett, Edelman, et al., 2012; Barretina, Caponigra, et al., 2012; Fallahi-Sichani, Monarnejad, et al., 2013; Yang, Soares, et al., 2013). Since this is a single-time-point measurement, we refer to it as a 'static' drug effect metric. The data is then fit to the Hill equation (Goutelle, Maurin, et al., 2008), a four-parameter log-logistic function, to produce a sigmoidal dose–response curve that summarizes the relationship between drug effect and concentration. Parameters extracted from these curves include the maximum effect (*E*max), half-maximal effective concentration (EC50), half-maximal inhibitory concentration (IC50), area under the curve (AUC), and activity area (AA) (Garnett, Edelman, et al., 2012; Barretina, Caponigra, et al., 2012; Fallahi-Sichani, Monarnejad, et al., 2013; Yang, Soares, et al., 2013). These are useful for quantitatively comparing various aspects of drug activity across drugs and cell lines (Figure 3.1).

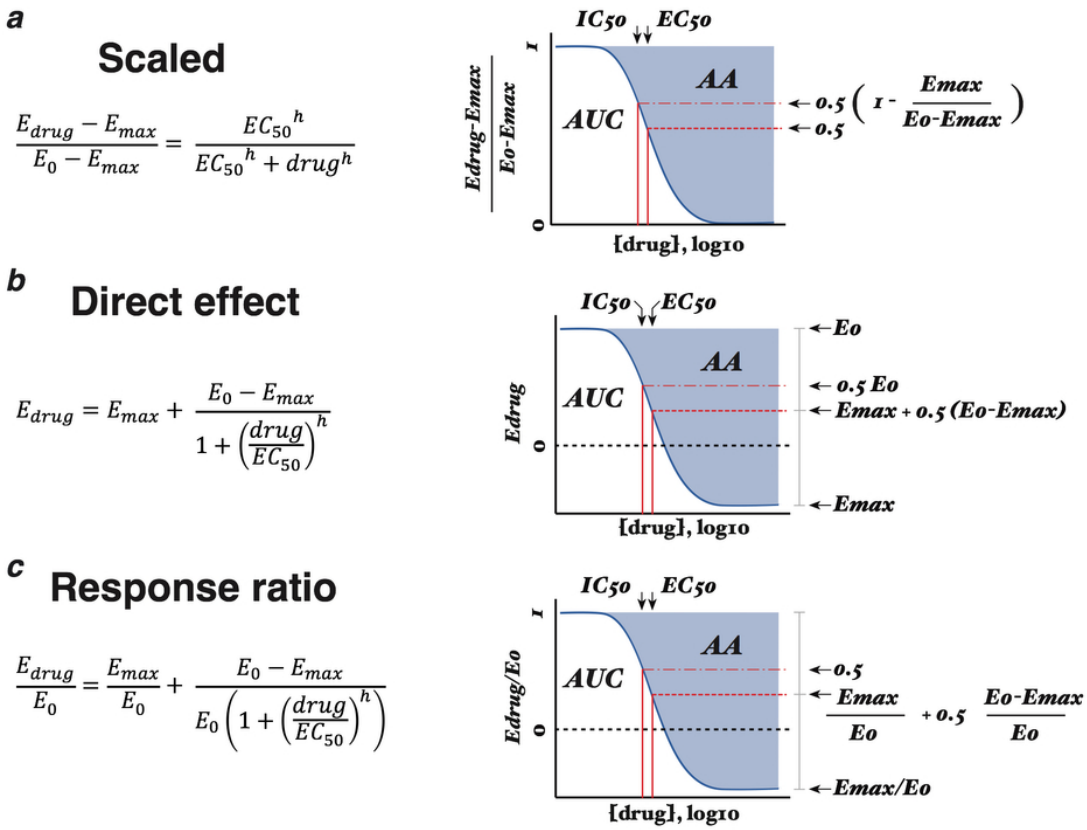

Figure 3.1: Different Formulations of Dose Curve Parameters. Potency parameters EC_{50} and IC_{50} are shown, as are area under the curve (AUC) and activity area (AA; the inverse of AUC), parameters that attempt to capture both potency and efficacy in a single quantity**. (a)** The "scaled" form given in equation (S2); (b) The "direct effect" form obtained by rearranging equation (S2) to solve for E_{drug}; (c) The "response ratio" form obtained by dividing the direct-effect form by E_0. Note that we consider here a case where $E_{max} < 0$, which is possible when using a dynamic drug effect metric such as DIP rate. This results in $IC_{50} < EC_{50}$ (see equation S5). In cases like this, the IC_{50} is sometimes referred to as the GI_{50} (half-maximal growth inhibitory concentration). (Figure Contribution: Leonard Harris and Darren Tyson)

We contend that dose–response curves constructed using standard metrics of drug effect can result in erroneous and misleading values of drug-activity parameters, skewing data interpretation. This is because these metrics suffer from time-dependent bias: i.e., the metric value varies with the time point chosen for experimental measurement. We identify two specific sources of time-dependent bias: (i) exponential growth and (ii) delays in drug effect stabilization. The former can lead to erroneous conclusions (e.g., that a drug is increasing in efficacy over

time), while the latter requires shifting the window of evaluation to only include data points after stabilization has been achieved (Figure 3.2).

To overcome this problem of bias, we propose as an alternative drug effect metric the drug-induced proliferation (DIP) rate (Tyson, Garbett, et al. 2012; Frick, Paudel, et al. 2015), defined as the steady-state rate of proliferation of a cell population in the presence of a given concentration of drug. Using related approaches, we previously quantified clonal fitness (Frick, Paudel, et al. 2015) and heterogeneous single-cell fates (Tyson, Garbett, et al., 2012) within cell populations responding to perturbations. Here, we show that DIP rate is an ideal metric of antiproliferative drug effect because it naturally avoids the bias afflicting traditional metrics, it is easily quantified as the slope of the line on a plot of the doubling of cell populations versus time (Figure 3.2), and it is interpretable biologically as the rate of regression or expansion of a cell population.

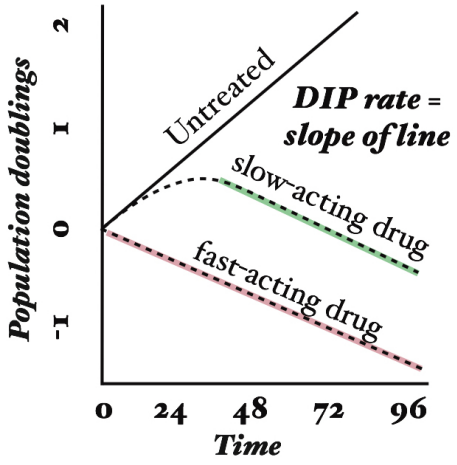

Figure 3.2: Action of Drugs On Proliferation. Hypothetical growth curves (in log scale) for a cell line untreated and treated with two different drugs: a fast-acting drug where the full effect is achieved immediately, and a slow-acting drug that causes a temporal delay in the stabilization of the drug effect. Also shown is drug-induced proliferation (DIP) rate, defined as the slope of the line after the drug effect has stabilized (in this case, immediately for the fast-acting drug and ≥48h for the slow-acting drug). Note that the DIP rate is shown as equivalent for both the fast- and slow-acting drugs for illustration purposes only. (Figure Contribution: Leonard Harris and Darren Tyson)

Results:

Theoretical Illustration of Biases in Drug Dose-Response Curves

To theoretically illustrate the consequences of time-dependent bias in standard drug effect metrics, we constructed a simple mathematical model of cell proliferation that exhibits the salient features of cultured cell dynamics in response to drug (Figure 3.3). The model assumes that cells experience two fates, division and death, and that the drug modulates the difference between the rates of these two processes, i.e., the net rate of proliferation. Drug action may occur immediately or gradually over time, depending on the chosen parameter values. In all cases, a stable DIP rate is eventually achieved and, when calculated over a range of drug concentrations, a sigmoidal dose–response relationship emerges (Figure 3.3).

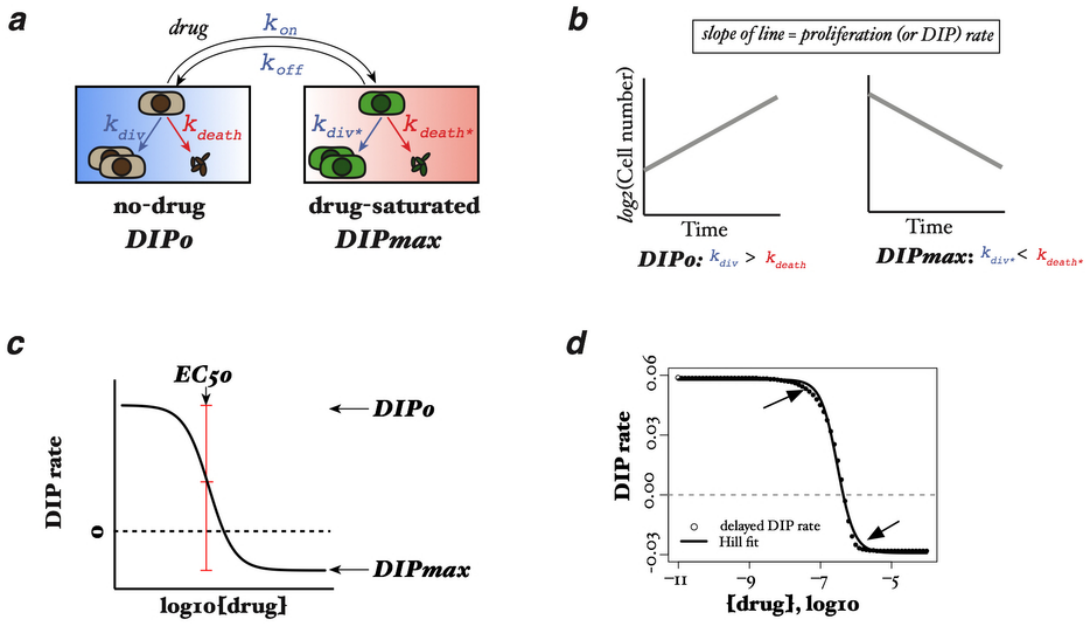

Figure 3.3: Figure legend on next page.

Figure 3.3: Mathematical Model of Cell Proliferation. (a) The model assumes two states, a drug-naïve state and a drugged state, each with its own characteristic rate of proliferation (DIP_0 and DIP_{max}, respectively), which is the difference between the rates of cell division and death. The rate of transition from the drug-naïve state to the drugged state depends on the concentration of drug, while the reverse transition does not. Hence, as the concentration of drug increases, the dynamic equilibrium between states shifts increasingly in favor of the drugged state. (b) Since the action of an antiproliferative drug is to reduce, and perhaps reverse, the rate of proliferation of a cell population, we assume that the proliferation rate of the drug-naïve state is positive and greater than that of the drugged state (which may be positive or negative). In Figure 3.4 of this chapter, we assume that in each case the drug is cytotoxic at saturating drug concentrations (i.e., causes regression of the cell population). Hence, the DIP rate of the drugged state (DIP_{max}) is assumed to be negative. (c) An example dose–response curve predicted by the two-state model under the partial equilibrium assumption (PEA). The curve was generated from equation (S27) with EC_{50} = 1e–8 M, $DIP_0 = 0.06*\ln(2)$ h^{-1}, and $DIP_{max} = –0.03*\ln(2)$ h^{-1}. (d) An example dose–response curve predicted by the two-state model in conditions where the PEA does not hold. The curve was generated by numerical integration of equations (S12) and (S13) with k_{on} = 1e5 M^{-1} h^{-1}, k_{off} = 1e–3 h^{-1}, $k_{div} – k_{death} = 0.06*\ln(2)$ h^{-1}, and $k_{div*} – k_{death*} = –0.03*\ln(2)$ h^{-1}. Note that these are consistent with the values used in part (c); see equations (S22), (S23), and (S26). Arrows highlight largest differences between calculated values (circles) and the Hill equation fit (black line). (Figure Contribution: Leonard Harris and Darren Tyson)

We model three scenarios: treatment of a fast-proliferating cell line with a fast-acting drug (Figure 3.4, part a), treatment of a slow-proliferating cell line with a fast-acting drug (Figure 3.4, part b), and treatment of a fast-proliferating cell line with a delayed-action drug (Figure 3.4, part c). In each case, we generate simulated growth curves in the presence of increasing drug concentrations (Figure 3.4, columns 1 and 2) and from these produce static dose–response curves by taking cell counts at single time points between 12 h and 120 h (Figure 3.4, column 3). As expected, in each scenario the shape of the dose–response curve varies depending on the time of measurement. Consequently, parameter values (EC50 and AA) extracted from these curves also vary (Figure 3.4, columns 4 and 5). Similar results are obtained for an alternative drug effect metric proposed by the U.S. National Cancer Institute's Developmental Therapeutics Program (Shoemaker, 2006). In contrast, as DIP rate is the slope of a line, it is independent of measurement time. Using it as the drug effect metric gives a single dose–

response curve (Figure 3.4, columns 3 and 6) and single values of the extracted drug-activity parameters (Figure 3.4, columns 4 and 5).

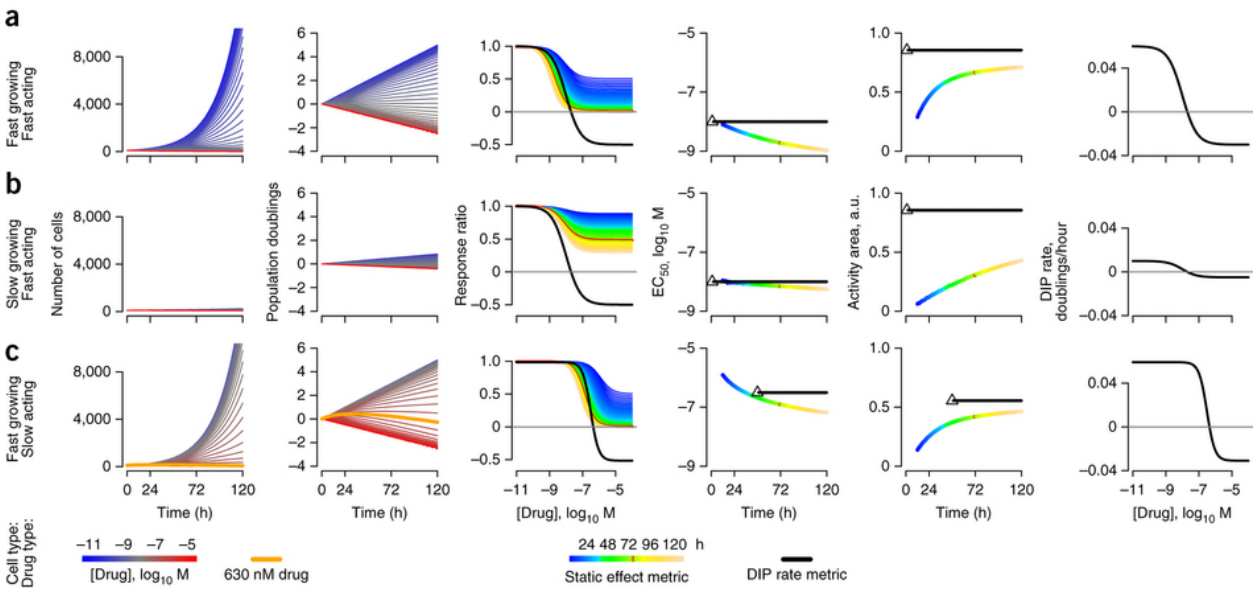

Figure 3.4: Theoretical Illustration of Time-dependent Bias. Computational simulations of the effects of drugs on: **(a)** a fast-growing cell line treated with a fast-acting drug; **(b)** a slow-growing cell line treated with a fast-acting drug; **(c)** a fast-growing cell line treated with a slow-acting drug. In all cases, *in silico* growth curves, plotted in linear (*column 1*) and log2 (*column 2*) scale, are used to generate static- (*column 3*) and DIP rate-based (*columns 3 and 6*) dose–response curves, from which values of *EC*50 (*column 4*) and activity area (AA; *column 5*) are extracted. For DIP rate-based values of *EC*50 and AA, the black triangle denotes the first time point used to calculate the DIP rate (i.e., after the drug effect has stabilized; see Online Methods); the black dashed line signifies that the value remains constant for all subsequent time points. Note that the "response ratio" (*column 3*) and "direct effect" (*column 6*) versions of the DIP rate-based dose–response curves (Figure 3.1) convey complementary information about the activity of a drug on a cell line. (Figure Contribution: Leonard Harris and Darren Tyson)

Experimental Demonstration of Time-Dependent Biases

As a first confirmation of our theoretical findings, we subjected triple-negative breast cancer cells (MDA-MB-231) to the metabolic inhibitors rotenone (Figure 3.5, part a) and phenformin (Figure 3.5, part b). Using fluorescence microscopy time-lapse imaging (Tyson, Garbett, et al., 2012; Frick, Paudel, et al., 2015; Quaranta, Tyson, et al., 2009), we quantified changes in cell number over time for a range of drug concentrations. For both drugs, we observed a rapid stabilization of the drug effect (<24 h delay) and stable exponential proliferation thereafter, reminiscent of the growth dynamics of the theoretical cell lines treated with fast-acting drugs. We generated dose–response curves from these data using the standard static effect metric and DIP rate for various drug exposure times. Consistent with our theoretical results, the shape of the static-based dose–response curve strongly depended on the time point at which cell counts were taken, an illustration of time-dependent bias. The DIP rate, on the other hand, was free of time-dependent bias and produced a single dose–response curve in both cases.

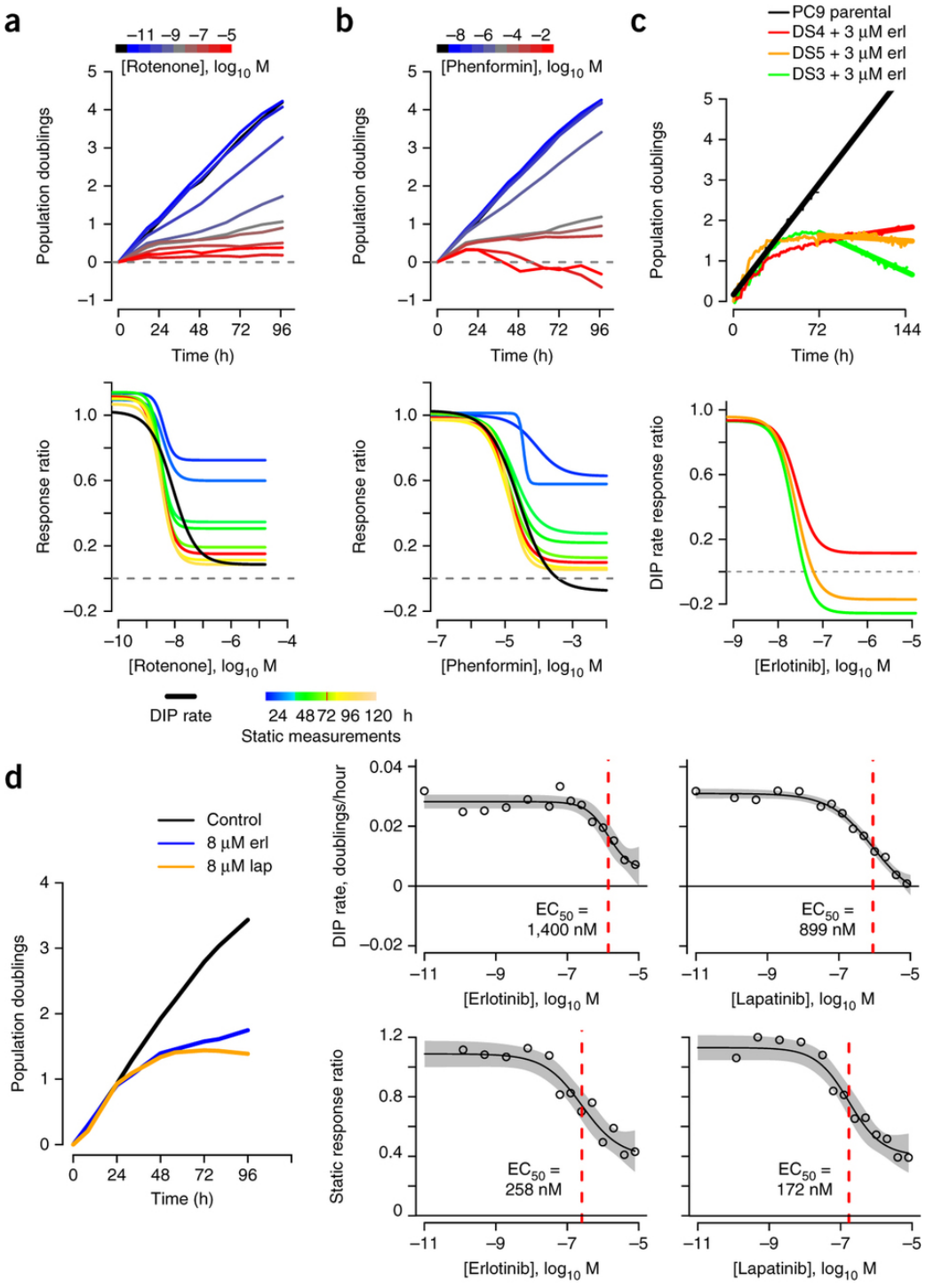

Figure 3.5: Figure legend on next page.

Figure 3.5: Experimental Confirmation of Time-dependent Bias. Population growth curves (log2 scaled) and derived dose–response curves (static- and/or DIP rate-based) for **(a)** MDA-MB-231 triple-negative breast cancer cells treated with rotenone; **(b)** MDA-MB-231 cells treated with phenformin; **(c)** three single-cell-derived drug-sensitive (DS) clones of the EGFR mutant-expressing lung cancer cell line PC9 treated with erlotinib; **(d)** HCC1954 HER2-positive breast cancer cells treated with erlotinib and lapatinib. Data for (*a*) and (*b*) are from single experiments with technical duplicates; data in (*c*) are from individual wells for two experiments containing technical duplicates (growth curves) and from a single experiment with technical duplicates (dose–response curves); data in (*d*) are sums of technical duplicates from a single experiment (growth curves) and mean values (circles) with 95% confidence intervals (gray shading) on the log-logistic model fit (dose–response curves; n=4, 6 for erlotinib and lapatinib, respectively).

These DIP-rate-based dose–response curves produce interesting insights (Figure 3.5, parts a and b). For example, they indicate that while rotenone is much more potent than phenformin (EC50 ≅ 8.5 nM versus 25 μM), phenformin is more effective (Emax/E0 ≅ −0.1 versus 0.1). The static dose–response curves can discriminate the ordering of potencies (rotenone >> phenformin) but not the ordering of efficacies: i.e., the static drug effect metric obscures the crucial fact that at saturating concentrations phenformin is cytotoxic (cell populations regress) while rotenone is partially cytostatic (cell populations continue to expand slowly). This information is critical to studies assessing drug mechanism of action. This example illustrates the perils of biased drug effect metrics and the ability of DIP rate to produce reliable dose–response curves from which accurate quantitative and qualitative assessments of antiproliferative drug activity can be made.

To illustrate the confounding effects that a delay in the stabilization of the drug effect can have, we examined single-cell-derived clones of the lung cancer cell line PC9, which is known to be hypersensitive to erlotinib (Gong, Somwar, et al., 2007), an epidermal growth factor receptor (EGFR) kinase inhibitor. Consistent with our previous report (Tyson, Garbett, et al., 2012), three drug-sensitive PC9-derived clones (DS3, DS4, and DS5) each responded to 3 μM erlotinib with nonlinear growth dynamics over the first 48–72 h, followed by stable exponential proliferation

thereafter (Figure 3.5, part c). These dynamics are reminiscent of those for the theoretical fast-proliferating cell line with a delayed-action drug (Figure 3.4, part c). Because of the delay in drug action, all three clones had nearly identical population sizes 72 h after drug addition for all concentrations considered. The static 72-h metric thus produces essentially identical dose–response curves for all clones (data not shown). In contrast, dose–response curves based on DIP rate make a clear distinction between the clones in terms of their long-term response to drug: i.e., erlotinib is cytotoxic (negative DIP rate) for two of the clones but partially cytostatic (positive DIP rate) for the other (Figure 3.5, part c).

We then investigated the effects of erlotinib and lapatinib (a dual EGFR/human EGFR 2 (HER2) kinase inhibitor) on HER2-positive breast cancer cells (HCC1954; delay ~48 h; Figure 3.5, part d). In each case, DIP-rate-based dose–response curves produced EC50 values more than five-fold larger than their static counterparts; i.e., by the static drug effect metric the drugs appeared significantly more potent than they actually were. Taken together with the PC9 results (Figure 3.5, part c), these data illustrate the importance of accounting for delays in drug action when assessing antiproliferative drug activity, and they further emphasize the ability of the DIP rate metric to produce accurate drug-activity parameters and qualitative conclusions about drug-response dynamics.

Biases Found For Melanoma Cell Lines In Public Data Sets

Within the last several years, a number of studies have been published reporting drug responses for hundreds of cell lines derived from various cancer types (Garnett, Edelman, et al., 2012; Barretina, Caponigra, et al., 2012; Yang, Soares, et al., 2013; Seashore-Ludlow, Rees, et al., 2015; Rees, Seashore-Ludlow, et al. 2016) and organ sites (Fallahi-Sichani, Honarnejad, et

al., 2013; McDermott, Sharma, et al., 2008; Heiser, Wang, et al., 2009). Raw data are available for the responses of over 1,000 cancer cell lines to a panel of 24 drugs in the Cancer Cell Line Encyclopedia (CCLE) (Barretina, Caponigra, et al., 2012) and for the responses of over 1,200 cell lines to 140 drugs in the Genomics of Drug Sensitivity in Cancer (GDSC) project (Yang, Soares, et al., 2013). These data are largely based on 72-h cell counts, a metric that we have shown contains time-dependent bias.

To investigate bias in these data sets, we treated four $BRAF^{V600E}$- or $BRAF^{V600D}$-expressing melanoma cell lines with various concentrations of the BRAF-targeted agent PLX4720, an analog of vemurafenib. We produced experimental growth curves (Figure 3.6, part a) and static- and DIP-rate-based dose–response curves (Figure 3.6, part b), and we extracted IC50 values for each cell line and compared these to IC50 values obtained from the CCLE and GDSC data sets (Figure 3.6, part c). In all cases, our IC50 values corresponded closely to the value from at least one of the public data sets. While in three cases the static- and DIP-rate-based IC50 values corresponded within an order of magnitude, in one case (A375), they differed by nearly two orders of magnitude. This discrepancy can be traced to a period of complex, nonlinear dynamics (brief regression followed by rebound) observed for this cell line between 24 h and 72 h post drug addition (Figure 3.6, part a). This result is particularly intriguing because it shows that, based on DIP rate, this cell line is not much different than the other three cell lines in terms of drug sensitivity. Using the biased static drug effect metric, however, one would be led to the incorrect conclusion that it is significantly more sensitive. It is likely that cases like this abound within these and other similar data sets (Seashore-Ludlow, Rees, et al. 2015; Rees, Seashore-Ludlow, et al. 2016), and this likelihood illustrates the critical need for new antiproliferative drug effect metrics.

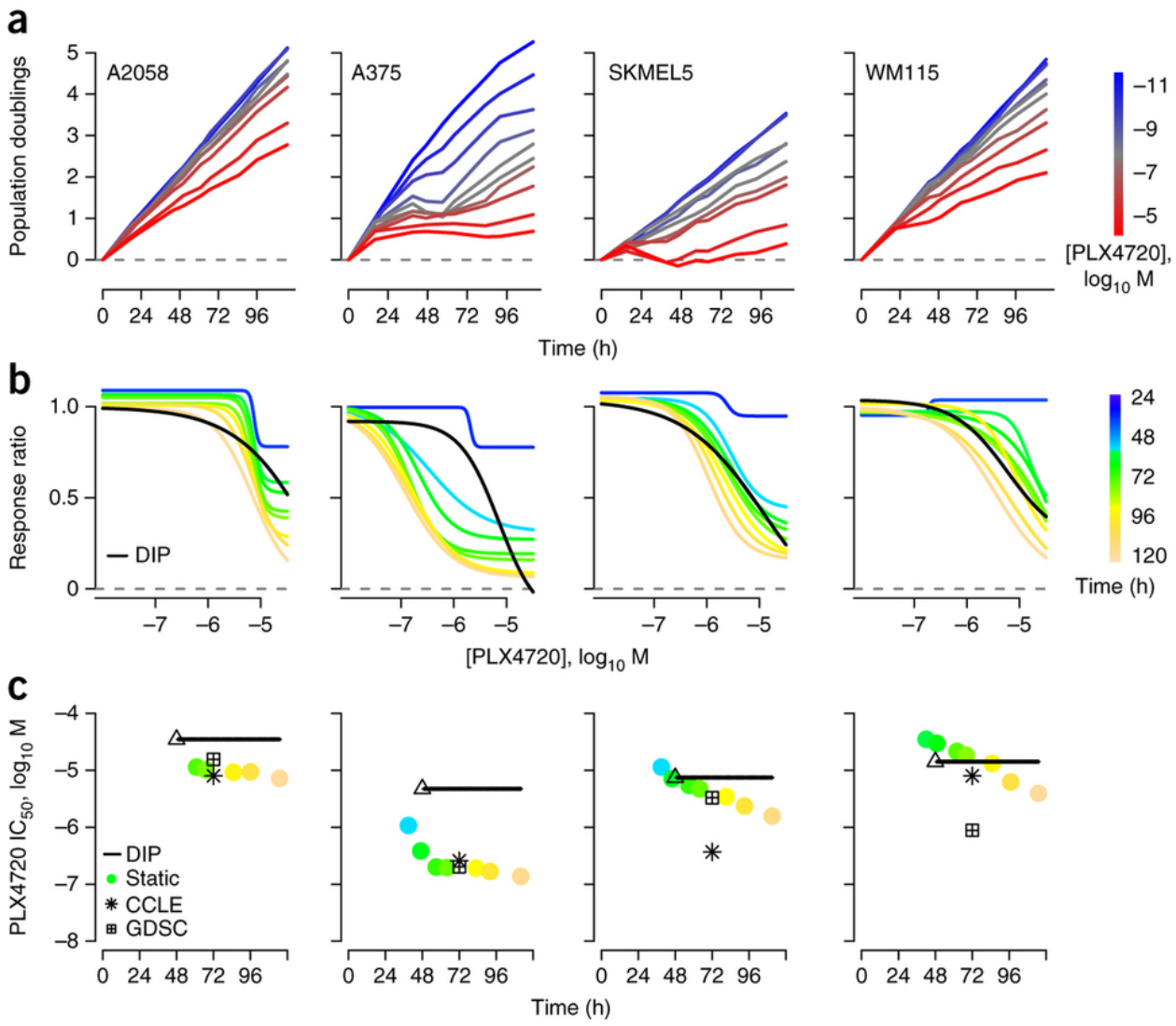

Figure 3.6: Bias In Potency Metrics Found In Public Datasets. (a) Population growth curves (log2 scaled) for four select BRAF-mutant melanoma cell lines treated with various concentrations of the BRAF inhibitor PLX4720; (b) dose–response curves based on the static effect metric (colored lines) and DIP rate (black line); (c) static- (circles) and DIP rate-based (triangle+line) estimates of *IC*50 for each measurement time point. *IC*50 values obtained from public data sets (CCLE: Cancer Cell Line Encyclopedia; GDSC: Genomics of Drug Sensitivity in Cancer), based on the static 72h drug effect metric, are included for comparison. The triangle denotes the first time point used in calculating the DIP rate and the black line signifies that the value remains constant for all subsequent time points. Data shown are from a single experiment with technical duplicates. Experiment has been repeated at least twice with similar results.

Discussion:

Current protocols for cell proliferation assays are based on informal 'rules of thumb', for example, counting cells after 72 h of treatment to ameliorate the impact of complex dynamics and delays in drug response. However, these de facto standards have no theoretical basis and, as demonstrated here, they suffer from time-dependent bias that leads to erroneous conclusions. In light of the widespread applications of cell proliferation assays in oncology, pharmacology, and basic biomedical science (Sporn, & Harris, 1981) (for example, to assess activity of cytokines, cell surface receptors, altered signaling pathways, gene overexpression and silencing, or cell metabolic adaptation to varied microenvironmental conditions), it is imperative that the quality of the metric for antiproliferative assays be improved. Toward this end, we have proposed DIP rate as a viable, unbiased alternative antiproliferative drug effect metric. DIP rate overcomes time-dependent bias by log-scaling cell count measurements to account for exponential proliferation and by shifting the time window of evaluation to accommodate lag in the action of a drug, changes that do not substantially alter experimental design (Supplementary Note and Supplementary Figs. 6, 7, 8, 9). Moreover, DIP rate is an intuitive, biologically interpretable metric with a sound basis in theoretical population dynamics, and it faithfully captures, within a single value, the long-term effect of a drug on a cell population.

Acknowledgements:

We are grateful to R. Feroze, J. Hao, K. Jameson, and C. Peng for support in experimental data acquisition; to J. Guinney, T. de Paulis, and J.R. Faeder for critical reviews of the manuscript; to W. Pao (Vanderbilt University, Nashville, Tennessee) for providing the PC9 cell line; and to M. Herlyn (Wistar Institute, Philadelphia, Pennsylvania) for providing the

WM115 cell line. This work was supported by Uniting Against Lung Cancer 13020513 (D.R.T.), Vanderbilt Biomedical Informatics Training Program NLM 5T15-LM007450-14 (L.A.H.), and the National Cancer Institute U54-CA113007 (V.Q.), U01-CA174706 (V.Q.), and R01-CA186193 (V.Q.), and partially supported by the National Cancer Institute (P50-CA098131) and the National Center for Advancing Translational Sciences (UL1-TR000445-06). This work was also supported by the National Science Foundation (grant MCB-1411482 to C.F.L.) and the VICC (Young Ambassador Award to C.F.L.). Its contents are solely the responsibility of the authors and do not necessarily represent official views of the National Cancer Institute, the National Center for Advancing Translational Sciences, or the National Institutes of Health.

CHAPTER IV

DEPENDENCE ON GLYCOLYSIS SENSITIZES BRAF-MUTATED MELANOMA FOR INCREASED RESPONSE TO BRAF INHIBITION

Adapted From: Hardeman KN, Peng C, Paudel BB, Meyer CT, et al. (2017). "Dependence On Glycolysis Sensitizes BRAF-mutated Melanoma For Increased Response To BRAF Inhibition." *Scientific Reports* 7; 42604.

Abstract:

Dysregulated metabolism can broadly affect therapy resistance by influencing compensatory signaling and expanding proliferation. Given many BRAF-mutated melanoma patients experience disease progression with targeted BRAF inhibitors, we hypothesized therapeutic response is related to tumor metabolic phenotype, and that altering tumor metabolism could change therapeutic outcome. We demonstrated the proliferative kinetics of BRAF-mutated melanoma cells treated with the BRAF inhibitor PLX4720 fall along a spectrum of sensitivity, providing a model system to study the interplay of metabolism and drug sensitivity. We discovered an inverse relationship between glucose availability and sensitivity to BRAF inhibition through characterization of metabolic phenotypes using nearly a dozen metabolic parameters in Principle Component Analysis. Subsequently, we generated rho0 variants that lacked functional mitochondrial respiration and increased glycolytic metabolism. The rho0 cell lines exhibited increased sensitivity to PLX4720 compared to the respiration-competent parental lines. Finally, we utilized the FDA-approved antiretroviral drug zalcitabine to suppress

mitochondrial respiration and to force glycolysis in our cell line panel, resulting in increased PLX4720 sensitivity via shifts in EC50 and Hill slope metrics. Our data suggest that forcing tumor glycolysis in melanoma using zalcitabine or other similar approaches may be an adjunct to increase the efficacy of targeted BRAF therapy.

Introduction:

Melanoma is the most malignant form of skin cancer, and roughly 50% of clinical isolates have a mutation in the BRAF kinase of the mitogen-activated protein kinase (MAPK) pathway (Davies, Bignell, et al., 2002; Ribas and Flaherty, 2011). Ninety percent of those BRAF mutations are missense mutations that change the valine at position 600 to glutamic acid (V600E) or aspartic acid (V600D) (Ascierto, Kirkwood, et al., 2012). The mutation confers constitutive activation of the BRAF kinase and drives oncogenic signaling through MEK phosphorylation. Targeted therapies against the mutant BRAF have prolonged progression-free survival and overall survival in Phase III clinical trials (Chapman, Hauschild, et al., 2011). Unfortunately, most patients will exhibit some degree of disease progression while treated with a BRAF inhibitor, with nearly 50% of patients progressing after only 6 to 7 months of initial treatment (Chan, Haydu, et al., 2014). There have been a variety of mechanisms that underlie initial and acquired drug resistance described in the literature. Generally, mechanisms of resistance to anti-BRAF therapies are put into MEK-dependent and MEK-independent categories. MEK-dependent mechanisms include mutations in NRAS, MEK1 and MEK2 (Nazarian, Shi, et al., 2010), loss of RAS regulation by NF1 (Hodis, Watson, et al., 2012; Whittaker, Theurillat et al., 2013), COT overexpression driving MEK signaling (Johannessen, Boehm, et al., 2010), and genetic alterations in BRAF itself, such as truncation or amplification (Poulikakos, Persaud, et al., 2011). MEK-independent mechanisms of resistance include receptor

tyrosine kinase protein and ligand overexpression, such as cMET, IGF1R, and PDGFRb (Nazarian, Shi, et al., 2010), and signaling through PI3K (Villanueva, Vultur and Herlyn, 2011). Unfortunately, more than 40% of the resistance found in patients who progressed on targeted therapy cannot be attributed to any of these mechanisms Rizos, Menzies, et al., 2017). One of the features common to all of the known pathways that contribute to resistance is that they exert direct or indirect control of multiple cellular metabolic pathways—contributing to the single "hallmark" of metabolic reprogramming. In the last several years, there has been an increasingly intense focus on tumor metabolism as an exploitable therapeutic avenue (Vander Heiden, Cantley, et al., 2009; DeBerardinis, Lum, et al., 2008; DeBerardinis, and Chandel, 2016; Hanahan and Weinberg, 2011), with the success of asparaginase in the treatment of acute lymphoblastic leukemia (ALL) being just one example that has achieved widespread clinical use (Clavell, Gelber, et al., 1986; Silverman, Gelber, et al., 2001), and with many other metabolism-based therapies under active development (Wang, Karamanlidis, and Tian, 2016; Zhao, Butler, and Tan, 2013).

Dysregulated metabolism in cancer has been shown to affect treatment outcome via multiple pathways, including the activation of compensatory receptor tyrosine kinase signaling to bypass molecular targeted therapies, the repression of pro-apoptotic signaling, and limitation of drugs' access to molecular targets through active and passive mechanisms (Zhao, Butler, and Tan, 2013). Komurov et al showed chronic lapatinib treatment of HER2+ breast cancer cell lines produced cells with an advanced nutrient starvation phenotype Komurov, Tseng, et al., 2012). Furthermore, the cells were sensitive to the antihelminthic pyrvinium pamoate, which targets mitochondrial function under various conditions (Tomitsuka, Kita, and Esumi, 2012), particularly glucose deprivation (Esumi, Kurashima, and Hanaoka, 2004). Recently, it has been

shown in BRAF-mutated melanoma that chronic treatment with BRAF inhibitor induces glutamine dependence that correlates with drug resistance (Baenke, Chaneton, et al., 2015; Hernandez-Davies, Tran, et al., 2015). We were interested in the prospect that the molecular metabolic landscape of any individual tumor might have a direct relationship to its sensitivity to targeted therapies.

The same metabolic pathways that have been targets for investigation in other malignancies have also been explored in BRAF-mutated melanoma, but a consensus of the major metabolic program exhibited by BRAF-mutated melanomas, or even whether a single dominant metabolic program exists, is lacking. BRAF-mutated melanomas have conversely been characterized as exhibiting primarily aerobic glycolysis (Parmenter, Kleinschmidt, et al., 2014) or oxidative phosphorylation (Vazquez, Lim, et al., 2013; Haq, Shoag, et al., 2013). Moreover, the relationship between metabolic program and therapeutic response in BRAF-mutated melanoma is poorly understood, so we set out to probe the phenotypic relationship of metabolism and responses to the BRAF inhibitor vemurafenib.

In the present study, we used a panel of human BRAF-mutated melanoma cell lines to demonstrate *in vitro* variability in response to PLX4720, a BRAF inhibitor and analogue of vemurafenib. Utilizing our previously described method for measuring proliferative rate under various treatment conditions (Harris, Frick, et al., 2016), we calculated a metric describing the dependence of proliferation on drug concentration to place the cell lines on a continuum of sensitivity to PLX4720. We then examined baseline glycolytic and oxidative metabolism and found a relationship between reliance on glycolysis and sensitivity to inhibition by PLX4720. Building upon this observation, we show that forcing exclusive reliance on glycolysis via mitochondrial DNA depletion using either ethidium bromide or zalcitabine (a first generation

antiretroviral used to treat HIV) significantly attenuates intrinsic resistance to PLX4720 in our cell line panel.

Results:

PLX4720 Response Spectrum and Global Metabolism

To confirm the variability in response to mutant BRAF inhibition observed in patients could be modeled *in vitro*, we measured the cell lines' proliferative responses to BRAF inhibition. The proliferative kinetics of the cell lines were quantified in the presence of PLX4720. Based on the PLX4720-treated DIP rates, BRAF-mutated melanoma cell lines fall along a response spectrum or continuum (Figure 4.1), from highly sensitive (e.g., WM164) to largely insensitive (A2058). The IC50 metric is calculated from a log-logistic curve fit to the estimated rate of proliferation obtained at each drug concentration, known as the drug-induced proliferation (DIP) rate (Harris, Frick, et al., 2016).

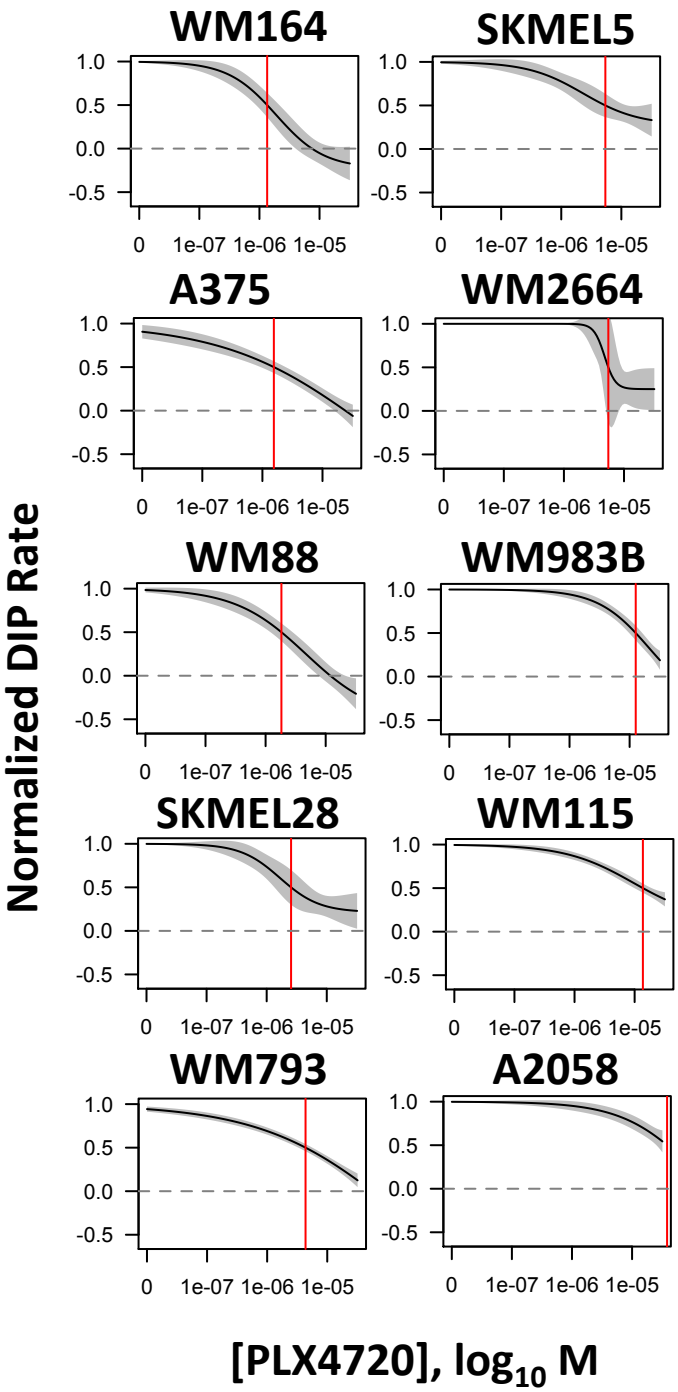

Figure 4.1: Heterogeneous Responses to BRAF Inhibition. Proliferative spectrum of IC50's for PLX4720 based on DIP rate. The dose-response curves are generated using a 2-fold dilution of PLX4720 from 32 μM down to zero (DMSO). The proliferative rates are calculated using the slope of the log2-normalized population curve after 48 hours. Mean responses are shown as solid lines, 95% confidence intervals as shaded regions. All results are based on 3+ biological replicates.

We next wanted to confirm that the measured variability in response to PLX4720 treatment was not due to phenotypic selection of drug-resistant subclones during the short 4-5 day timeframe of our experiments. We leveraged a fluorescent ubiquitin-dependent cell cycle indicator (FUCCI; mAG-gem1-110) to detect cells that have committed to cell division (i.e. passed the G1/S transition). We reasoned that if intrinsically resistant clones exist within the population, they would be enriched in cells that continue to proliferate in the presence of BRAF inhibition and would remain resistant after isolation. To test this, we treated the BRAF-mutated melanoma lines with PLX4720 or DMSO for 72 hours followed by flow sorting for the actively dividing FUCCI+ cells from both groups, then re-plated them in the absence of drug for 24 h and treated a second time with PLX4720. The proliferative responses of the two groups were essentially the same, indicating that PLX4720 does not appear to select for resistant populations in the short term (Figure 4.2). Stated differently, cells that actively divide in the presence of PLX4720 have similar proliferation kinetics when re-challenged with the drug.

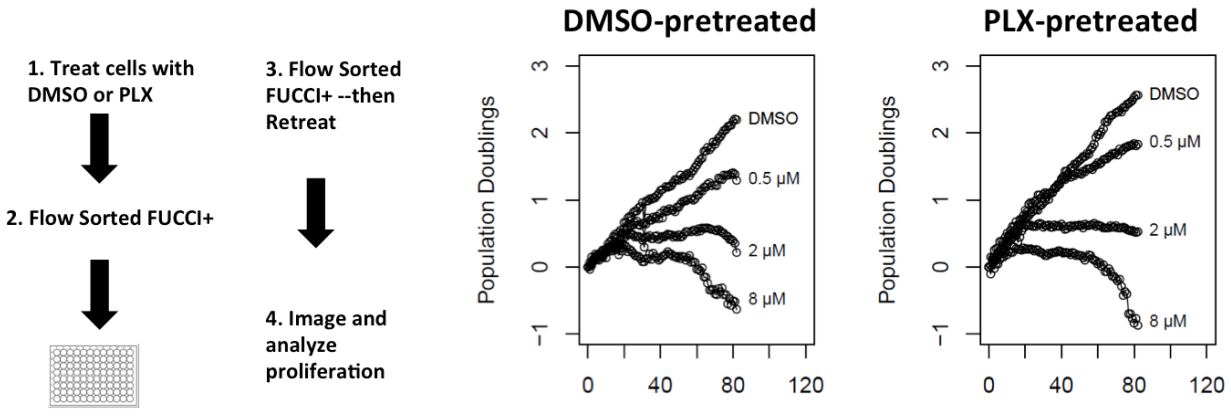

Figure 4.2 Figure legend on next page.

Figure 4.2: FUCCI-sorting Experiment: Cells Retain No Memory. Schematic outline of the flow of the experimental design: A375 cells were pre-treated for 72 hours with either DMSO or PLX4720, then flow sorted for positive fluorescence-ubiquitin-linked cell cycle indicator (FUCCI). Those cells were seed in 96 well plates overnight, then retreated with PLX4720. The proliferation was log-2 normalized and plotted as population doubling (y-axis) over time (x-axis, in hours). Data shown are from a single experiment with technical duplicates; experiment has been repeated with similar results.

To determine the metabolic profiles exhibited by our panel of BRAF-mutated melanomas, we quantified lactate-producing glycolysis and mitochondrial oxidative metabolism using the Seahorse extracellular flux analyzer platform. Using a panel of 10 BRAF-mutated melanoma cell lines, we found most lines can variably utilize glucose and consume oxygen as part of mitochondrial respiration (Figure 4.3). Notably, most cells have minor glycolytic reserve after the addition of oligomycin (Figure 4.3, lower), indicating most of the melanoma cell lines are functioning at or near their glycolytic capacity. The basal respiration and oxygen consumption also varied across cell lines. Additionally, the subsequent decreases in oxygen consumption rate (OCR) after the addition of oligomycin (Figure 4.3, upper) suggest varying dependencies on ATP-linked respiration (or ATP turnover supported by oxidative phosphorylation) across the cell lines. In totality, these data suggest broad, intrinsic metabolic heterogeneity across the cell line panel.

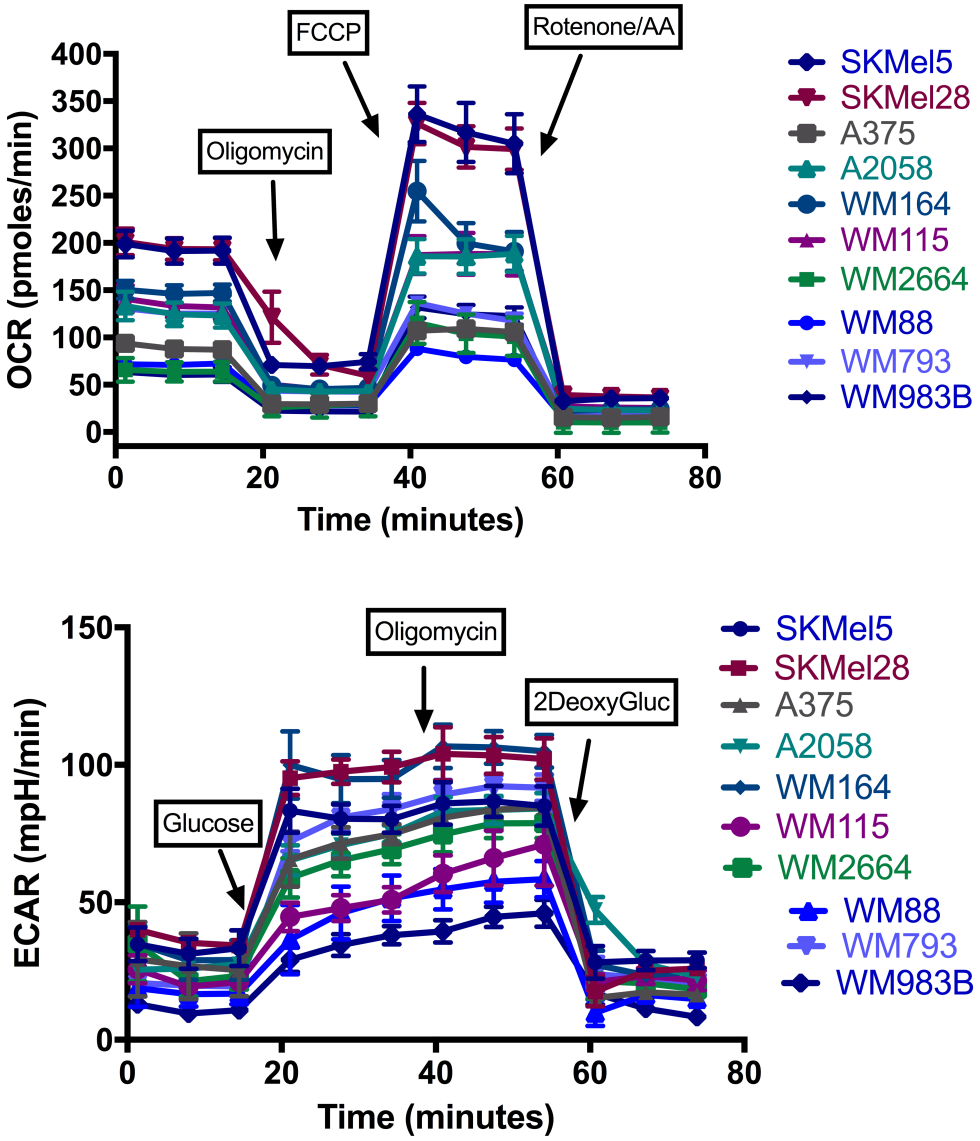

Figure 4.3: Global Oxidative Phosphorylation and Glycolysis. Upper: Oxygen consumption profiles for the cell lines with sequential additions of oligomycin (1 μM), FCCP (1 μM) and Rotenone/Antimycin A (0.5 μM). Lower: Extracellular pH profiles for the cell lines with sequential additions of glucose (10 mM), oligomycin (1 μM), and 2-deoxyglucose (0.5 μM). Data shown are from a single experiment with minimum 5 technical replicates; experiment has been repeated at least twice with similar results. Error bars are standard deviation.

Given the observed heterogeneity in PLX4720 responses without an obvious biological mutational trend (Figures 4.1 and Table 1) and the variable metabolic strategies employed by our panel of BRAF-mutated melanomas, we sought to examine more closely whether a direct relationship exists between metabolism and drug response.

Table 1. BRAF-Mutated Melanoma Cell Lines Exhibit Heterogeneity

	Relevant Mutation/Biology			IC50 Metrics
Cell Line	**BRAF Mutation**	**P53 Status**	**PTEN Status**	**IC50 (uM)**
WM164	V600E	MU	WT	1.34
A375	V600E (HOMOZ)	WT	WT	1.55
WM88	V600E	WT	WT	1.83
SKMEL28	V600E (HOMOZ)	MU	MU	2.55
WM793	V600E	WT	MU/HEM DEL	4.35
SKMEL5	V600E	WT	WT	5.42
WM2664	V600D	WT	HEM DEL	5.49
WM983B	V600E	MU	WT	12.6
WM115	V600D	WT	HEM DEL	13.7
A2058	V600E	MU	MU	38.3

Table 1. Relevant Mutation Biology and Calculated IC50. Cell line mutation information from WISTAR Institute website, COSMIC website, and Birgit Schittek, et al., Int J. of Cancer; 82, 583-585 (1999). HOMOZ=homozygous; MU=mutated; WT=wild type; HEM DEL=hemizygous deletion

Glucose Is A Key Nutrient Influencing Response

To quantify the relationship between the metabolic program of BRAF-mutated melanoma cell lines and PLX4720 response, eleven metabolic parameters were calculated from measurements of mitochondrial oxygen consumption and glycolytic function curves for nine cell lines (parameters described in Figure 4.4 schema).

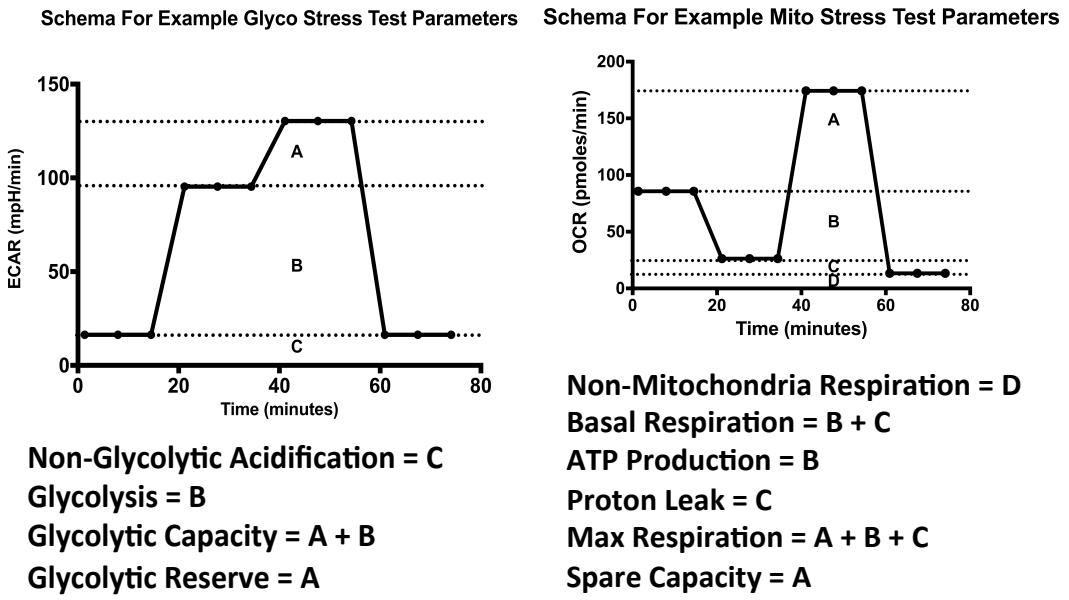

Figure 4.4: Schema For Principal Component Analysis. Schematic diagram describing the components and metrics from Seahorse assays used in the PCA; Bioenergetic Health Index (BHI) calculation is described in methods.

Each metabolic parameter was independently tested for correlation with the measured IC50 for PLX4720 for each cell line (Figure 4.5). We found a significant inverse correlation ($r = -0.495$) between glycolysis and the measured IC50 values, suggesting increased glycolysis in BRAF-mutant cell lines is indicative of greater sensitivity to BRAF inhibition (and thus a lower IC50).

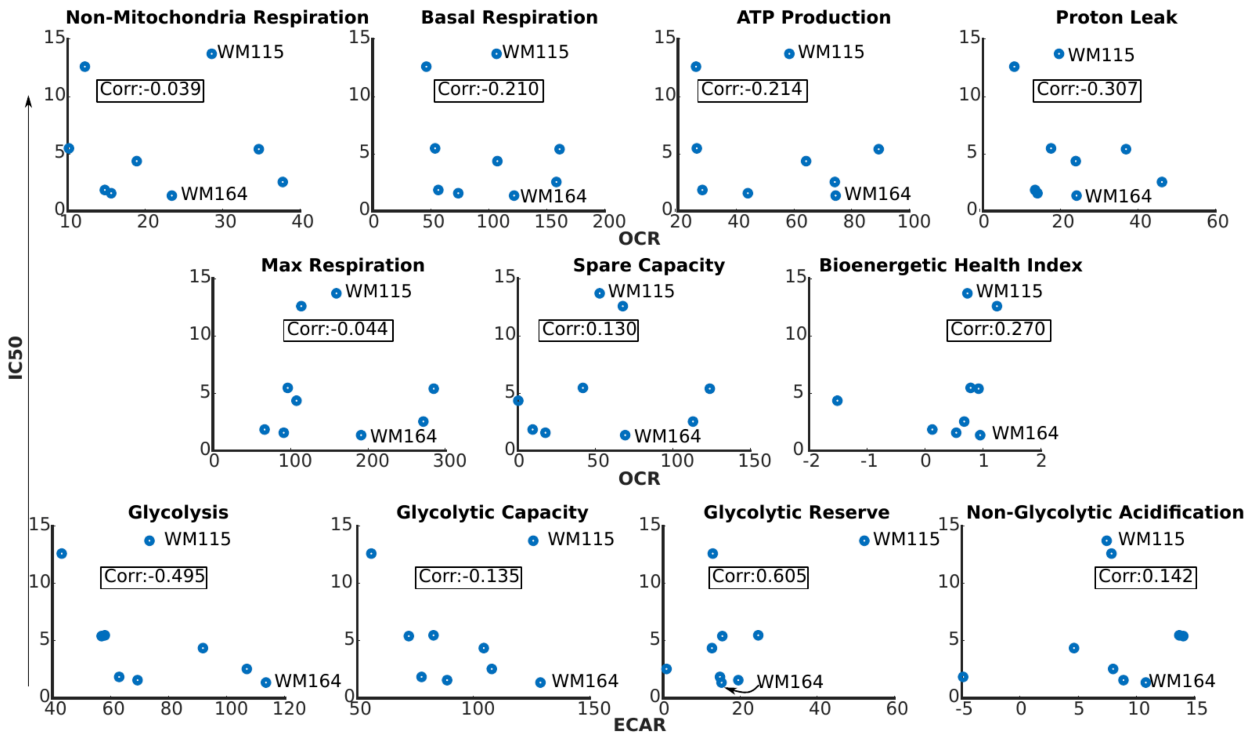

Figure 4.5: Independent Correlation Analysis. Metabolic parameters individually tested for correlation (Pearson) to PLX4720 IC50 of the cells. Parameters include: Non-mitochondrial respiration; Basal respiration; ATP production; Bioenergetic health index; Proton leak; Max respiration; Spare capacity; Glycolysis; Glycolytic capacity; Glycolytic reserve; and Non-glycolytic acidification.

Next we determined how different combinations of the metabolic parameters correlated with drug sensitivity using Principle Component Analysis (PCA). This analysis comparing all possible combinations of parameters identified a linear combination of glycolysis and glycolytic reserve as strongly correlating to the cell line's IC50 values, with the combination of these two metabolic parameters accounting for more than two-thirds (69.7%) of the variance in the parameter ensemble across the cell line panel (Figure 4.6). Based on these results, we predicted increasing the rate of glycolysis while depleting glycolytic reserve would decrease the IC50 value for a BRAF-mutated melanoma to PLX4720 treatment.

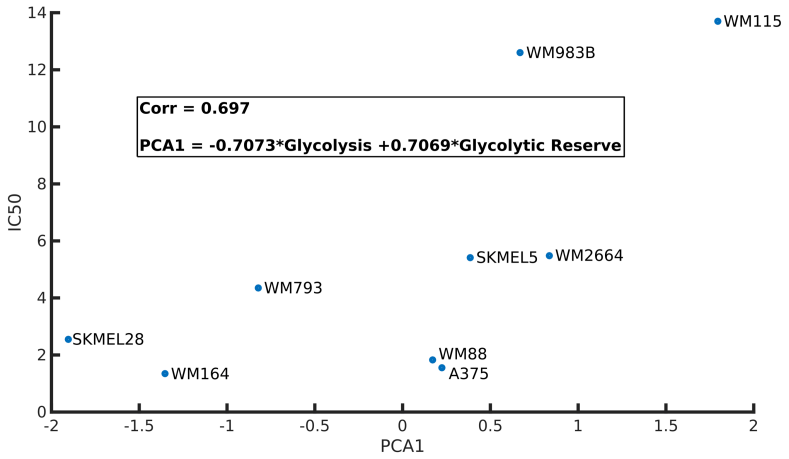

Figure 4.6: PCA Analysis. The first principle component of a linear combination of glycolysis and glycolytic reserve parameters (in cell lines) correlates with IC50. Corr=correlation.

We titrated across serial dilutions of PLX4720 and glucose concentrations to test whether glucose availability and PLX4720 response were functionally related. We first quantified drug-induced proliferative (DIP) rates across the spectrum of glucose/PLX4720 conditions in 6 melanoma cell lines. We found that the DIP rate responses are largely linear and glucose/PLX4720 concentration dependent, as shown in Figure 4.7. Glucose-replete conditions exhibited the "best" or highest DIP rates for each cell line (indicating more rapid cell proliferation), and the glucose-deprived conditions the poorest or lowest DIP rates, as might have been expected. The key finding was each cell line appears to have the capacity to revert phenotypically to a more PLX4720-sensitive phenotype (i.e. lower DIP rate) by simply lowering the glucose in the medium, and every cell line exhibited sensitivity to glucose limitation to approximately the same degree. Using proliferation as a phenotypic output, every cells' phenotype is pushed into a more responsive zone of lowered proliferation. These data suggest that glucose is a key nutrient tied to BRAF inhibition, and PLX4720 efficacy is maximized in glucose-limiting conditions.

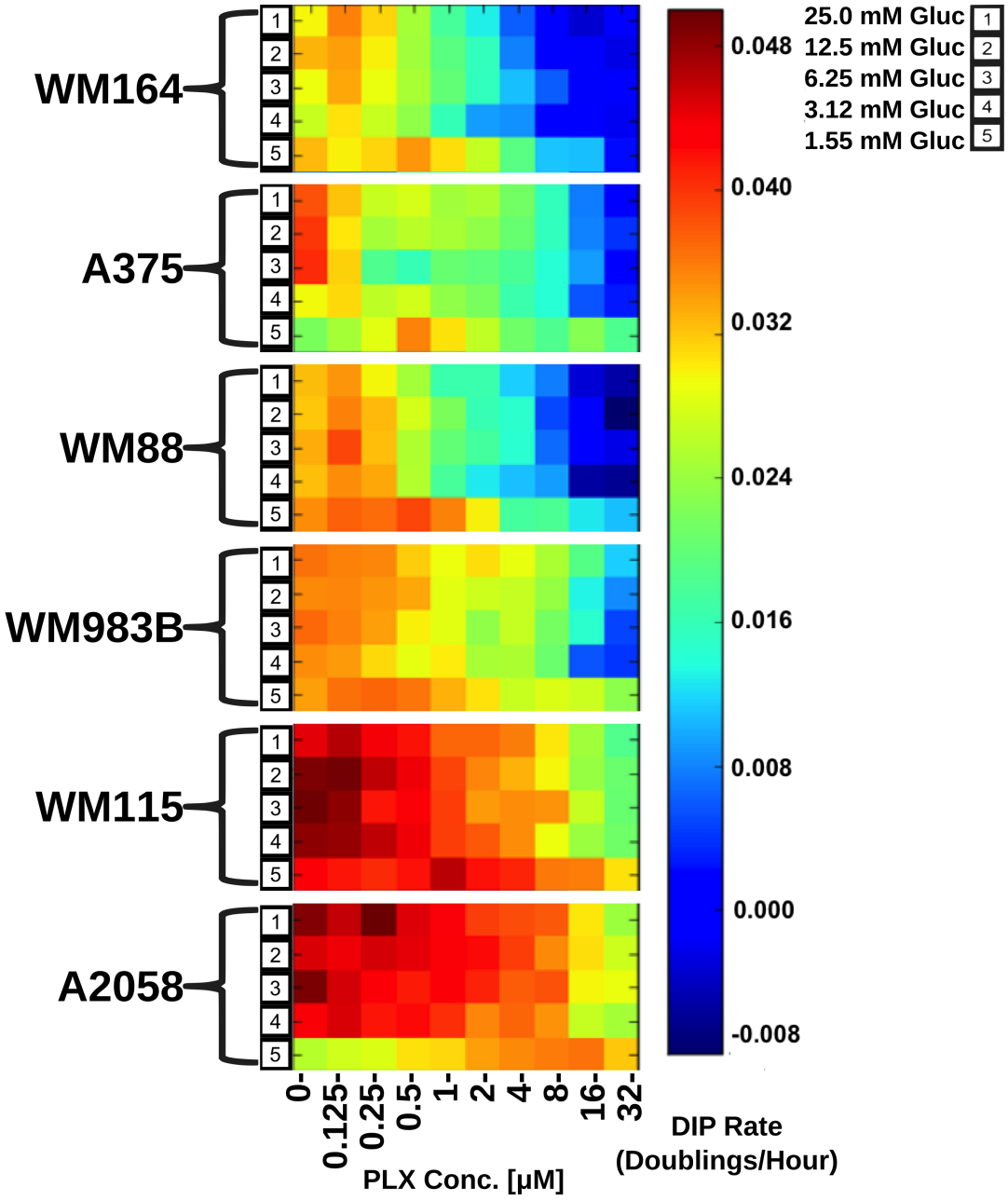

Figure 4.7: Glucose Affects PLX Response. Un-scaled heatmap of the proliferative responses of cell lines treated in PLX4720 dose-response assay coupled with varying glucose concentrations (indicated in legend, 5 glucose/media conditions total). The doses of PLX4720 are the x-axis (10 doses, from 32 μM to zero/DMSO) and concentrations of glucose are the y-axis (from 25 mM to 1.55 mM, labeled using legend key). Data shown are from a single experimental run; experiment has been repeated at least once with similar results.

To test the hypothesis that increased glycolytic dependence is functionally related to enhanced PLX4720 response, we generated rho0 variants of two of our melanoma lines, A2058 and WM164. These two lines were chosen because they represented the least and most sensitive lines, respectively, to PLX4720 in our assays. Generating rho0 variants (which lack mitochondrial DNA and, thus, lack a functional electron transport chain) allowed assurance of a quantitative shift to an exclusively glycolytic metabolic program. We confirmed depletion of mitochondrial DNA (data not shown) and showed absence of mitochondrial oxygen consumption and a significant increase in glycolytic rate combined with a significantly decreased glycolytic reserve (Figure 4.8) compared to the parent line for each variant.

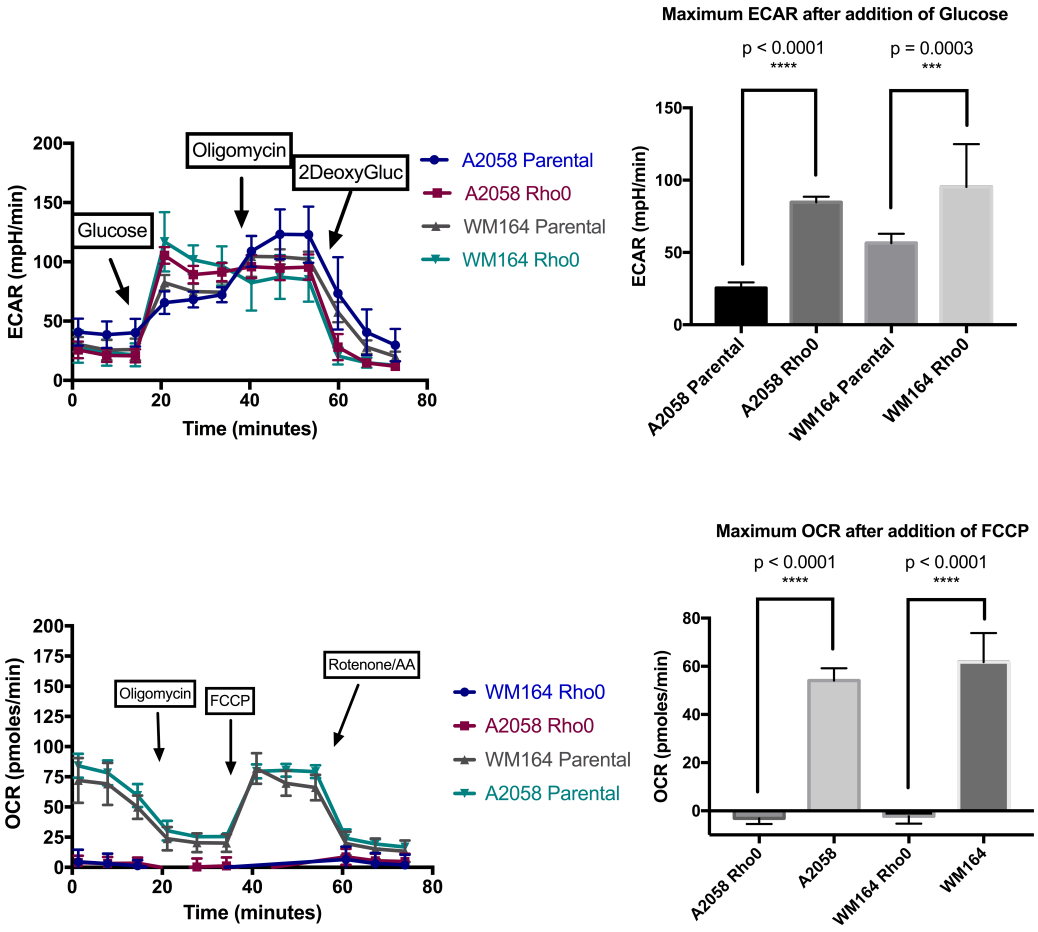

Figure 4.8: Metabolic Phenotype of Rho0 Variants. Extracellular pH or acidification rate of parental A2058 and WM164, and their Rho0 derived counterparts; bar plot showing maximum ECAR after adding glucose (10 mM), with t-test between parental and Rho0. Oxygen consumption rate of parental A2058 and WM164, and their Rho0 derived counterparts; bar plot showing maximum OCR after adding FCCP (1 μM), with t-test between parental and Rho0. Data shown are from a single experiment with 5-6 technical replicates; experiment has been repeated at least twice with similar results. Error bars are standard deviation.

Rho0 cells have been shown to be capable of apoptosis (Kukat, Kukat, et al., 2008; Gregoire, Morais, et al., 1984) and are largely reported as carrying "ghost" mitochondria that lack electron transport chain functionality. Using the rho0 cells as a model, we tested whether forced glycolysis impacts response to BRAF inhibition by treating the rho0 variants with increasing doses of PLX4720. We first noted that, as might be expected, the overall proliferative

rates of the rho0 cells were decreased compared to their parental counterparts (Figure 4.9). However, even taking this into account, the percent inhibition (based on the final population doublings) with PLX4720 treatment was significantly increased in the A2058 & WM164 Rho0 cells compared to their parental cell lines (Figure 4.9).

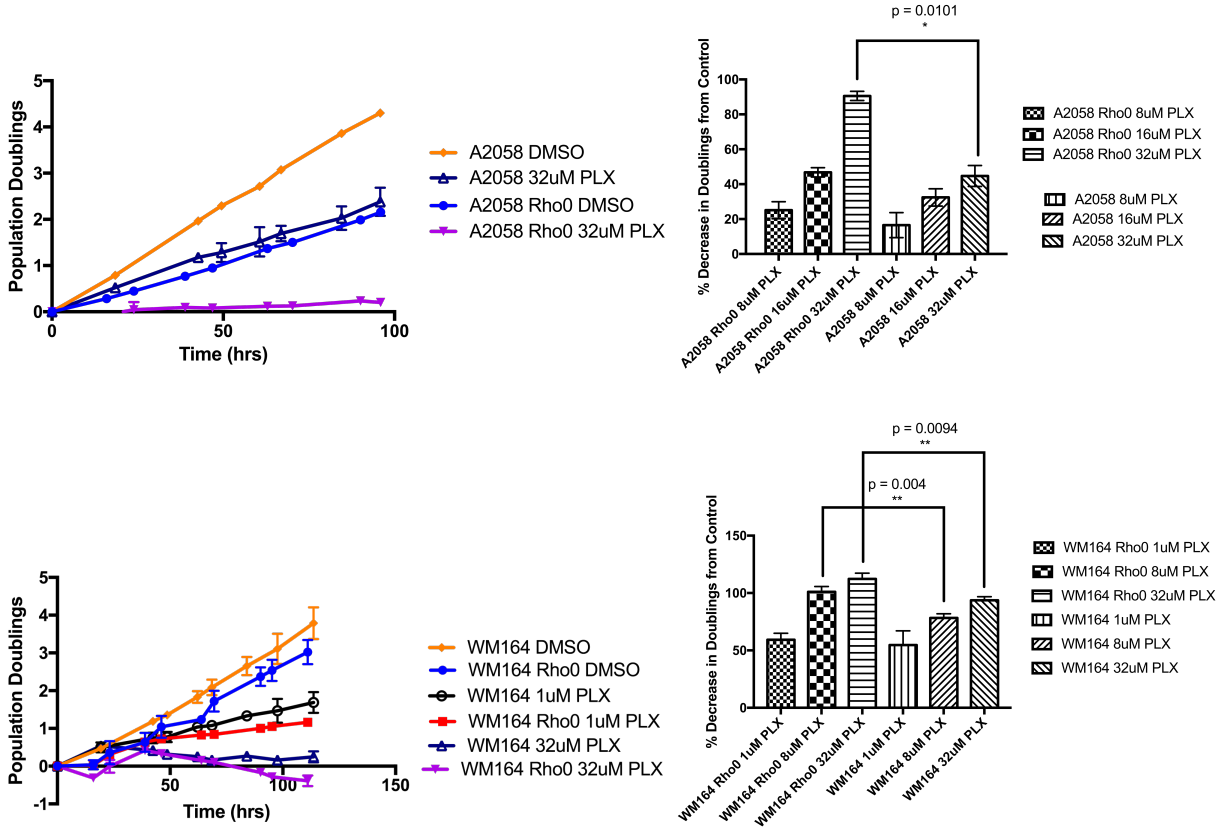

Figure 4.9: Rho0 Cells Have Increased Inhibition. Log2 normalized proliferation of parental A2058 treated with DMSO or 32 μM PLX4720, and Rho0 A2058 treated with DMSO or 32 μM PLX4720 (purple). Similar population doublings-time plot of WM164 (lower panel), with additional dose of 1 μM PLX4720. (D & E) Quantification of percent decrease in Doublings from respective DMSO control (ie., parental compared to parental, or Rho0 compared to Rho0). Data shown are from a single experiment with technical duplicates; experiment has been repeated at least twice with similar results. Error bars are standard deviation.

Anti-retrovirals Can Be Repurposed To Target BRAF-Mutated Melanomas

Finally, we sought to replicate these findings and to force glycolysis using an alternative method with greater translational potential than ethidium bromide treatment. To accomplish this, we utilized the FDA-approved antiretroviral drug zalcitabine, also called ddC, in our cell lines. Zalcitabine/ddC is a nucleoside analog utilized as a first generation antiretroviral in the treatment of HIV (Lee, Hanes, and Johnson, 2003), falling out of favor largely due to the mitochondrial toxicities it exerted on various tissues and organs and the development of less toxic and more effective antiretrovirals (Birkus, Hitchcock, and Cihlar, 2002; Dalakas, Semino-Mora, and Leon-Monzon, 2001). In humans, ddC has been shown to deplete mitochondrial DNA (Reiss, Casula, et al., 2004; Walker, Bauerle, et al., 2004), and in vitro assays have been utilized with up to 300 μM ddC (Birkus, Hitchcock, and Cihlar, 2002), with efficient mtDNA depletion typically observed at concentrations in the 10-50 μM range. In our melanoma cell lines, treatment with 40 μM ddC phenocopied the suppression of mitochondrial oxygen consumption, the increase in glycolysis, and the reduction in glycolytic reserve (Figure 4.10) seen in the rho0 cell lines.

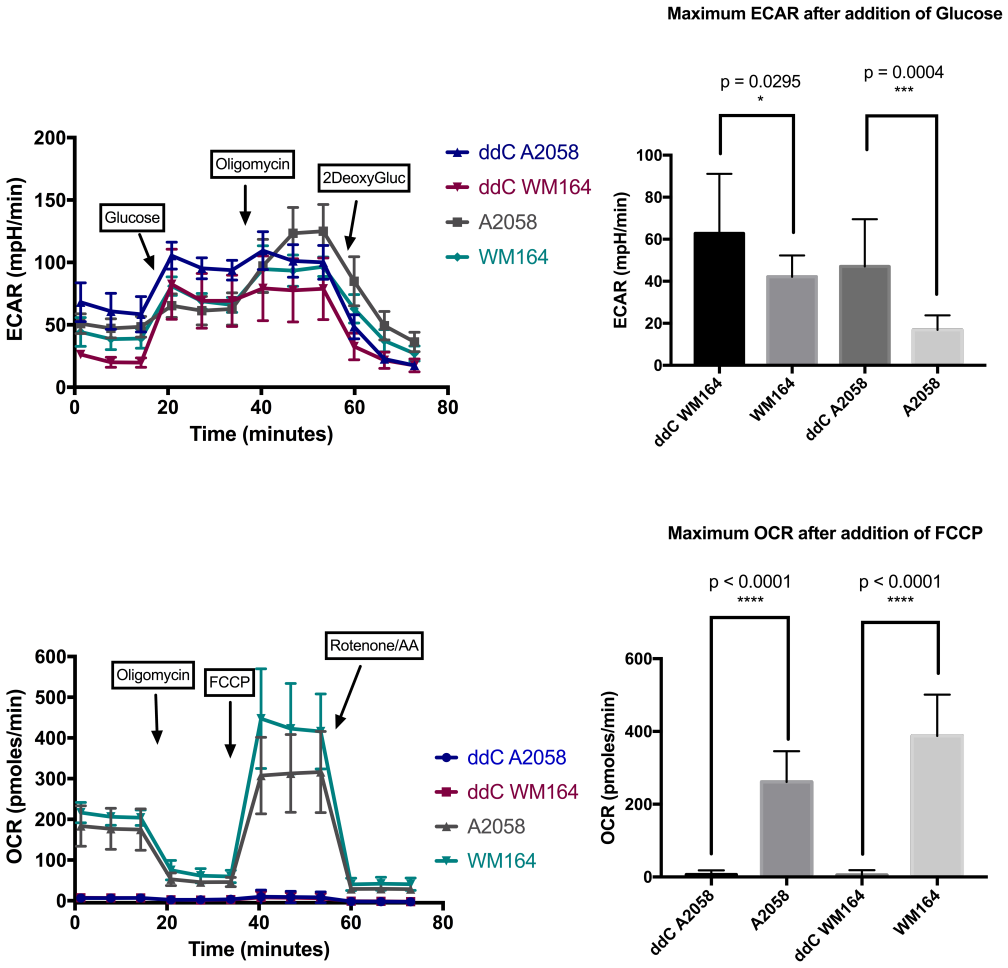

Figure 4.10: Anti-retrovirals Can Deplete mtDNA. (Upper) Extracellular pH or acidification rate of parental A2058 and WM164, and their ddC/zalcitabine treated counterparts (40 μM zalcitabine); bar plot showing maximum ECAR after adding glucose (10 mM), with t-test between parental and ddC treated cells. (Lower) Oxygen consumption rate of parental A2058 and WM164, and their ddC/zalcitabine treated counterparts (40 μM zalcitabine); bar plot showing maximum OCR after adding FCCP (1 μM), with t-test between parental and ddC treated cells.

Utilizing our previous model for in vitro assays (Harris, Frick, et al., 2016), we found the PLX4720 response in ddC-treated WM164 was significantly increased: the proliferative kinetics phenocopied the prior WM164 rho0 experiments and the percent decrease in doublings was statistically significant (Figure 4.11, upper). In contrast, the PLX4720-resistant line A2058 was more substantially affected by the attenuation of proliferation associated with ddC treatment itself: the percent decrease in doublings was not significant. However, the effect on proliferative kinetics of a single ddC treatment phenocopied the high-dose PLX4720 treatment (Figure 4.11).

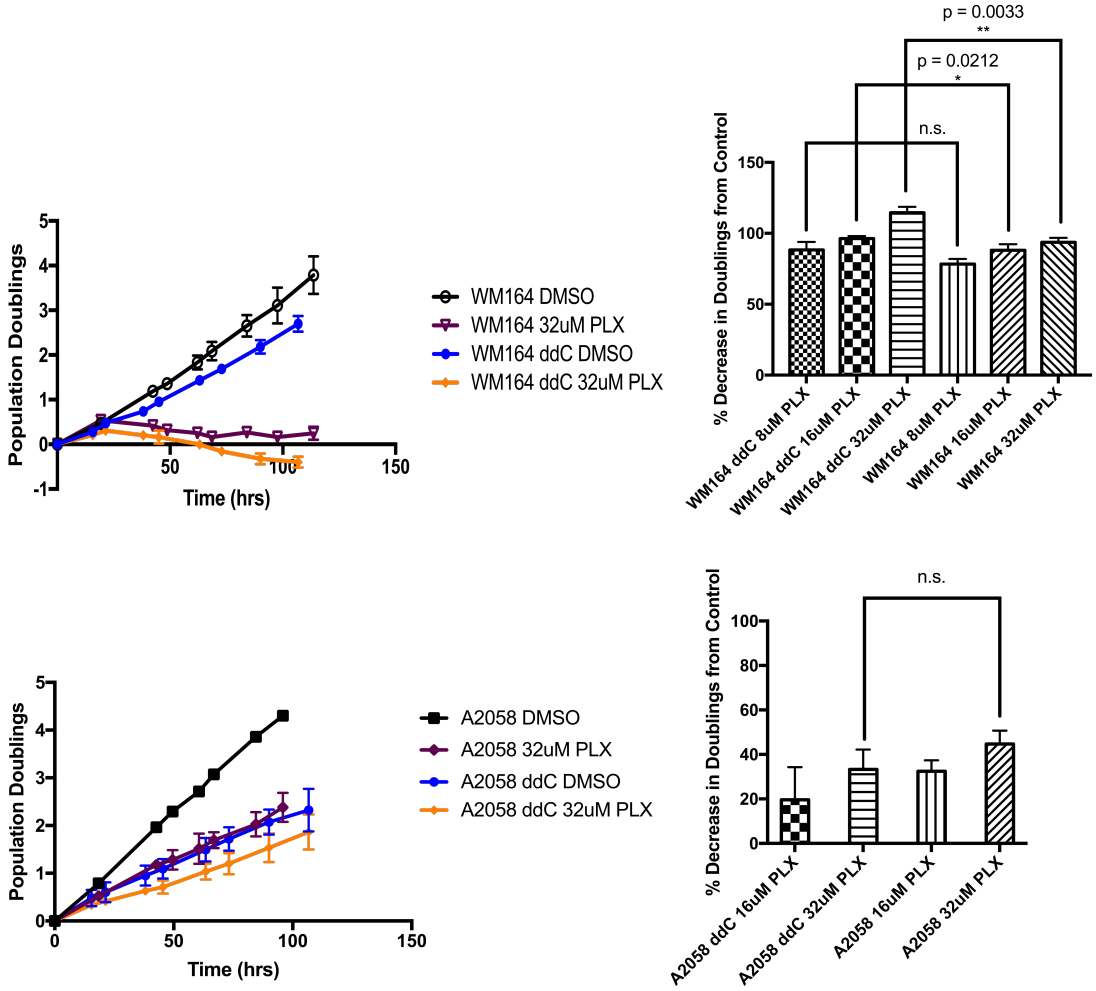

Figure 4.11: Figure legend on next page.

Figure 4.11: Anti-retroviral Effects On Proliferation. Left: Log2 normalized proliferation of ddC treated WM164 or ddC treated A2058. Right: Quantification of percent decrease in Doublings from respective DMSO controls for the cell lines (not statistically significant). Data shown are from a single experiment with technical duplicates; experiment has been repeated at least twice with similar results. Error bars are standard deviation.

Moreover, ddC treatment in A2058 reduced the EC50 for PLX4720 ten-fold and also substantially reduced Emax (Figure 4.12, upper), both effects consistent with significantly enhanced efficacy of PLX4720 in the context of ddC pretreatment. Additionally, the rate of proliferation affected the dose-response slopes, or Hill coefficients, revealing that ddC treatment decreased the Hill slope metric (Figure 4.12, lower).

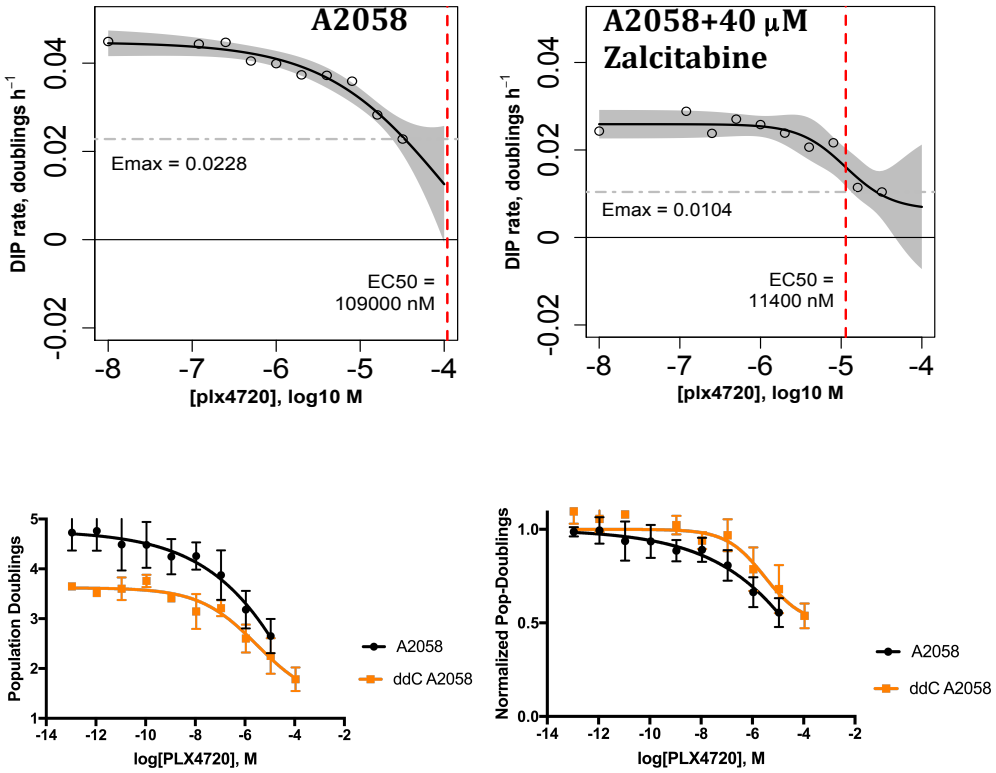

Figure 4.12: Anti-retrovirals Shift Dose Dynamics With BRAF Inhibition. Upper: Drug Induced Proliferative (DIP) metric dose response curves (non-normalized) marking model estimated EC50 values in nM (red dashed vertical line), and model estimated Emax values (grey dashed horizontal line). Lower: Non-normalized (bottom left) and normalized (bottom right) dose-response curves of A2058 parental and A2058 pre-treated with ddC/Zalcitabine.

Mitochondrial respiration provides more than just ATP through oxidative phosphorylation, as rho0 cells and electron deficient cells can still proliferate if provided uridine and pyruvate (King and Attardi, 1989; King and Attardi, 1996a; King and Attardi, 1996b). To test whether increased PLX4720 sensitivity in the ddC –treated A2058 might be due to a deficiency in the necessary biosynthetic intermediate aspartate, which is normally produced through mitochondrial respiration (Sullivan, Gui, et al., 2015; Birsoy, Wang, et al., 2015), we supplemented both pyruvate and exogenous aspartate to attempt to rescue the ddC-treated A2058 cells. Not only did this not rescue the proliferative response, proliferative rates were actually further decreased upon treatment with PLX4720 (Figure 4.13).

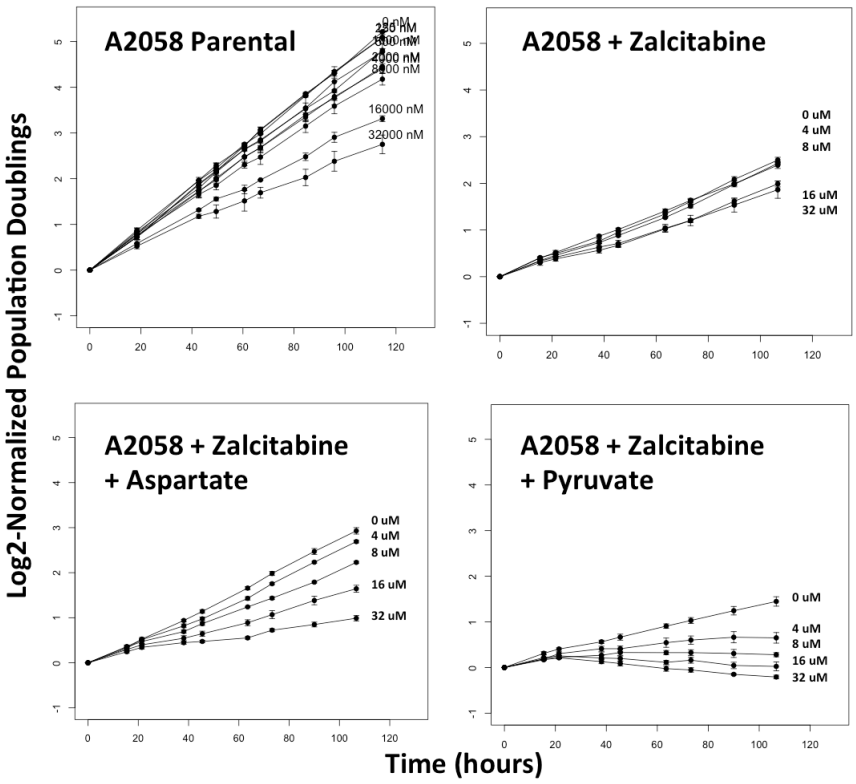

Figure 4.13: No Rescue From Aspartate Nor Pyruvate During BRAF Inhibition. Log2-normalized proliferation of parental A2058 (top left plot) and pre-treated ddC/zalcitabine A2058 (remaining 3 plots, pre-treated with 40 μM of zalcitabine for ~5 days). 10 mM Aspartate (bottom left) or 10 mM Sodium Pyruvate (bottom right) was added to the medium. Data shown are from a single experiment with technical duplicates.

Discussion:

All cells, including tumor cells, have basic energy and metabolic needs for survival and proliferation. Cellular responses—such as adaptation, differentiation, proliferation, and signal transduction—are inherently complex and dynamic in nature. Therefore, sustained proliferation in the presence of targeted inhibitors is likely shaped by a cell's dynamic metabolic constraints. In our study we investigated whether there exists a direct link between overall metabolic program and sensitivity to targeted BRAF inhibition, and if that relationship could be exploited to increase sensitivity in the cells. Our results demonstrate over-reliance on glycolysis can sensitize BRAF-mutated melanoma cells to targeted BRAF inhibitor treatment. The cells had significantly reduced proliferation (even death) when co-treated with PLX4720 and zalcitabine. This finding is in agreement with earlier reports (Haq, Shoag, et al., 2013; Hall, Meyle, et al., 2013) suggesting mitochondrial inhibitors like oligomycin would be therapeutically beneficial in this cancer type. However, the use of oligomycin in humans would be difficult due to its extreme toxicity, and other mitochondrial inhibitors, like metformin and phenformin, probably exert antitumor effects but have potential dosage issues (Chandel, Avizonis, et al., 2016) and lactic acidosis problems (Shitara, Nakamichi, et al., 2013), respectively. Antiretrovirals like zalcitabine, in contrast, have toxicities that may be easier to manage, and the portfolio of nucleoside analogs has been greatly expanded compared to the clinically available mitochondrial inhibitors (Lee, Hanes, and Johnson, 2003; Dalakas, Semino-Mora, and Leon-Monzon, 2001). Moreover, there is a tremendous amount of clinical experience with antiretrovirals used alone, in combinations, and in the context of many other drugs. The dose of ddC used in our studies is admittedly high in comparison to plasma concentrations typically achieved with conventional dosing to treat HIV infections, though our timeframe for treating cells to achieve mtDNA

depletion was also very short. In translating these findings to in vivo studies, lower doses of ddC for longer periods of time would be expected to produce the same effects while allowing toxicities to remain manageable. The DIP rate metric overcomes time-related biases of slow acting vs. fast acting drugs, fast vs. slow-proliferating cells, and complex contributions of cell death and division that plague typical end-point assays. Interestingly, though, the Hill slope (or Hill coefficient) emerges as an important metric for evaluating antiretrovirals in the context of cancer therapeutics, and it has already been postulated by others to be clinically important when assessing drug sensitivity in the context of non-genetic influences (Fallahi-Sichani, Honarnejad, et al., 2013). Moreover, as a consequence of "washing out" time-dependent biases, the DIP rate metric may miss potentially clinically meaningful findings. This can be seen with ddC treatment of A2058, where a major effect of high dose, short duration ddC treatment is to slow proliferative rate. This is problematic for DIP rate-based assessments, but clinically, a slower growing tumor would generally be regarded more favorably than a rapidly growing one. Moreover, DIP rate analysis alone would miss the 10-fold shift in the EC50 for PLX4720 in ddC-treated A2058. Should this effect translate fairly directly into in vivo studies, this would represent a shift of EC50 for BRAF inhibitor from outside the typically achievable range into a dose range that is readily achievable and that may allow for lower doses to limit toxicities.

However, there still remain questions about what physiological role glycolysis, oxidative phosphorylation, or the mitochondria play for BRAF-mutated melanomas, particularly under the context of drug treatment. It can be speculated that BRAF inhibition cuts off the oncogenic signaling that is ramping up the metabolism and ATP production. ATP hydrolysis and glucose flux have been postulated to be intimately linked in highly proliferative cells: the ATP/AMP ratio is repressed and kept to a minimum by linking high ATP consumption activities (like N-

glycosylation and folding of proteins (Fang, Shen, et al., 2010)) with increased glycolytic flux for biosynthetic production. Thus, the high amounts of ATP generated from glycolysis are shuttled in order to relieve negative feedback inhibition on major glycolysis enzymes such as PFK. Other mechanisms to control ATP/AMP levels involve the tumor suppressor LKB1 and its target the AMP-activated Kinase: loss of function mutations and deletions of LKB1 in non-small cell lung cancers (Whang, Park, et al., 2016) and Peutz-Jeghers Syndrome (Beggs, Latchford, et al., 2010), and activating mutations in PI3K and AKT that lead to strong signaling increasing glycolytic flux and ATP (and thus preventing the activation of AMPK through high levels of AMP) (Hardie, 2004; Shaw, Kosmatka, et al., 2004; Schaffer, Levin, et al., 2015). In BRAF-mutated melanomas it has been shown that the strong signaling down the MEK-ERK-RSK pathway enables negative regulation on LKB1 through phosphorylation of S325 and S428 sites (Zheng, Jeong, et al., 2009). Interestingly, WT BRAF immuno-precipitates with AMPK (Shen, Yuan, et al., 2013) and high phospho-ERK staining inversely correlated with low phospho-AMPK staining in vivo under the context of WT BRAF (Shen, Yuan, et al., 2013). To put these finding into context WT BRAF uses AMPK in the context of integrating energy metabolism with proliferation; mutant $BRAF^{V600E}$ will dampen the influence of AMPK, possibly because it is not needed for downstream metabolic signaling. BRAF inhibition may relieve the negative feedback regulation on LKB1 and thus, provide an avenue of metabolic rescue that would include mitochondrial biogenesis to make up for the resultant diminished ATP production. Therefore, in our work when we targeted mitochondrial DNA and rendered the cells functionally deficient, we metabolically constrained the cells to rely on glycolysis for all ATP (and redox regeneration).

Our approach of targeting differential tumor metabolism represents a break from previous models constrained within the more narrow scope of looking upstream and downstream along

the RAS-RAF-MEK-ERK signaling axis. Identifying avenues of resistance through "non-oncogenic vulnerabilities" has been suggested (Adler and Gough, 2011; Singh, Joshi, and Komurov, 2015), particularly since many cancers are multifaceted and resistant to single target therapies. The functional integration of drug resistance mechanisms leads to adaptive, independently actionable phenotypes. Targeting the metabolic phenotype rather than a single genetic driver appears promising: the phenotype sustains the tumor--not necessarily the pathway, due to signaling plasticity and mechanistic redundancies. Thus, the benefit of targeting a terminal phenotypic state and bypassing the risk of oncogene switching or secondary mutations can be realized with current FDA-approved drugs such as zalcitabine. The strength of this study is that we used a large panel of cell lines, treated with physiologically relevant doses of the BRAF inhibitor PLX4720.

Acknowledgements:

We thank Meenhard Herlyn (Wistar Institute, Philadelphia, Pennsylvania), Kimberly Dahlman, and Ann Richmond for kindly providing BRAF mutated melanoma cell lines. We are grateful to Jing Hao for support in data acquisition and James Pino for help with Python coding. The Seahorse Biosciences Extracellular Flux Analyzer used in this study is housed and managed within the Vanderbilt High-Throughput Screening Core (an institutionally supported facility) and was funded by NIH Shared Instrumentation Grant S10 OD018015.

CHAPTER V

DYSFUNCTIONAL MITOCHONDRIA LEADS TO A NON-QUIESCENT IDLING STATE IN DRUG TREATED BRAF MUTATED MELANOMA CELLS

Adapted From: Paudel BB, Harris LA, Hardeman KN, Abugable A, Lizama-Manibusan B, McLaughlin BA, Tyson DR, Fessel JP, and Quaranta V. "Dysfunctional Mitochondria Leads To A Non-quiescent Idling State In Drug Treated BRAF Mutated Melanoma Cells." (In Preparation To Be Submitted Spring of 2017)

Abstract:

Therapeutic resistance to targeted, small molecule inhibitors remains a clinical challenge for melanoma patients with the BRAF-V600 mutations. We sought to understand the proliferative dynamics of these cancer cells during the course of treatment, and utilized a battery of *in vitro* assays to illuminate cellular responses. We found that exposure of BRAF-mutated melanoma cells to BRAF inhibitors induces complex, non-linear proliferation dynamics followed by transition into a non-quiescent state of balanced death and division that we term "idling" state. Experiments with single cell-derived clonal lineages suggest that the response dynamics are a combined effect of clonal selection and drug-induced reversible phenotypic state transitions. Our results indicate that previously reported differences in cell line sensitivity to BRAF inhibitors are misleading, as they only occur on short time scales and dissipate ~100 hours after drug addition. Instead, all cell lines that we tested, including clonal isolates, transition into the idling state in the presence of continued BRAF inhibition. Interestingly, this idling state has features of

significantly decreased metabolism, and poor mitochondrial function despite prior up-regulation of PGC1α. Because of the continued division observed at the single-cell level, idling melanoma cells are potential reservoirs for genetic mutations and may represent an untapped phenotypic bottleneck susceptible to therapeutic targeting. My contribution to this developing manuscript is with data acquisition at the population level (Figures 5.1, 5.3, 5.4) and phenotypic characterization of the subclones in regards to metabolism (Figures 5.5 and 5.6). Presently, I am working with the first author to develop final key experiments to finish the manuscript and submit to a peer-reviewed journal.

Introduction:

Targeted small molecule inhibitors of BRAF (Flaherty, Yasothan and Kirkpatrick, 2011) show remarkable, short-term efficacy in melanoma patients with tumors harboring $BRAF^{V600}$ mutations (Flaherty, Puzanov, et al., 2010; Chapman, Hauschild, et al., 2011). However, clinical responses are variable, short-lived, and tumor recurrence is almost universal within a few months of initiation of therapy (Chapman, Hauschild, et al., 2011; Sosman, Kim, et al., 2012). Overcoming inherent and acquired resistance to targeted therapy is a major goal of current melanoma research, which uncovered two categories of resistance mechanism: (i) re-activation of mitogen-activated protein kinase (MAPK) signaling cascades (Poulikakos, Persaud, et al., 2011; Montagut, Sharma, et al., 2008; Wagle, Emery, et al., 2011; Shi, Moriceau, et al., 2012; and Villanueva, Vultur, et al., 2010), and (ii) activation of MAPK-pathway independent signaling pathways (Wagle, Emery, et al., 2011; Nazarin, Shi, et al., 2010; Shi, Hugo, et al., 2014; Rizos, Menzies, et al., 2014; and Whittaker, Theurillat, et al., 2013). This has led to the development of combination therapies of BRAF inhibition with other targeted agents (Larkin, Ascierto, et al., 2014; Menzies and Long, 2014; Greger, Eastman, et al., 2012; Long,

Stroyakovskiy, et al., 2014; Flaherty, Infante, et al., 2012; and Whittaker, Cowley, et al., 2015) or in conjunction with immunotherapy (Hu-Lieskovan, Robert, et al., 2014). While these therapies improve clinical responses, variation in treatment outcomes persists and benefits remain transient and unpredictable (Long, Stroyakovskiy, et al., 2014).

Most of our knowledge of melanoma tumor recurrence is derived from analysis of post-resistant tumors or cells (Rizos, Menzies, et al., 2014); the proliferation dynamics of drug-treated tumor cells prior to resistance is poorly understood (Smith, Brunton, et al., 2016). Resistance is usually attributed to rare, resistance-conferring genetic alterations that either preexist (Greaves and Maley, 2012; Shackleton, Quintana, et al., 2009; and Nowell, 1976) or develop during therapy (Shi, Hugo, et al., 2014; and Johnson, Menzies, et al., 2015). However, there is accumulating evidence that non-mutational processes play a significant role in the response of cancer cells to drug treatment (Smith, Brunton, et al., 2016; Raj and van Oudenaarden, 2008; Vandamme and Berx, 2014; Niepel, Spencer, and Sorger, 2009). It has been suggested that cancer cells employ a dynamic survival strategy involving phenotypic state transitions, governed by epigenetic alterations to evade lethal external cues (Sharma, Lee, et al., 2010; and Hugo, Shi, et al., 2015). These observations are consistent with preclinical and clinical evidence suggesting that cancer cells can become re-sensitized to therapy after a brief "drug holiday" (Sun, Wang, et al., 2014; Das Thakur, Salangsang, et al., 2013; and Cara and Tannock, 2001). It is likely, therefore, that both genetic and non-genetic processes are involved in the acquisition of drug resistance and/or relapse of melanoma tumors.

Here, we use experimentation to quantify drug-induced proliferation dynamics in numerous BRAF-mutated melanoma cell lines at the cell population, clonal, and single cell

levels. We show that treatment with a BRAF inhibitor induces entry into a previously unrecognized, non-quiescent state of balanced death and division (zero net growth), which we refer to as the "idling" state. Experiments with single cell-derived clonal lineages suggest that the drug-response dynamics are a combined effect of clonal selection and drug-induced phenotypic state transitions. We postulate that idling cancer cells may constitute a reservoir from which genetic mutations and, ultimately, tumor recurrence arises. They may also represent a previously unappreciated phenotypic bottleneck that can be targeted, and perhaps eliminated, with an appropriate secondary treatment.

Results:

To investigate drug-induced proliferation dynamics of BRAF-mutated melanoma cells to BRAF inhibition, we subjected populations of the BRAF-mutated human melanoma cell line SKMEL5 to varying concentrations of a small molecule BRAF kinase inhibitor (BRAFi) called PLX4720. Using fluorescent time-lapse imaging, we tracked cell numbers over time for a period of approximately two weeks. For intermediate drug concentrations, we observed complex, non-linear population dynamics (Figure 5.1). After an initial transient period (~24 hours), the cell population regressed significantly (for ~24 hours), rebounded (for ~100 hours), and then settled into a phase of near zero net growth. We confirmed that the zero-net-growth phase is not trivially due to confluency (data not shown). In addition, some cells (~10%) are positive for an exogenous marker of the S, G2, and M phases (Figure 5.1, part B), indicating continuing progression through the cell cycle, while other cells exhibit early nuclear morphological changes associated with apoptosis (Ziegler and Groscurth, 2004) (data not shown). Since cells continue to turnover (die and divide) but the cell population maintains a constant level, we refer to this phase as "idling". Furthermore, the idling phenotype is not specific to SKMEL5 cells; we also observe

it in A375, SKMEL19, SKMEL28, WM164, WM793 and WM88 cell lines (Figure 5.1, part C). Idling cells resume normal proliferation when switched to drug-free media and exhibit similar initial proliferation dynamics when re-challenged with the drug (Figure 5.1, part D), suggesting that the idling phase is both drug-induced and reversible. Taken together, these results indicate that entry into an idling phase in response to continued long-term BRAF inhibition is a general characteristic of BRAF-mutated melanoma cells.

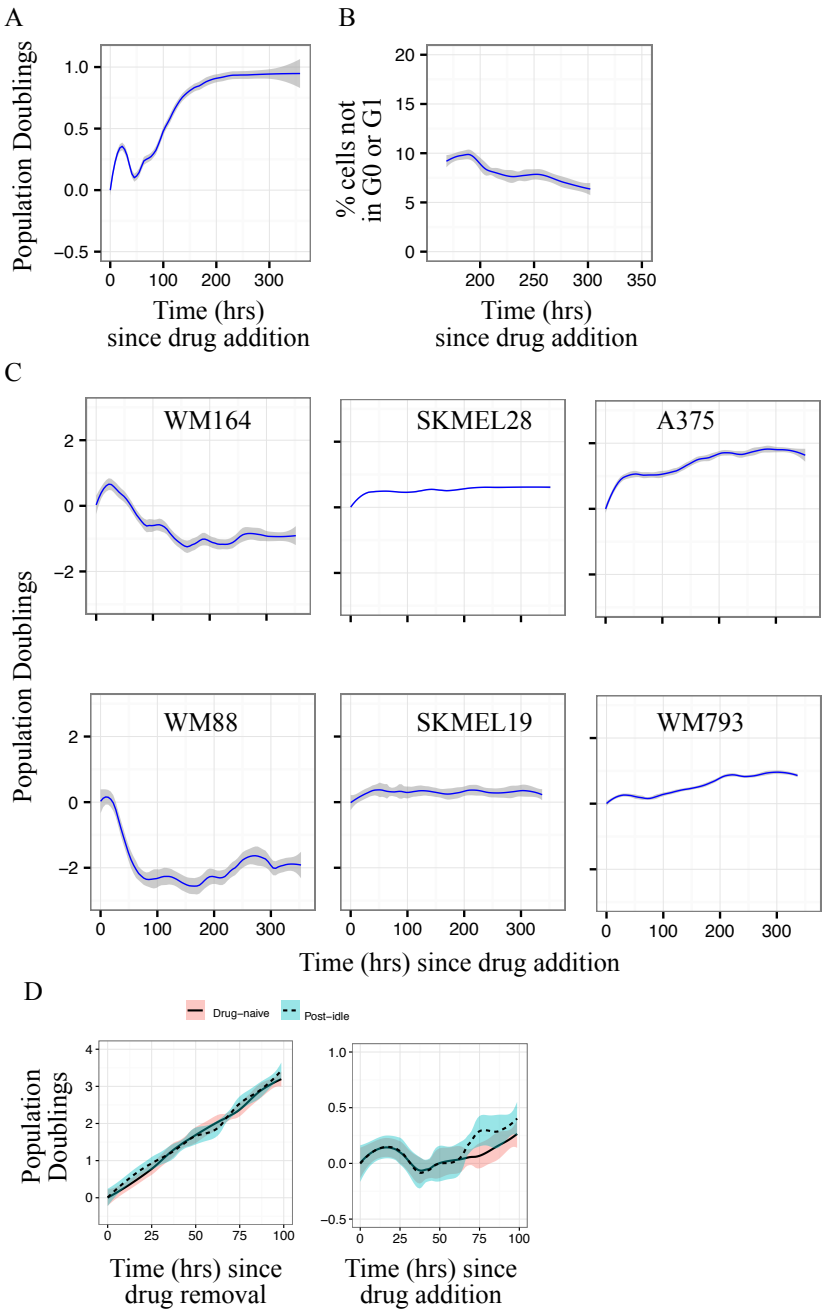

Figure 5.1: BRAF-Mutated Melanoma Cell Populations Idle Under Continued BRAF Inhibition. (a) Population growth curve (log2 normalized) for the SKMEL5 parental cell line treated with BRAFi. (b) Percentage of FUCCI-positive cells during 168-300h of BRAFi treatment for the SKMEL5 parental cell line. (c) Population growth curves for six additional BRAF-mutated melanoma cell lines in BRAFi. Mean responses are shown as solid lines, 95% confidence intervals as shaded regions. All results are based on 3+ technical replicates. (d) Idling cells respond similarly to BRAFi as drug-naive cells after a 24h drug holiday: (left) Population growth curves (log2 normalized) for drug-naive and post-idling SKMEL5 cells in complete-growth media; (right) Responses of drug-naive and post-idling cells to 8μM BRAFi.

We investigated more closely the short-term, non-linear population dynamics in the SKMEL5 cell line. We sought to determine whether all cells were adapting to BRAFi or whether the population-level response was a composite of clonal subpopulation responses, i.e., clonal selection (Nowell, 1976). To test these possibilities, we tracked ~200 single cell-derived colonies (~110 cells per colony) treated with BRAFi using the Clonal Fractional Proliferation (cFP) assay (Frick, Paudel, et al., 2015). Drug responses varied from clone to clone and encompassed a broad range of behaviors, from rapidly expanding to rapidly regressing (Figure 5.2, parts A and B). Further, the proliferation rate of a clonal lineage prior to treatment does not correlate to its proliferation rate in response to BRAFi (Figure 5.2, part C). The aggregate of the clonal responses qualitatively matches the short-term population-level response (Figure 5.2, part D), suggesting that the short-term dynamics are a result of clonal selection: the initial regression phase is due to depletion of the proportion of the population with negative proliferation rates and the subsequent rebound is due to expansion of positively proliferating clones. Similar results were obtained for other drug concentrations (data not shown). Moreover, to determine whether clonal heterogeneity is a general phenomenon, we tested two other BRAF-mutated melanoma cell lines in BRAFi and observed similar clonal variation in drug response (data not shown). Together, these results indicate that BRAF-mutated melanoma cell populations contain pre-existing hidden clonal heterogeneity that is revealed upon drug-exposure and shapes drug-response population dynamics in the short term.

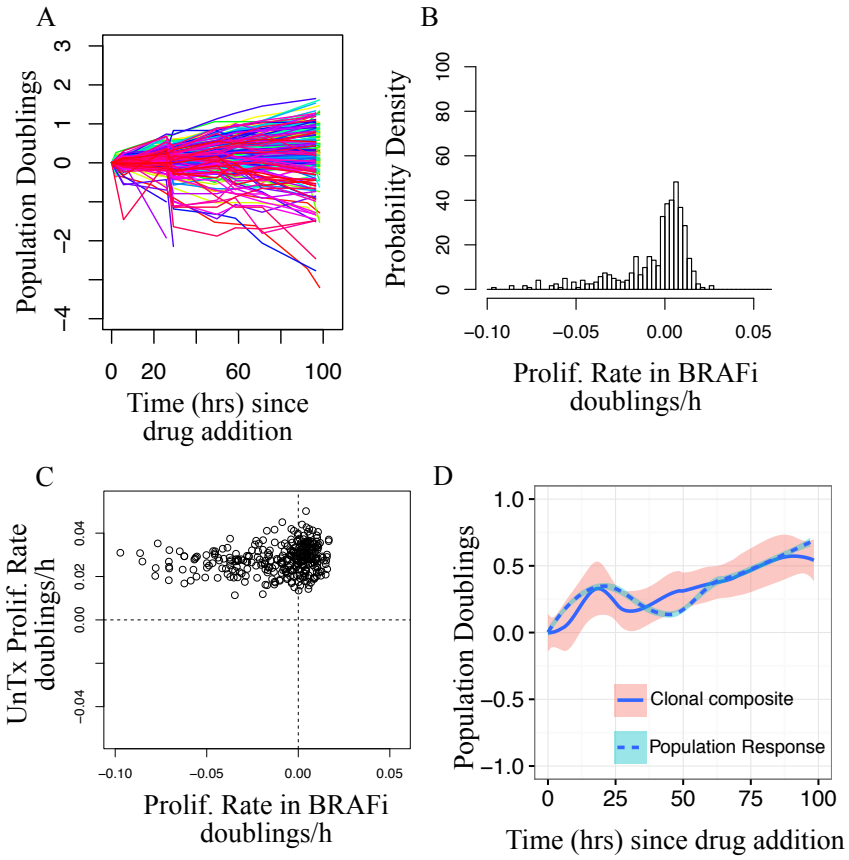

Figure 5.2: Short-Term Drug Response is Due to Clonal Heterogeneity. (a) Population growth curves (log2 normalized) for BRAFi-treated SKMEL5 single cell-derived colonies (n=203) obtained using the cFP assay. (b) Distribution of clonal proliferation rates of single cell-derived clones in BRAFi, quantified by linear fit to the response dynamics (d) Comparison of untreated and BRAFi-treated (8μM) proliferation rates (doublings/h) for SKMEL5 single cell-derived colonies (n=203) obtained using the cFP assay. (d) Comparison of the clonal composite (sum of cell counts from all colonies at each time point) to the SKMEL5 population-level response (means are shown as solid or dashed lines, 95% confidence intervals as shaded regions; the population-level response is the same data as in Figure 5.1, part A).

To reconcile the long-term population-level response (Figure 5.1) with the observed clonal heterogeneity (Figure 5.2), we sought to determine whether each clonal lineage enters an idling phase or whether only select clones do. To distinguish between these possibilities, we isolated over a dozen single cell-derived sublines from the SKMEL5 cell line. Upon exposure to BRAFi, the short-term dynamics (<100h) varied significantly across the clonal sublines, with

some expanding, some regressing, and some maintaining a stable population. We selected three sublines representative of the range of observed short-term responses for further experimentation: SC01 (expanding), SC07 (stable), SC10 (regressing). Upon prolonged exposure to BRAFi, despite their initial divergent responses, both SC01 and SC10 converged to approximately zero net growth, while SC07 maintained its initial zero-net-growth response (Figure 5.5, part A). In each case, we confirmed that entry into the idling phase is not due to confluence (Figure 5.3).

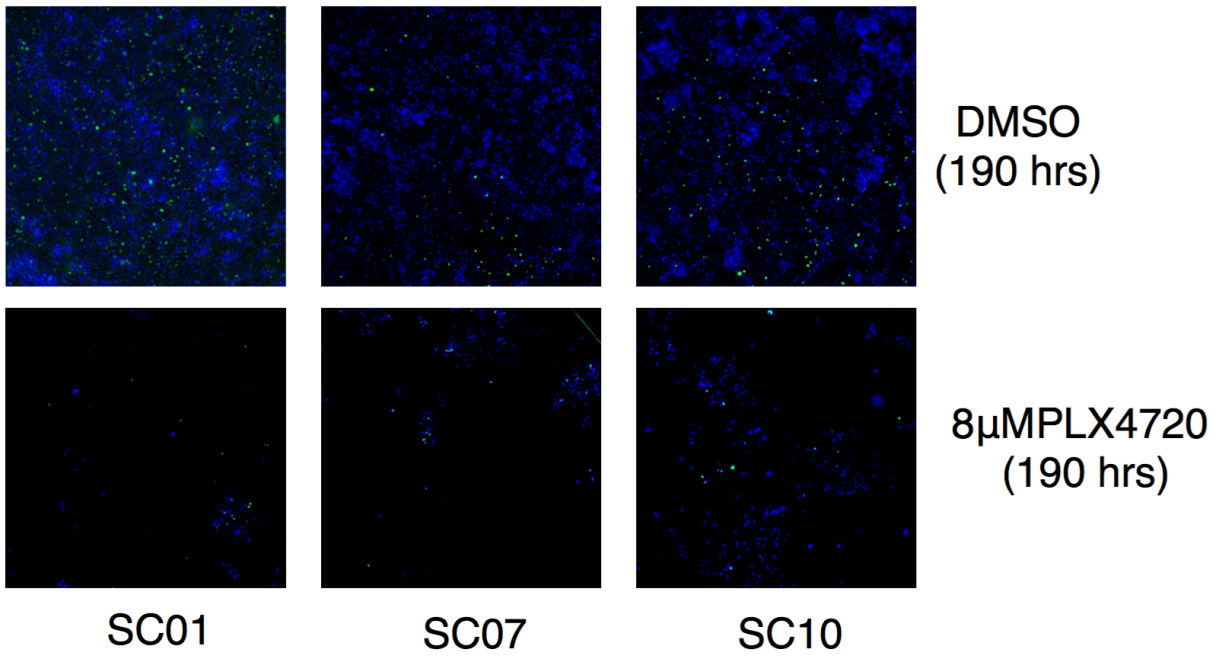

Figure 5.3. Plate Confluency Is Not Responsible For Idling Phase. Representative microscopy images at 190 hours with treatment of DMSO or 8 μM PLX4720. Cells are stained with Hoeschst stain (blue), and the image is overlayed with FUCCI-positive cells in green channel. The cell lines SC01, SC07, SC10 are single cell-derived sublines from the melanoma cell line SKMel5 (See text in this Chapter V for additional details, first paragraph page 79). Data shown are from a single experiment with technical replicates.

By manually tracking the fates of multiple individual cells over time, we also determined that all three clonal sublines experience both death and division events while in the idling phase (Figure 5.4, part B), confirming that idling is not due to quiescence but rather to balanced rates and death and division (concurrent death and division are also observed in the early response, data not shown). Together, these results suggest that idling is a phenotypic state that all clonal populations, regardless of initial sensitivity, can transition into in the continued presence of BRAF inhibition.

To determine whether the idling state could be targetable, we re-challenged (following a brief 24h drug holiday) idling cell populations of three clonal sublines (SC01, SC07, and SC10) with Trametinib (a MEK inhibitor), Cisplatin (a platinum-based chemotherapeutic), BEZ235 (a PI3K/mTOR dual inhibitor), and BKM120 (a PI3K inhibitor). Sensitivity to the PI3K inhibitors did not change in the idling cells as compared to their untreated counterparts. In contrast, idling cell populations of clonal sublines SC07 and SC10 acquired sensitivity to Trametinib and BKM120 (Figure 5.4, part C). Idling SC07 cells were also sensitive to Cisplatin. These preliminary results indicate that transition into the idling state indeed opens additional potential treatment avenues.

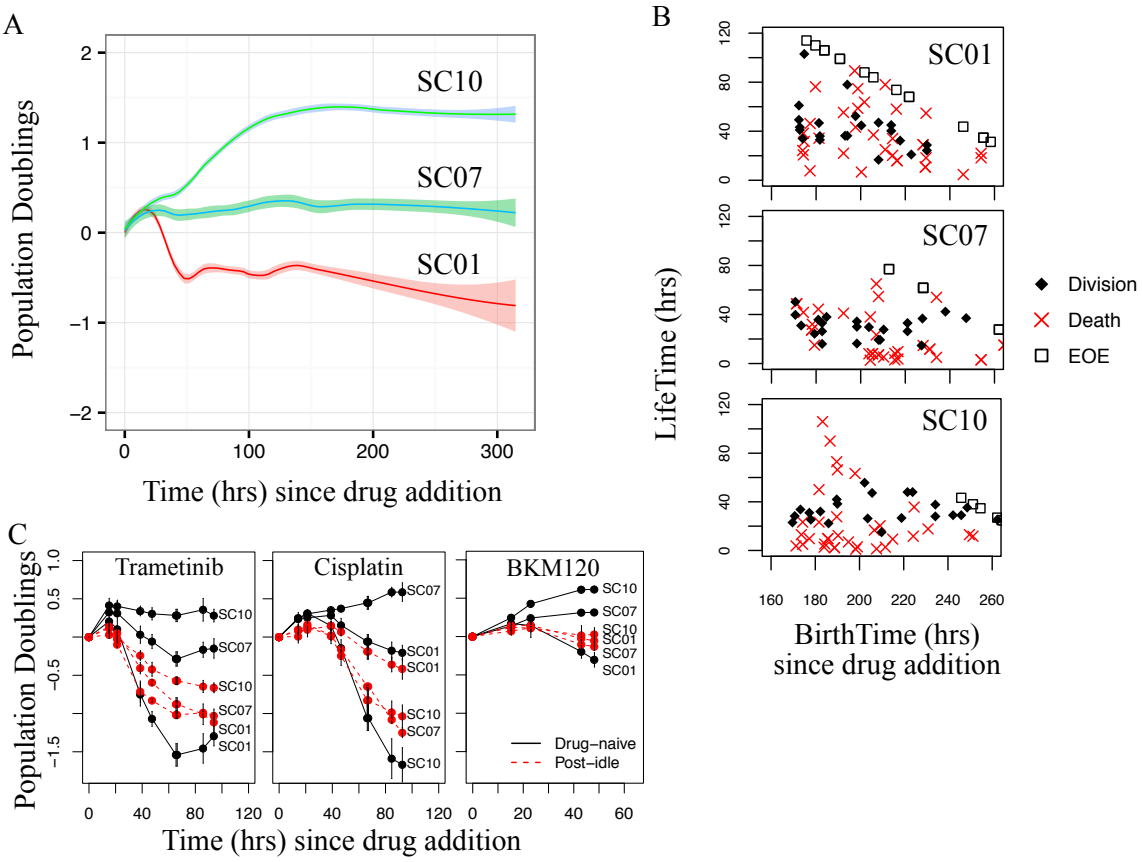

Figure 5.4: Single Cell-Derived Clonal Sublines Idle Independent of Short-Term Dynamics. (a) Population growth curves (log2 normalized) for three single cell-derived SKMEL5 sublines treated with BRAFi (means are shown as solid lines, 95% confidence intervals as shaded regions; all results are based on 3+ technical replicates). (b) Single cell lifespans vs. birth times (time of first mitotic event) for the three sublines after a week in BRAFi. Cells born during the experiment but reaching the end of the experiment (EOE) without a second mitotic event are plotted along the diagonal. (c) Population growth curves (log2 normalized) for three single cell-derived SKMEL5 sublines, either drug-naïve or following a week in BRAFi ("post-idle"), treated with trametinib, cisplatin and BKM120 (error bars are 1 standard deviation). For post-idle populations, BRAFi was removed less than 24h prior to subsequent drug addition. Data shown are from 3+ experiments.

BRAF inhibition might possibly relieve the negative regulation mutant-BRAF exerts on metabolic housekeeping strategies, via regulation of LKB1 (Zheng, Jeong, et al., 2009). Therefore, we decided to examine the global metabolism of the subclones, particularly the glycolysis and mitochondrial respiration using Glyco and Mito Stress Tests on the Seahorse Extracellular Flux Analyzer. Using sequential addition of metabolic inhibitors, we assessed the oxygen consumption and glycolysis (via lactate production) of the subclones in their basal (or untreated) and idling (7 days treatment with PLX4720) states. The untreated subclones have varying metabolic profile traces and it is interesting to note that the SC01 has little to know Glycolytic Reserve: after the three measurements of basal and glucose ECAR, the addition of oligomycin does not yield a subsequent increase in ECAR as it does in SC07 and SC10 (Figure 5.5., lower left side). Surprisingly, we found a significant metabolic depression in the idling cells (Figure 5.5, right side) across all three subclones. Others have reported increased oxygen consumption rates (OCR) upon BRAF inhibition (Haq, Shoag, et al., 2013; Corazao-Rozas, Guerreschi, et al., 2013), so the substantially decreased OCR at basal and FCCP-stimulated levels is unexpected.

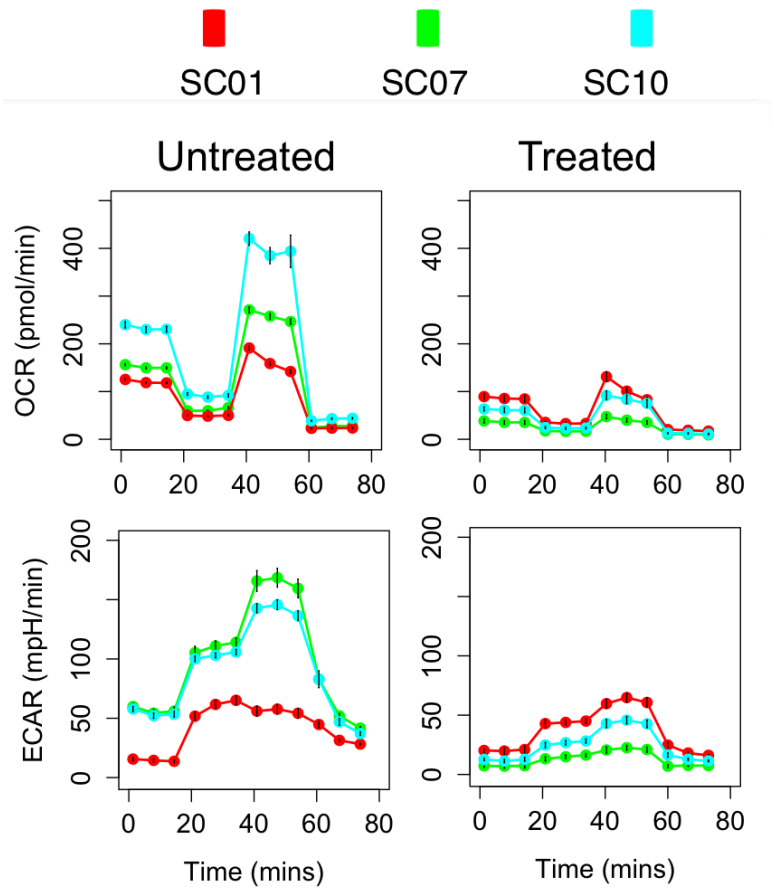

Figure 5.5: Prolonged BRAF Inhibition Causes Metabolic Depression. Upper: Oxygen consumption profiles for the cell lines with sequential additions of oligomycin (1 μM), FCCP (1 μM) and Rotenone/Antimycin A (0.5 μM). Lower: Extracellular pH profiles for the cell lines with sequential additions of glucose (10 mM), oligomycin (1 μM), and 2-deoxyglucose (0.5 μM).

Others have shown that mitochondrial biogenesis and a shift toward oxidative phosphorylation occurs in BRAF-mutated melanomas under PLX4720 treatment, so the prior result of decreased OCR led us to examine the mRNA expression of PGC1a. Looking at all three sublines (plus the parental cell line they were generated from), there is clear cessation of PGC1a expression over time, particularly after 120 hours of BRAF inhibition treatment (Figure 5.6).

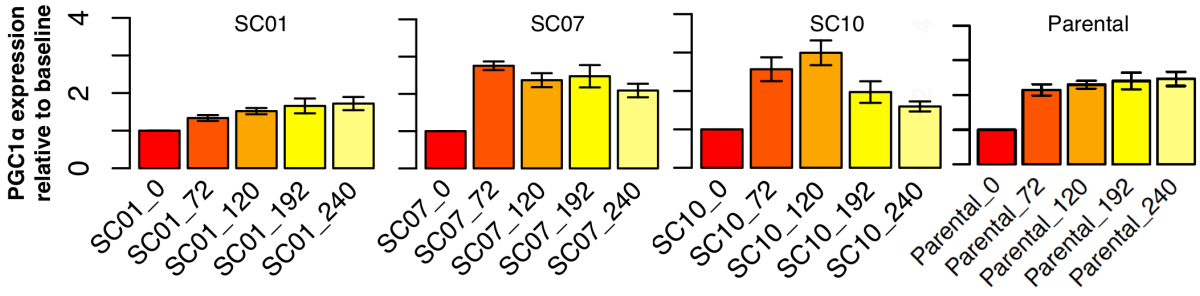

Figure 5.6: Increased PGC1a Levels Are Not Sustained. Using PCR, mRNA expression for each cell line is normalized to its own zero-hour time point. Relative expression is plotted with standard deviation (~2-3 replicates each time pt/cell line). SC01, SC07 and SC10 are single cell-derived sublines from the melanoma cell line SKMel5 (See text in this Chapter V for additional details, first paragraph page 79). Parental= SKMel5 cell line. On the x-axis the time lengths for drug exposure are indicated (0, 72, 120, 192, and 240 hours).

Finally, we decided to examine more closely the mitochondrial physiology of the subclones. MitoOrange and MitoGreen MitoTracker fluorescent probes were used to stain and visualize the mitochondria of the three sublines. MitoGreen will stain the mitochondria of all live cells without regards to the mitochondrial membrane potential; thus, we used MitoGreen to see if mitochondrial mass was increased in the idling cells. The total mass of mitochondria appear to decrease on SC07, increase in SC10, and stay relatively the same in SC01 (Figure 5.7, left panel). However, the average size of the mitochondria in SC10 appears to decrease significantly (Figure 5.7, middle panel) suggestive of mitochondrial fragmentation or fission. This led us to utilize MitoOrange CMTMR, which will only accumulate inside intact mitochondria that have retained their membrane potential. The overlap between MitoOrange and MitoGreen decreases significantly in the SC10 idling cells (Figure 5.7, right panel). These results indicate that the early increased expression of PGC1a does not lead to functional mitochondria in any of the sublines: SC07 actually decreases mitochondrial mass and SC10 exhibits signs of fragmented, damaged mitochondria.

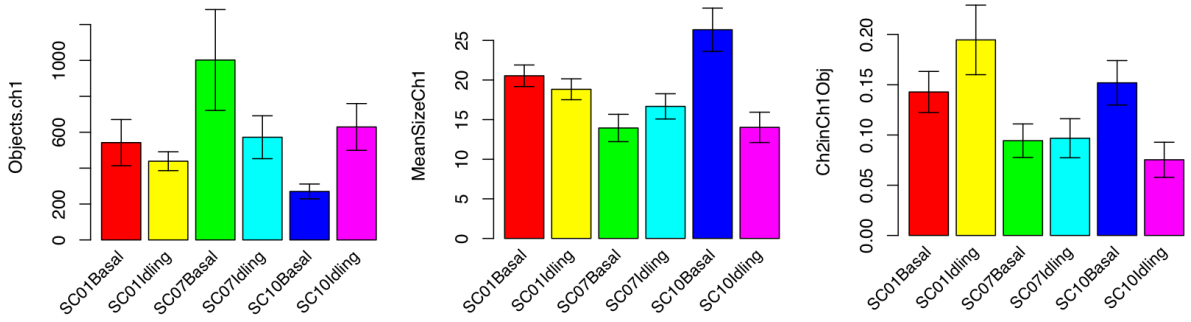

Figure 5.7: Mitochondrial Physiology Worsens Under Idling State. Plots of fluorescence intensity (left), size (middle, in arbitrary pixel units), and membrane potential per area (right). The cells were stained with MitoTracker MitoGreen (Ch1) and MitoTracker MitoOrange (Ch2). Basal indicates no drug treatment. Idling indicates cells exposed to 7 day PLX4720 treatment (8 μM). SC01, SC07 and SC10 are single cell-derived sublines from the melanoma cell line SKMel5 (See text in this Chapter V for additional details, first paragraph page 79).

Discussion:

We report here that sustained *BRAF* inhibition (>1 week) induces entry of BRAF-mutated melanoma cell populations into an idling state of balanced death and division, which results in ~zero net proliferation. Idling occurs at both the population and clonal levels, independent of variation in initial short-term response, and is drug-induced and reversible, consistent with non-mutational drug tolerance described in earlier reports (Smith, Brunton, et al., 2016). To our knowledge, the idling phenotype has not been previously described. We attribute this to the fact that drug response assays are usually performed over short observation times (72-96h) and proliferation rates are not usually measured (Tyson, Garbett, et al., 2012; Harris, Frick, et al., 2016; Frick, Paudel, et al., 2015), as we do in this work.

This indicates that previously reported differences in sensitivity among melanoma cell lines, measured on short time scale, might indeed be misleading. Our findings thus provide a unifying view of how *BRAF*-mutated melanomas respond to *BRAF* inhibition as well as a conceptual framework for how they might evade therapeutic interventions using both non-mutational and mutational means. It is possible that idling cancer cells constitute the bulk of the stable disease (tumors neither increasing nor decreasing in size) observed in patients following targeted therapy and preceding tumor recurrence (Casanovas, Hicklin, et al., 2005). This view is consistent with previous reports speculating that drug-induced tolerant cancer cells act as reservoirs from which genetic mutation, and ultimately tumor recurrence, arises (Sharma, Lee, et al., 2010; Ramirez, Rajaram, et al., 2016; Hata, Niederst, et al., 2016; Menon, Das, et al., 2015; Lito, Rosen, and Dolit, 2013). However, in contrast to those reports, we show here that idling cancer cells continue active division. We speculate that continued progression through the cell cycle during idling makes cells prone to accumulating deleterious mutations and, hence, a more

fertile ground for acquired resistance than quiescent (Sharma, Lee, et al., 2010; Haass, Sproesser, et al., 2008; Haass, Beaumont, et al., 2014) or senescent cells (Haferkamp, Borst, et al., 2013). Therapeutic approaches that suppress or eliminate this non-quiescent reservoir of idling cells could thus delay, perhaps indefinitely, tumor recurrence. Our model assumes that in the idling phase the majority of cells occupy a state of zero net proliferation. If this is true, then idling constitutes a phenotypic bottleneck that may be targetable with an appropriate secondary treatment. Initial experiments show that indeed new drug sensitivities are acquired by idling cells, although each clonal subline behaves differently in this respect. Future studies should focus, therefore, on identifying the molecular signatures of idling cancer cells and developing therapeutic approaches to eliminate them.

Many in the field have reached a consensus that some type of metabolic reprogramming in BRAF-mutated melanomas is occurring after therapy treatment: the details and the mechanism, however, remain unresolved. It was recently suggested that resistance to targeted BRAF inhibition requires two steps: first, a metabolic reprogramming during the early phases of treatment, then the acquisition of mutation(s) that will drive resistance, continued proliferation, etc. (Verduczo D, Flaherty KT, and Smalley, 2015). In this context, the mitochondria play a very important role of managing the bioenergetics demands within the cell. As a critical biosynthetic powerhouse, the mitochondria coordinates and integrates metabolite signaling from the cytosol to help build fatty acids, nucleotides and amino acids (Ahn and Metallo, 2015). Therefore, mutations or alterations related to the mitochondria can be the driving metabolic trigger for reprogramming before a mutation event. Our finding of mitochondrial fragmentation and dysfunction thus explain the idling phenotype and provide motivation for a two-hit model.

Under treatment, subclone 10 undergoes mitochondrial fragmentation that accompanies the physiological dysfunction (reduced oxygen consumption). Fission of mitochondria is generally thought to be pro-tumorigenic, as targeting mitochondrial fission can decrease proliferation, cell cycle progression, and cell viability (Rehman, Zhang, et al., 2012; Arismendi-Morillo, 2009; Chen, Dasgupta, et al., 2014; Inoue-Yamauchi and Oda, 2012; and Zhang, Jin, et al., 2013). Indeed, Kashatus and colleagues asked if "altering the balance of mitochondrial fusion and fission" could be targeted particularly in RAS mutated tumors, and demonstrated that MAPK signaling promotes mitochondrial fission via phosphorylation of Drp1 by ERK2 (Kashatus, Nascimento, et al., 2015). This brings the possibility of the SKMel5 clones, particularly subclone 10, undergoing a type of Mitochondrial Dysfunction-associated Senescence (MiDAS), termed by Wiley and co-authors (Wiley, Verlarde, et al., 2016).

Acknowledgements:

We are grateful to M. Herlyn, K.B. Dahlman, and A. Richmond for kindly providing *BRAF*-mutated melanoma cell lines; to J. Hao for support in experimental data acquisition; K.B. Dahlman, A. Richmond, J.A. Sosman, J.M. Irish, C.F. Lopez, and A.M. Weaver for critical reviews of the manuscript; and C. Meyer, E. Shockley, M. McKenna, and D. Wooten for useful discussions.

CHAPTER VI

SUMMARY, CONCLUDING REMARKS, AND FUTURE DIRECTIONS

Summary:

Melanoma is the most malignant form of skin cancer and around 50% of melanomas harbor a specific mutation in the MAPK family member BRAF kinase, predominantly V600E or V600D (Davies, Bignell, et al., 2002; Ribas and Flaherty, 2011; Ascierto, Kirkwood, et al., 2012). BRAF-targeted therapies like vemurafenib and dabrafenib have high response variability in patients, and the premise of this thesis work is to connect metabolic changes to response variability. Fortunately, there exist cell line models that could be used to test functional relationships of proliferative responses and intrinsic, cellular metabolism. Dysregulated metabolism has been shown to affect therapeutic responses, by influencing compensatory signaling, expanding proliferation, repressing apoptosis, and active/passive drug transport mechanisms. Interestingly, the main part of this thesis (Chapter IV) demonstrated that heavy reliance on glycolysis—with little to none Glycolytic Reserve—sensitizes cells for an increased response to targeted therapy. This result confirms early evidence of BRAF-mutated melanomas' addiction to glycolysis and adaptation towards oxidative phosphorylation. Furthermore, this is the first phenotypic exploration on how the FDA-approved antiretroviral zalcitabine affects proliferation of the melanoma cells' co-treated with vemurafenib. Figure 6.1 illustrates a schematic model of resistant, oxidative cells.

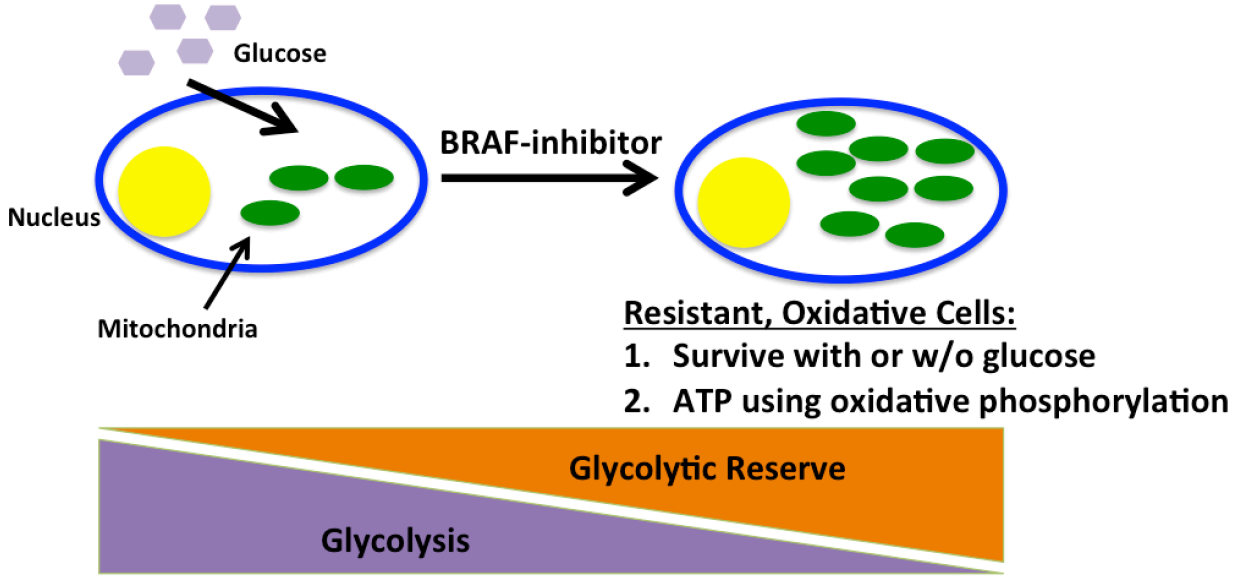

Figure 6.1: Model of Metabolic Phenotypic Resistance to BRAF Inhibition. Conceptual diagram visualizing how BRAF-mutated cells may become increasingly oxidative as a mechanism of resistance.

Given the results confirming a functional interaction between glucose metabolism and PLX4720 response (Figures 4.6 and 4.7), we set out to probe the details of this interaction with respect to particular metabolic strategies. Oxidative phosphorylation was inhibited at its terminal step using the ATP synthase inhibitor oligomycin (Appendices B and C), and lactate-producing glycolysis was inhibited at its terminal step using the lactate dehydrogenase inhibitor oxamic acid (Appendix D). Ordered and viewed according to the PLX4720 response spectrum (Figure 4.1), PLX-insensitive cell lines are more resistant to LDH inhibition; this makes sense, as the PCA data suggested that PLX-insensitive cells have more Glycolytic Reserve and metabolic flexibility. Oxamic acid exhibited a fairly wide dose-response relationship with regard to cell proliferation in our cell line models. By contrast, oligomycin had an almost binary effect, with melanoma lines being either extremely sensitive to every dose or tolerant of every dose with an identical DIP rate approximately ½ of their respective untreated control. This result, in

combination with the oxygen consumption results (Figure 4.3), suggests that variable ATP-linked respiration only translates to 2 proliferative outcomes: extreme sensitivity or adaptable tolerability. These data suggest that forcing a glycolytic metabolic strategy in the context of PLX4720 treatment may enhance the antitumor effect of mutated BRAF inhibition in relatively insensitive lines like A2058 and WM115.

As detailed in Chapter V, the dynamics and biology of drug-treated tumor cells prior to the observation of treatment failure or resistance is generally understudied. However, with powerful models such as single cell-derived subclones, we can attempt to dissect the variability and the dynamic biology occurring within the first stages of BRAF inhibition. Single cell-derived subclones are about as genetically similar as it can possibly exist; thus, their usage allows for a type of experimental control against the varied background constellation of mutations cancers typically bear. Nonetheless, we still can observe varied responses at the clonal level, adding credibility to the accumulating evidence that non-mutational, epigenetic processes influence the response of cancer cells to therapeutics (Smith, Brunton, et al., 2016; Raj and van Oudenaarden, 2008; Vandamme and Berx, 2014; Niepel, Spencer, and Sorger, 2009). With this report on the idling cancer cells in Chapter V, I can easily see the link towards what clinicians deem stable disease: a period before resistance or recurrence is reported where the tumor neither increases nor decreases. A type of metabolic reprogramming in BRAF-mutated melanomas is likely occurring after BRAF inhibitor treatment, and the idling state is simply a reservoir where the cells are not only dynamically adjusting their oxidative phosphorylation and mitochondrial operations, but likely acquiring mutations that will help drive their metabolic recovery.

It is important to consider the value-added or contribution this body of work gives to the field of melanoma cellular biology. Thinking back to Meenhard Herlyn's gene expression

analysis (Zhang, Frederick, et al., 2016), part of this work has given more resolution on the particular phenotype of glycolysis that makes some melanomas super-sensitive and responsive to BRAF inhibition. The key role of glycolytic reserve in determining the ability of a cell to overcome addicting oncogene inhibition (ie., BRAF inhibition) is an important discovery. Furthermore, the suggestion to use anti-retrovirals creates a clear translational path to repurpose those drugs in the treatment of these cancers. I am not alone in this thought process: the MITF/PAX inhibition screen that Smith et al. used led them to target melanomas with protease inhibitor anti-retrovirals (Smith, Brunton, et al., 2016). Additionally, coupling a dozen metabolic metrics to build a PCA is unusual in the field: most Seahorse Bioanalyzer users do not assay and measure both Glyco and Mito Stress Tests in their systems. High-throughput metabolic analyses and nutrient screenings should become the norm and Gohil et al. suggest a great design/platform for such experiments: using either glucose- or galactose-containing media, they screened over 3,000 compounds to find even modest, subtle shifts in metabolism (Gohil, Sheth, et al., 2010). A screening design such as this should be employed to find novel inhibitors that shift metabolism of BRAF-mutated melanomas. Of course, the assays should employ the more powerful DIP rate metric as detailed in Chapter III of this thesis. Gohil et al. used static metrics (number of cells remaining after 3 days) but the static dose–response curves can only separate and enrich for highly potent compounds (like the rotenone >> phenformin example in Chapter III). Efficacy is obscured or lost when examining static dose-response analyses. All in all, the work described in this thesis dissertation provides an important contribution to response variability and assay development, the glycolytic biology in relation to BRAF inhibition, and a finer inspection of variability within a tumor. These findings help resolve discordant reports in the literature and link a targetable metabolic phenotype to cellular proliferation.

Concluding Remarks:

BRAF-mutated cells may be addicted to glucose, due to reducing equivalents (NADH) produced for redox balance and the production of the central metabolite acetyl-CoA from the pyruvate generated through glycolysis. Acetyl-CoA is a 2 carbon acetyl group (CH3CO) linked by a thioester bond to the vitamin derivative coenzyme A; the molecule is impermeable to membranes (except passive diffusion through nuclear pores) and acts as a central metabolite by linking glycolysis to oxidative phosphorylation, influencing functionality and stability of proteins from translation through post-translation, and participating in cell cycle/mitosis via histone acetylation (Pietrocola, Galluzzi, et al., 2015). Histone acetylation is important to drive preferential gene expression of high target genes involved for cell proliferation, glycolysis, and to counter oxidative stress (Pietrocola, Galluzzi, et al., 2015). Acetyl-CoA is the sole donor or "obligate cofactor" for histone acetyltransferases, thus centering this metabolite in epigenetic processes. There is subcellular compartmentalization of Acetyl-CoA, and in the context of the mitochondrial matrix, the alkaline pH of the negatively charged matrix can allow for non-enzymatically driven acetylation due to physiochemical properties of generated acetyl-phosphate intermediates (Kuhn, Zemaitaitis, et al., 2014).

In regards to the reported glutamine dependency as a mechanism of resistance (Baenke, Chaneton, et al., 2015; Hernandez-Davies, Tran, et al., 2015), reductive carboxylation of glutamine happens frequently when glycolysis is blocked, hypoxic conditions arise or in the setting of mitochondrial defects. Glutamine dependence, therefore, is probably a bioenergetic strategy for BRAF-mutated melanomas to recover Acetyl-CoA. Upon transport into the cytosol from a carrier, glutamine is metabolized to glutamate, then the glutamate is transported into the mitochondria via the glutamate-aspartate carrier SLC25A13. Enzymes glutamate dehydrogenase

2 (GLUD2) or glutamic-oxaloacetic transaminase 2 (GOT2) metabolize glutamate into α-KG, which then goes into the TCA cycle backwards (reductive carboxylation) to make citrate. Citrate can leave the mitochondria by the transporter SLC25A1 and is metabolized to acetyl-CoA (and oxaloacetate) by the enzyme ATP citrate lyase (ACLY). Interestingly, AKT1 phosphorylates ACLY on Ser455 to increase its activity (Lee, Carrer, et al., 2014); thus, it can be argued that activation of AKT1 signaling can help drive a glutamine dependency under BRAF-treatment in the end-goal of generating and accumulating acetyl-CoA. A key question to address would be if we could rescue a metabolic catastrophe phenotype by using cell-permeable dimethyl α-ketoglutarate. In like manner, the cell membrane impermeant nicotinamide adenine dinucleotide (NAD+) has a central role in cellular metabolism and it can be postulated that the inhibition of BRAF signaling may also disturb the reductive-oxidative balance in BRAF-mutated melanomas.

Future Directions:

<u>The WNT pathway</u>

WNT5A can drive Beta catenin expression and metastasis in melanoma. Hoek, et al describes phenotype switching model where melanoma cells are "growing or going": proliferating/dividing versus metastasizing or invading (Hoek, Eichhoff, et al., 2008). BRAF mutated melanomas with high levels of Beta catenin are more sensitive to apoptosis from BRAFi (Biechele, Kulikauskas, et al., 2012). That same group later showed that WNT5A is increased in cell lines made resistant through chronic exposure to BRAF inhibitor PLX4720 (Anastas, Kulikauskas, et al., 2014).

Utilizing a high-throughput approach I found interesting preliminary data regarding the WNT inhibitor, pyrvinium pamoate (PP). PP is an antihelminthic or parasitic inhibitor that

inhibits WNT pathway signaling via the activation of Casein Kinase 1-α (Thorne, Hanson, et al., 2010; Li, Flaveny, et al., 2014). Figure 6.2 shows the DIP rates of BRAF-mutated melanomas treated with PP alone or with combination of PLX4720. Several phenotypes can be discerned from the data: PP appears to have additive effects with PLX in WM2664 and SKMel5 cells; combination has no effect in WM88 and WM164; and, an interesting PLX-rescue phenotype is observed in A375 and WM1799. These results are very preliminary and due to the design of the screen and drug solubility issues, dose optimization has not been completed.

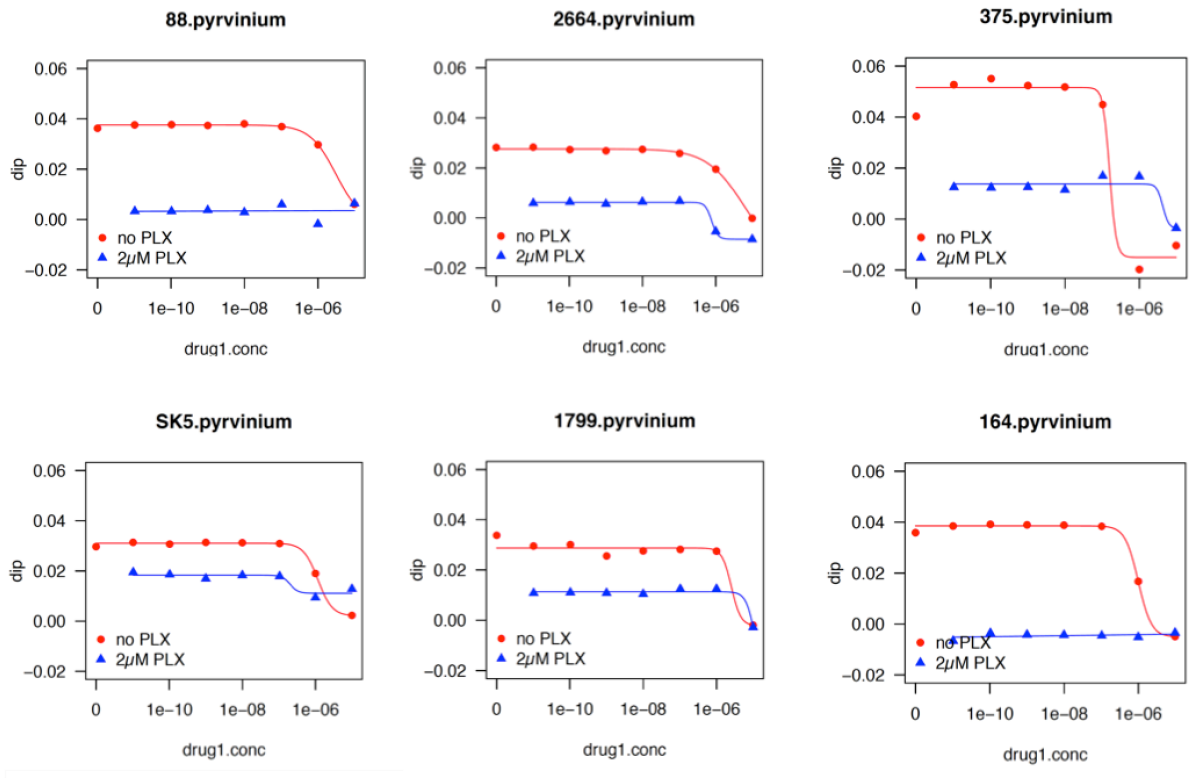

Figure 6.2. Figure legend on next page.

Figure 6.2: Phenotypes of WNT Inhibition Varies. High-throughput result of pyrvinium pamoate alone (red line) and with 2 μM PLX combination (blue line). Non-normalized DIP rate (slope of proliferation, per hour) are plotted as IC50 dose curve response with 10-fold dilutions of pyrvinium. Source drug plates are made first using the Echo 550/555 by Labcyte. Echo provides acoustic liquid transfer and distributes the drugs into target plates at 8X final concentration via acoustic wave in units of 2.5 nano-L droplets (these drug plates are kept in -80 & sealed until needed; 50uL media added later when used). The Bravo by Agilent (Velocity 11) is used for automated pipette liquid transfer and serial dilutions on the morning of the experiment. The plates are housed in a Cytomat incubator that can hold up to 42 individual plates; every plate is barcoded and read by a barcode reader before each data acquisition. Utilizing only the inner 308 wells of the 384 plate, the drug dilutions are done in either duplicate or triplicate; takes about 10 mins to image ea plate on an ImageXpress Micro XL automated microscope imager from Molecular Devices, and data is acquired every 8-9 hrs. Each experimental run produces about 2.5-3.5 TB of data. The cell lines shown here are WM88 ("88.pyrvinium"), WM2664 ("2664.pyrvinium"), A375 ("375.pyrvinium"), SKMel5 ("SK5.pyrvinium"), WM1799 ("1799.pyrvinium"), and WM164 ("164.pyrvinium").

Nonetheless, it is not discouraging to see the variable responses to PP. In fact, another set of high-throughput data suggests that a strong differential response to WNT inhibition is correlated to the varying inherent metabolism of these cells. Data from the Cancer Therapeutics Response Portal version 2.0 (CTRPv2) were downloaded and pharmacological data extracted. An intelligent string classifier is used to parse the accompanying annotation, and the drugs are divided and binned based on their mechanism of action. Out of nearly 550 drugs, groups such as "EGFR," "Proteasome," "PI3K," "DNA damage," etc. are created; this also includes a "WNT" group consisting of 2 drugs—JW-74 and CCT036477. JW-74 (Broad Institute ID BRD-K75664313) inhibits WNT signaling by stabilizing a component of the Beta catenin destruction complex (Stratford, Daffinrud, et al., 2014); CCT036477 (Broad Institute ID BRD-A22997170) targets a Beta catenin-mediated transcription complex (Mathur, Sehgal, et al., 2015). WNT inhibition significantly correlates to an unintuitive mix of the Seahorse metabolic parameters, thus highlighting a complex relationship of inherent cellular metabolism and WNT signaling.

.

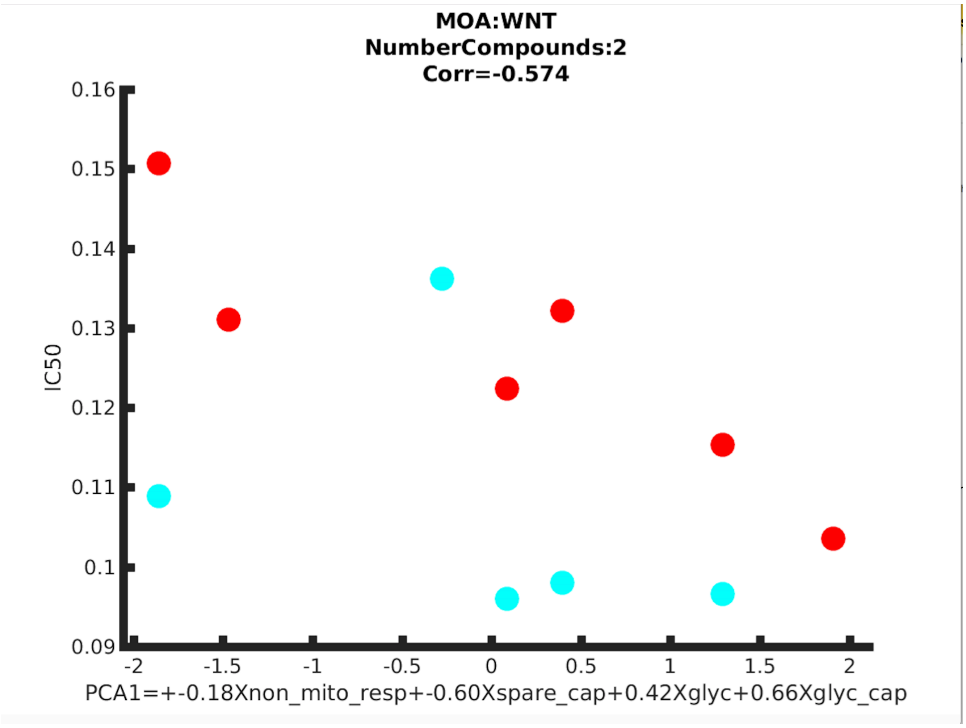

Figure 6.3: WNT Inhibition Correlates To Metabolic Parameters. PCA of IC50 data of 2 WNT compounds, JW-74 and CCT03677, on y-axis versus and the first principle component of a linear combination of Seahorse metabolic parameters. IC50 data is from the CTRPv2. JW-74 was tested at drug ranges of 0.002 μM to 66 μM; CCT036477 was tested at 0.001 μM to 33 μM. A normalization was done on the IC50 data in order to roughly compare all drugs together in groups.

Lactate Dehydrogenase and Glycolytic Intermediates

Membrane potential Δψ and (ΔpH) can significantly affect the distribution of reduced forms of products, substrates, reactants, and mediators of electron transfer. Craig Thompson's group just showed that an acidic pH promotes an unusual production of the stereoisomer L-2-hydroxyglutyrate (L-2HG) via ' "promiscuous" reduction of the alternative substrate α-KG' by lactate dehydrogenase (LDH) (Intlekofer, Wang, et al., 2017). LDH does not normally reduce α-KG, but usually has pyruvate as a canonical substrate, producing lactate. The acidic pH results in a protonated form of α-KG that can stably bind LDH, and the resulting L-2HG stabilizes HIF1α and is a purported cellular adaptation to acidic environments or acidosis under normoxia for

highly proliferative cells (Intlekofer, Wang, et al., 2017). In our melanoma cell line models, A2058—the most insensitive BRAF-mutated cell line—loses its concentration-dependent response to PLX4720 when treated with the LDH inhibitor Oxamic acid (Figure 6.4). It is intriguing to postulate that the inability of cells to make lactate may create a substrate and cytosolic pH bottleneck.

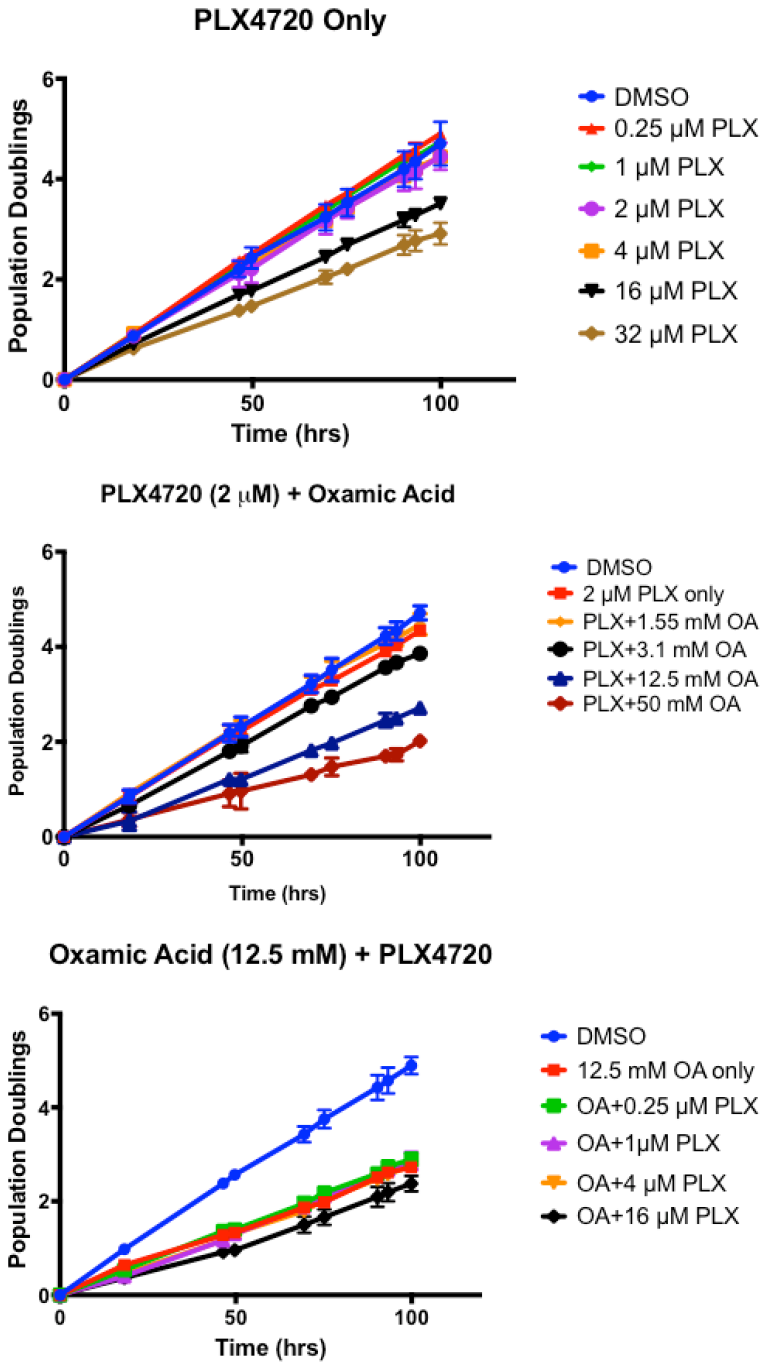

Figure 6.4: Oxamic Acid Constrains Proliferation Under BRAF Inhibition. Population doublings of cell line A2058 treated with BRAF inhibitor PLX4720 (left), varied Oxamic acid with constant 2 μM PLX (middle) and varied PLX with constant 12.5 mM Oxamic acid. Data shown are from a single experiment with technical duplicates; experiment has been repeated at least twice with similar results for single drug doses only (not combination conditions). Error bars are standard deviation.

It would be interesting to probe the dependency and flexibility of the cells lines on the three major oxidation substrates of the mitochondria: fatty acids, pyruvate, and glutamine. Dependency is defined as the absolute need of a carbon source for oxidation and usage; flexibility, on the other hand, is a measure of adaptability when inhibited from using a particular fuel source. The concept of creating Fuel Dependency and Fuel Flexibility analyses is relatively new (propelled by the works of Anne Murphy, Christian Metallo, Nika Danial, and others).

Mitochondrial Inhibition

Mitochondrial DNA (mtDNA) have a high mutation rate, mostly due to poor 3 to 5 prime exonuclease activity of the polymerase gamma, the lack of protective histones, assault of ROS due to the close proximity to the ETC, and a unique exposure to an enrichment of xenobiotics—the negative charge on the inner matrix-side of the membrane is needed to maintain membrane potential and ATP production, but it also encourages the accumulation of lipophilic cations like toxins and dyes. Lastly, it has been shown that p53 helps with the stability of the polymerase gamma, yet many cancers have mutant p53 (and about 10% of melanomas have a mutated p53). Given the crucial role oxidative phosphorylation and mitochondrial respiration plays in phenotypic resistance, I can imagine or postulate that combination BRAF inhibitors and anti-retrovirals would bring about positive or favorable composite endpoints: decreased clinical worsening, categorical increase in functioning or quality of life, etc. However, the combination of mitochondrial and BRAF inhibitors is not trivial, as Livingston and colleagues point out: dabrafenib- or vemurafenib-treated patients with concomitant use of the mitochondrial inhibitor and anti-diabetic treatment metformin had no improved survival or response benefits in the BREAK-3 clinical trial data (Livingston, Swann, et al., 2015).

Evaluating the Role of ROS in the Context of PLX4720 Treatment

Early in this thesis project I sought to dissect the relative contributions or importance of varied biology subsequent of mitochondrial inhibition. Specifically, targeting the mitochondria produces 3 broad conditions that can significantly affect downstream phenotypes such as proliferation: 1) decrease in in ATP production from oxidative phosphorylation; 2) decrease in biosynthesis through mitochondrial pathways (metabolites for lipid generation and protein post-translational modifications); and 3) increase in ROS generation. I sought to test in several ways the importance of ROS in our model system by attempting to answer 2 broad questions: 1) Is the response machinery used to handle or dispose of ROS defective in these cells? 2) Does PLX4720 treatment significantly increase ROS in a manner that is detrimental to these cells (and thus amplified by combination with other metabolic inhibitors)? The data in the following two figures helped shape my thinking and steer my thesis work away from ROS studies, by essentially eliminating ROS as a sensitizer and/or modulator of BRAF inhibition.

To answer the first question about the ROS machinery in BRAF-mutated melanoma cells, I designed an experiment to see if targeting proteins involved in disposal of ROS would give strong decreases in proliferation. Raj et al. reported a small molecule inhibitor called Piperlongumine that is selectively toxic to cancer cells (*in vitro*); even a breast cancer mouse model showed differential toxicity to cancer cells, as the other tissues in the mice showed no clinical signs of adverse effects (Raj, Ide, et al., 2011). The authors used a combination method of stable isotope labeling with amino acids (SILAC) and small molecule affinity beads (Ong, Schenone, et al., 2009) to show that piperlongumine binds to proteins involved in responding to oxidative stress like Glutathione S-transferase pi 1 (GSTP1) (Raj, Ide, et al., 2011). This drug

interacts with proteins like GSTP1 and CBR1 to yield the cellular phenotype of depleted total glutathione, protein glutathionylation and increased ROS (Adams, Dai, et al., 2012). Piperlongumine's bioactivity is related to its chemical structure: it has multiple electrophilic sites and two crucial olefin moieties (C2-C3 & C7-C8) that are essential for its cellular toxicity and ROS elevation (these moieties have Michael acceptor functionalities where a nucleophilic species is added) (Adams, Dai, et al., 2012). Adams et al. proposed a model where glutathione is added to the C2-C3 site 1st because the C2-C3 is more electrophilic/potent than C7-C8. Secondly, the piperlongumine-glutathione adduct will bind to a glutathione binding protein on its glutathione side and the entire complex is stabilized by the 2nd Michael addition of a nucleophilic part of the protein reacting with the C7-C8 electrophilic site (Adams, Dai, et al., 2012). Based on work from Raj et al., we know that the increased ROS in cancer cells treated with piperlongumine is probably nitric oxide and hydrogen peroxide but not superoxide anion (Raj, Ide, et al., 2011). Therefore, I treated two BRAF-mutated cell lines to varying concentrations of Piperlongumine—a typical dose-curve experiment—to see if differential proliferative responses would occur. SKMel5 and SKMel28 were the cell lines I used: at the time they had common media (DMEM/F12) as this was prior to the acquisition of WM lines from M. Herlyn and the transition to DMEM media for all cells lines. Additionally, these cells had vastly different response dynamics evident from their population growth curves, and preliminary single-cell tracking revealed SKMel5 to display dramatic cell death (deemed a "Death Burst" at the time) during treatment with PLX4720. Piperlongumine, however, had no differential effects between SKMel5 and SKMel28 (Figure 6.5, lower right panel). Trying to design a more specific experiment, I created a rescue experiment by first treating the cells with the Complex 1 inhibitor, Rotenone to find an IC50 value that would reduce proliferation but not kill too many cells (data

not shown). Then, I treated the cell lines with a combination of Rotenone (218 nM) and varying does of the general antioxidant N-acetylcysteine or NAC. I surmised that NAC should rescue or increase the proliferation rate and this would be evident in the growth plots (Figure 6.5, lower left panel). However, there was no rescue in the SKMel5 nor SKMel28 (data not shown). The caveat of the NAC+Rotenone experiment is that Complex I respiration may not be important in these cells; thus there would be little ROS produced to demonstrate measurable rescue benefits with the addition of NAC. Indeed, oxygraph measurements of oxygen consumption revealed that Patient Derived Xenograft (PDX) models of BRAF-mutated tumor samples consumed very little oxygen until the Complex II substrate (succinate) is added (PDX #1218, kindly provided by Ann Richmond; data not shown). Due to the complexity of ROS effects, I consulted with other experts and acquired samples of two reagents: mitoTEMPO and mitoEbselen.

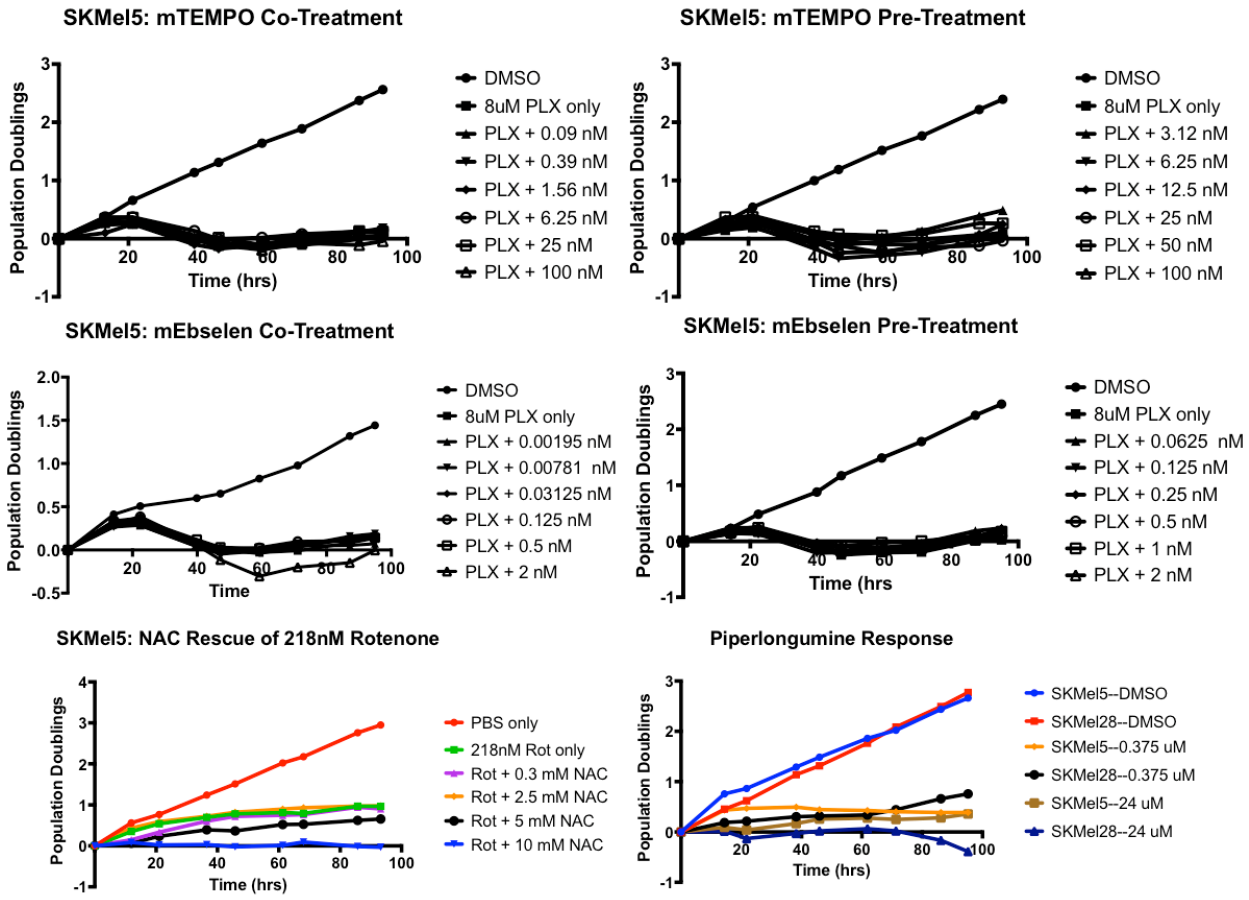

Figure 6.5: ROS Does Not Modulate Proliferation In The Context of BRAF Inhibition. Population doublings of either SKMel5 or SKMel28 treated with indicated compound. For Pre-Treatment experiments (top-right and middle-right panels) the mEbselen or mTEMPO was added to the wells first (in the dose-dependent fashion) and allowed to incubate for 15 mins; the controls (PLX only or DMSO had nothing added to them). Afterwards, the media was aspirated, washed 1x with PBS gently, and then replaced with fresh media plus 8 μM PLX4720 (or DMSO). For the NAC+Rotenone and Piperlongumine experiments, additional drug doses were examined but not included in these graphs for sake of clarity. Data shown are from a single experiment with technical duplicates.

mitoTEMPO and mitoEbselen are mitochondria-targeted antioxidants designed with classic triphenylphosphonium moiety that allows for concentration within the mitochondria (Daiber, Di Lisa, et al., 2015). Functionally, mitoTEMPO targets superoxide, and mitoEbselen targets hydrogen peroxide. I executed another rescue experiment but this time using a co- and pre-treatment design. Furthermore, I used PLX4720 as the putative ROS-producing perturbation:

since my initial questions revolved around the importance of ROS under the context of variable responses to BRAF inhibition, then the most convincing rescue would be in the context of BRAF treatment. There was no evidence of rescue in the SKMel5 nor SKMel28 (data not shown for SKMel28). This led to the final experiments of measuring ROS directly in the cell lines. Initially, the dye CellROX was used to stain ROS in 96-well plates, but despite including H_2O_2 and untreated controls, I experienced quantitation problems (data not shown). Thus, high-pressure liquid chromatography (HPLC) was employed to directly measure the ROS-dye product from the cells. Untreated and 8 μM PLX4720-treated cells (48 hr treatment) were incubated with 1 μM MitoSOX for 20 mins right before analysis. MitoSOX, or hydroethidine, is a mitochondria-targeted probe that reacts with superoxide to generate the red product 2-hydroxyethidium or dihydroethidium (Zielonka and Kaylanaraman, 2010). The prior experiment with CellROX was thought to be confounded due to quantitation problems with the microscope but also the generality of CellROX acting in the cytosol. Thus, probing with MitoSOX and HPLC quantification was intended as a more refined and targeted approach. 48 hours of treatment with 8 μM PLX4720 did not result in a statistically significant difference from the DMSO controls; in fact, it was surprising to observe a trending decrease of superoxide formation (Figure 6.6.)

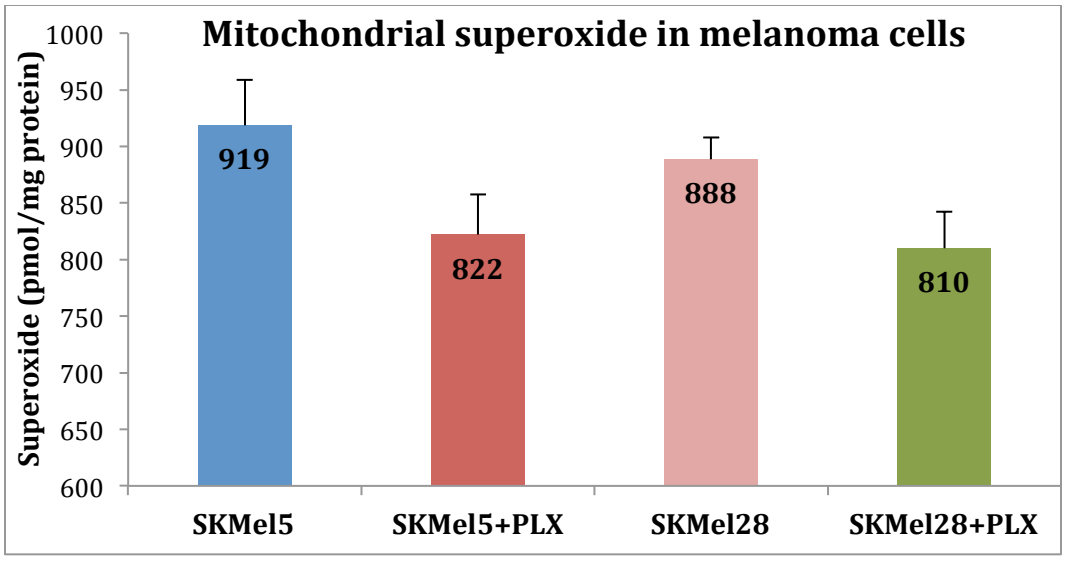

Figure 6.6: PLX4720 Does Not Form Differential Superoxide in BRAF-mutated Melanoma Cells. HPLC (used in conjunction with fluorescence detection for robust quantitation) on Shimatzu HPLC system with temperature control and automated sampling. Reverse-phase HPLC is done on a C18 column (Nucleosil 250 to 4.5 mm) and a mobile phase containing 0.1% trifluoroacetic acid and an acetonitrile gradient (from 37% to 47%). Results are normalized and reported based on protein concentration; all done in triplicate, error bars are SEM. Analysis provided by Sergey Dikalov and Alfiya Bikineyeva.

Even though MitoSOX can be sequestered and concentrated in the mitochondria by ~500 fold in comparison to cytosol, the probe has two significant limitations: interference from heme enzymes, cytochrome c and peroxidases (Zielonka and Kaylanaraman, 2010), and the similarly fluorescent waste product, ethidium (Dikalov and Harrison, 2012). It is still unclear what role ROS plays in defining or shaping the variability found in BRAF-mutated melanoma cell lines, however these initial experiments can help lay groundwork for further work. Understanding the confounding factors and limitations of these probes and reagents can influence more intelligent experimental designs; additionally, based on the work with clonal population in Chapter V, some of these results may very well be averaged out due to the population level responses being measured. It would be interesting to see if subclones with differential responses to PLX4720 engender differential 1) ROS formation, or 2) detoxification.

APPENDICES

Media Composition or Formulations

Media Name	Glucose (mM)	Glutamine (mM)	Glycine (mM)	Serine (mM)	Calcium Pantothenate (mM)	Niacinamide (mM)
DMEM, high glucose	25	4	0.4	0.4	0.0083	0.0327
Ham's F12	10.0111	1	0.1	0.1	0.001	0.0002
DMEM/F12 1:1 Mix	17.5055	2.5	0.25	0.25	0.0046	0.0165
RPMI-1640	11.1111	2.0547	0.1333	0.2857	0.0005	0.0081
McCoy's 5A	16.6666	1.5013	0.1	0.2504	0.0004	0.004

Appendix A: Media Formulations (Comparisons). Table highlighting a few of the prominent nutrients in the media utilized within this thesis. All values are in mM concentrations.

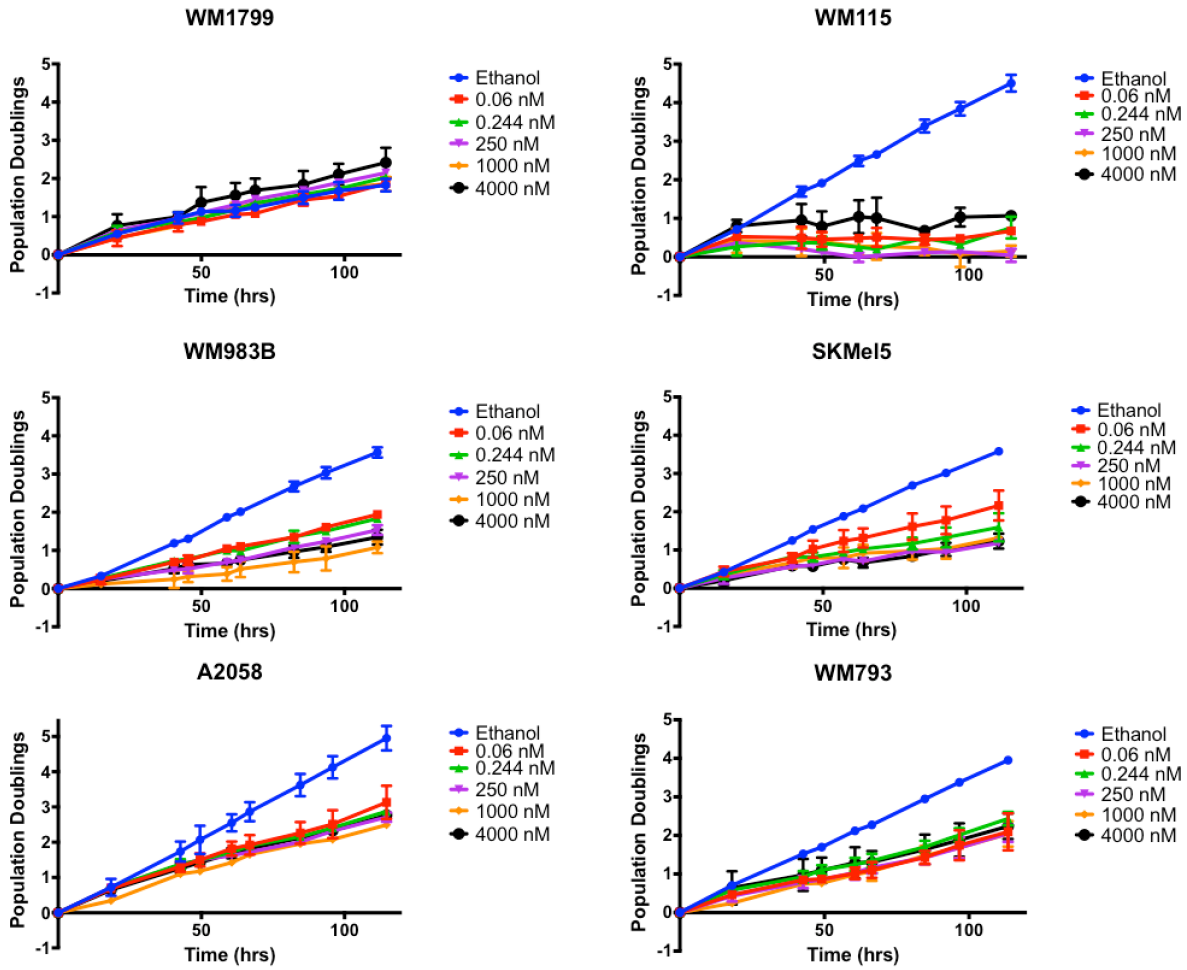

Appendix B: Growth Curves and Population Doublings of Melanoma Cell Lines In the Presence of Oligomycin (Part 1/2). Representative experiments of BRAF-mutated cell lines treated with oligomycin (first set of six cell lines). The proliferation was log-2 normalized and plotted as population doubling (y-axis) over time (x-axis, in hours). The concentrations of oligomycin started at 4 μM, going down 4-fold to zero control (ethanol). Therefore, the doses used are as follows: 4000 nM, 1000 nM, 250 nM, 62.5 nM, 15.625 nM, 3.9 nM, 0.97 nM, 0.244 nM, 0.06 nM, and ethanol control. For graph clarity, some of the concentrations are not shown, in order to eliminate crowding of the graph curves. Data shown are from a single experiment with technical duplicates; experiment has been repeated at least twice with similar results. Error bars are standard deviation. Additionally, for perspective about the dosing: 1 μM is needed to adequately inhibit oxygen consumption in our Seahorse assays.

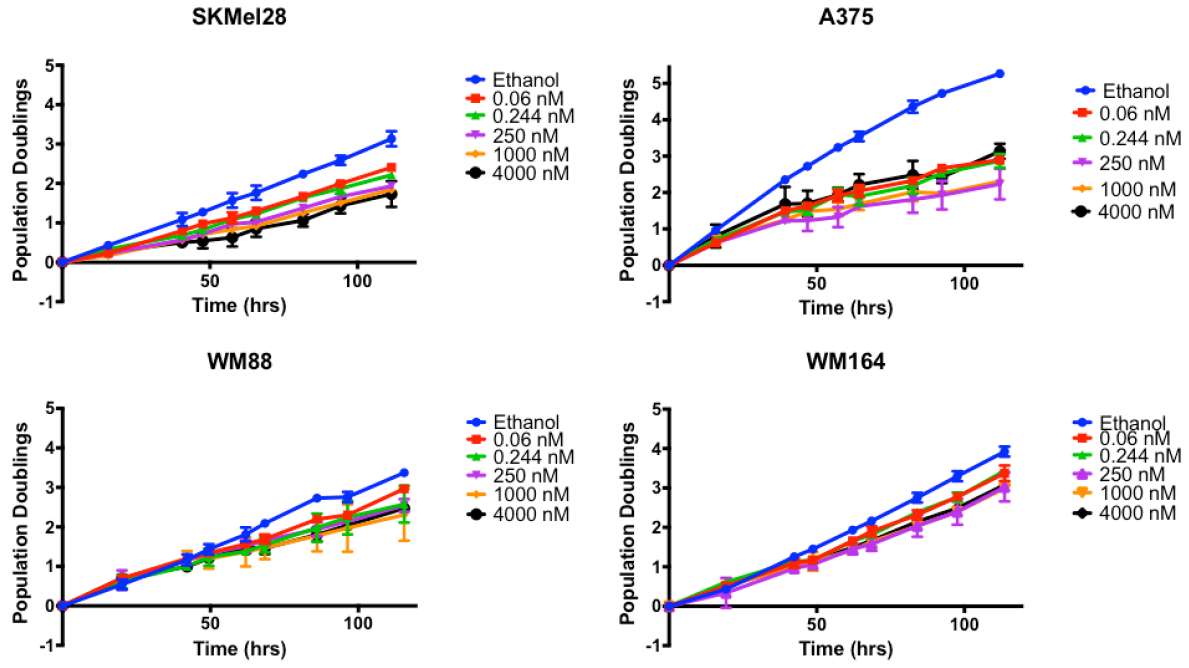

Appendix C: Growth Curves and Population Doublings of Melanoma Cell Lines In the Presence of Oligomycin (Part 2/2). Representative experiments of BRAF-mutated cell lines treated with oligomycin. The proliferation was log-2 normalized and plotted as population doubling (y-axis) over time (x-axis, in hours). The concentrations of oligomycin started at 4 μM, going down 4-fold to zero control (ethanol). Therefore, the doses used are as follows: 4000 nM, 1000 nM, 250 nM, 62.5 nM, 15.625 nM, 3.9 nM, 0.97 nM, 0.244 nM, 0.06 nM, and ethanol control. For graph clarity, some of the concentrations are not shown, in order to eliminate crowding of the graph curves. Data shown are from a single experiment with technical duplicates; experiment has been repeated at least twice with similar results. Error bars are standard deviation. Additionally, for perspective about the dosing: 1 μM is needed to adequately inhibit oxygen consumption in our Seahorse assays.

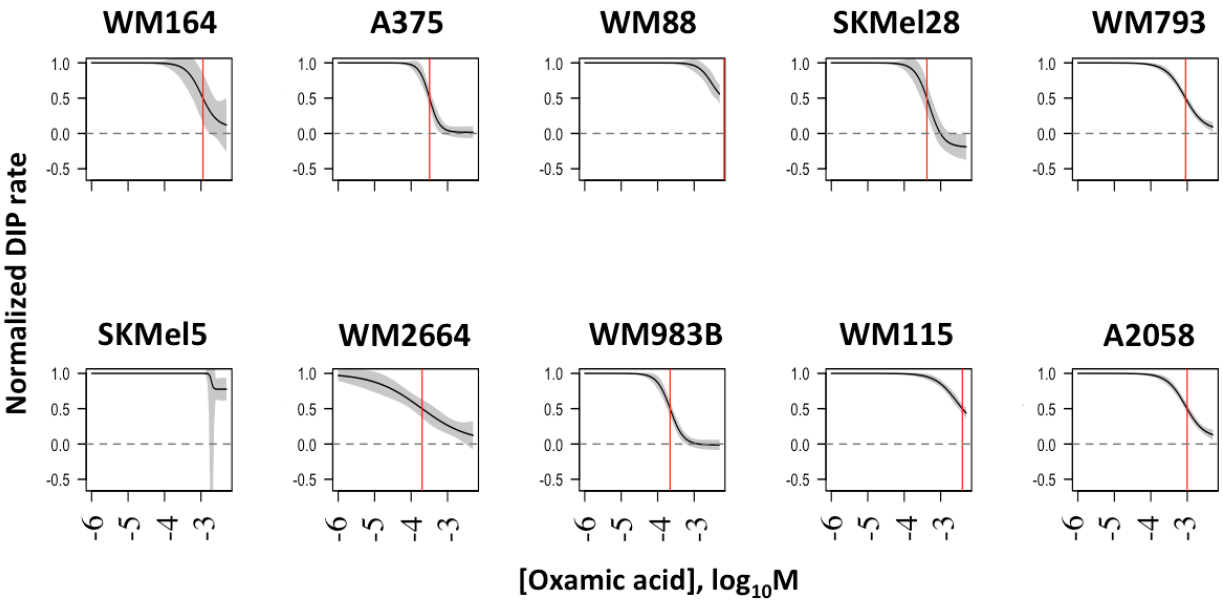

Appendix D: Variability of Response to Oxamic Acid in Melanoma Cell Lines. Proliferative, dose-response spectrum of IC50's for Oxamic acid based on DIP rate. The dose-response curves are generated using a 2-fold dilution of Oxamic acid from 50 mM down to zero (PBS). The proliferative rates are calculated using the slope of the log2-normalized population curve after 48 hours. Data shown are from 3+ experiments and 95% confidence intervals are the shaded regions.

REFERENCES

1. Adams, D. J. *et al.* Synthesis, cellular evaluation, and mechanism of action of piperlongumine analogs. *Proc. Natl. Acad. Sci.* **109,** 15115–15120 (2012).
2. Adler, E. M. & Gough, N. R. Focus issue: Rendering resistance futile. *Sci. Signal.* **4,** eg3 (2011).
3. Ahn, C. S. & Metallo, C. M. Mitochondria as biosynthetic factories for cancer proliferation. *Cancer Metab.* **3,** 1 (2015).
4. Akbani, R. *et al.* Genomic Classification of Cutaneous Melanoma. *Cell* **161,** 1681–1696 (2015).
5. American Cancer Society. *Cancer Facts & Figures 2017* (2017).
6. Anastas, J. N. *et al.* WNT5A enhances resistance of melanoma cells to targeted BRAF inhibitors. *J. Clin. Invest.* **124,** 2877–2890 (2014).
7. Ascierto, P. A. *et al.* The role of BRAF V600 mutation in melanoma. *J. Transl. Med.* **10,** 85 (2012).
8. Baenke, F. *et al.* Resistance to BRAF inhibitors induces glutamine dependency in melanoma cells. *Mol. Oncol.* 1–12 (2015).
9. Barretina, J. *et al.* The Cancer Cell Line Encyclopedia enables predictive modelling of anticancer drug sensitivity. *Nature* **483,** 603–7 (2012).
10. Beggs, a D. *et al.* Peutz-Jeghers syndrome: a systematic review and recommendations for management. *Gut* **59,** 975–986 (2010).
11. Benjamin, D. I., Cravatt, B. F. & Nomura, D. K. Global profiling strategies for mapping dysregulated metabolic pathways in cancer. *Cell Metab.* **16,** 565–577 (2012).
12. Berns, K. *et al.* A large-scale RNAi screen in human cells identifies new components of

the p53 pathway. *Nature* **428,** 431–437 (2004).

13. Birket, M. J. *et al.* A reduction in ATP demand and mitochondrial activity with neural differentiation of human embryonic stem cells. *J. Cell Sci.* **124,** 348–358 (2011).
14. Birkus, G., Hitchcock, M. & Cihlar, T. Assessment of mitochondrial toxicity in human cells treated with tenofovir: comparison with other nucleoside reverse transcriptase inhibitors. *Antimicrob Agents Chemother* **46,** 716–723 (2002).
15. Birsoy, K. *et al.* An Essential Role of the Mitochondrial Electron Transport Chain in Cell Proliferation Is to Enable Aspartate Synthesis. *Cell* **162,** 540–551 (2015).
16. Bollag, G. *et al.* Clinical efficacy of a RAF inhibitor needs broad target blockade in BRAF-mutant melanoma. *Nature* **467,** 596–599 (2010).
17. Bonnans, C., Chou, J. & Werb, Z. Remodelling the extracellular matrix in development and disease I E r. *Nat. Publ. Gr.* **15,** 786–801 (2014).
18. Breslow, A. Thickness, cross-sectional areas and depth of invasion in the prognosis of cutaneous melanoma. *Ann. Surg.* **172,** 902–908 (1970).
19. Bucheit, A. D. *et al.* Complete loss of PTEN protein expression correlates with shorter time to brain metastasis and survival in stage IIIB/C melanoma patients with BRAFV600 mutations. *Clin. Cancer Res.* **20,** 5527–5536 (2014).
20. Buck, M. D. D. *et al.* Mitochondrial Dynamics Controls T Cell Fate through Metabolic Programming. *Cell* **166,** 63–76 (2016).
21. Canto, C., Menzies, K. J. & Auwerx, J. NAD+ Metabolism and the Control of Energy Homeostasis: A Balancing Act between Mitochondria and the Nucleus. *Cell Metab.* **22,** 31–53 (2015).
22. Capaldo, B. J. *et al.* Systems analysis of adaptive responses to MAP kinase pathway

blockade in BRAF mutant melanoma. *PLoS One* **10,** 1–25 (2015).

23. Cara, S. & Tannock, I. Retreatment of patients with the same chemotherapy: implications for clinical mechanisms of drug resistance. *Ann. Oncol.* **12,** 23–7 (2001).
24. Casanovas, O., Hicklin, D. J., Bergers, G. & Hanahan, D. Drug resistance by evasion of antiangiogenic targeting of VEGF signaling in late-stage pancreatic islet tumors. *Cancer Cell* **8,** 299–309 (2005).
25. Chacko, B. K. *et al.* The Bioenergetic Health Index: a new concept in mitochondrial translational research. *Clin. Sci. (Lond).* **127,** 367–73 (2014).
26. Chan, M. M. K. *et al.* The nature and management of metastatic melanoma after progression on braf inhibitors: Effects of extended BRAF inhibition. *Cancer* **120,** 3142–3153 (2014).
27. Chandel, N. S. *et al.* Are Metformin Doses Used in Murine Cancer Models Clinically Relevant? *Cell Metab.* **23,** 569–570 (2016).
28. Chapman, P. B. *et al.* Improved survival with vemurafenib in melanoma with BRAF V600E mutation. *N. Engl. J. Med.* **364,** 2507–2516 (2011).
29. Chen, D. *et al.* SKI knockdown inhibits human melanoma tumor growth in vivo. *Pigment Cell Melanoma Res.* **22,** 761–72 (2009).
30. Chen, K. H. *et al.* Role of mitofusin 2 (Mfn2) in controlling cellular proliferation. *FASEB J.* **28,** 382–394 (2014).
31. Christofk, H. R., Vander Heiden, M. G., Wu, N., Asara, J. M. & Cantley, L. C. Pyruvate kinase M2 is a phosphotyrosine-binding protein. *Nature* **452,** 181–186 (2008).
32. Clark, W. H. *et al.* The Histogenesis and Biologic Behavior of Primary Human Malignant Melanomas of the Skin The Histogenesis Malignant Behavior of Primary

Melanomas of the Skin1. *Cancer Res.* 705–727 (1969).

33. Corazao-Rozas, P. *et al.* Mitochondrial oxidative phosphorylation controls cancer cell's life and death decisions upon exposure to MAPK inhibitors. *Oncotarget* **5,** (2016).

34. Crowson, A. N., Magro, C. M. & Mihm, M. C. Prognosticators of melanoma, the melanoma report, and the sentinel lymph node. *Mod. Pathol.* **19 Suppl 2,** S71–S87 (2006).

35. Daiber, A. *et al.* Crosstalk of mitochondria with NADPH oxidase via reactive oxygen and nitrogen species signalling and its role for vascular function. *Br. J. Pharmacol.* n/a-n/a (2015).

36. Dalakas, M. C., Semino-Mora, C. & Leon-Monzon, M. Mitochondrial alterations with mitochondrial DNA depletion in the nerves of AIDS patients with peripheral neuropathy induced by 2'3'-dideoxycytidine (ddC). *Lab. Invest.* **81,** 1537–44 (2001).

37. Dang, C. V. Links between metabolism and cancer. *Genes Dev.* **26,** 877–890 (2012).

38. Dang, L. *et al.* Cancer-associated IDH1 mutations produce 2-hydroxyglutarate. *Nature* **462,** 739–44 (2009).

39. Das Thakur, M. *et al.* Modelling vemurafenib resistance in melanoma reveals a strategy to forestall drug resistance. *Nature* **494,** 251–255 (2013).

40. Davies, H. *et al.* Mutations of the BRAF gene in human cancer. *Nature* **417,** 949–954 (2002).

41. Deberardinis, R. J. & Chandel, N. S. Fundamentals of cancer metabolism. (2016).

42. DeBerardinis, R. J., Lum, J. J., Hatzivassiliou, G. & Thompson, C. B. The biology of cancer: metabolic reprogramming fuels cell growth and proliferation. *Cell Metab.* **7,**

11–20 (2008).

43. DeBerardinis, R. J. *et al.* Beyond aerobic glycolysis: transformed cells can engage in glutamine metabolism that exceeds the requirement for protein and nucleotide synthesis. *Proc. Natl. Acad. Sci. U. S. A.* **104,** 19345–50 (2007).

44. DeBerardinis, R. J. & Thompson, C. B. Cellular Metabolism and Disease: What Do Metabolic Outliers Teach Us? *Cell* **148,** 1132–1144 (2012).

45. Dikalov, S. I. & Harrison, D. G. Methods for Detection of Mitochondrial and Cellular Reactive Oxygen Species. *Antioxid. Redox Signal.* **0,** 121019094741000 (2012).

46. Dupuy, F. *et al.* PDK1-dependent metabolic reprogramming dictates metastatic potential in breast cancer. *Cell Metab.* **22,** 577–589 (2015).

47. Esumi, H., Lu, J., Kurashima, Y. & Hanaoka, T. Antitumor activity of pyrvinium pamoate, 6-(dimethylamino)-2-[2- (2,5-dimethyl-1-phenyl-1H-pyrrol-3-yl)ethenyl]-1-methyl-quinolinium pamoate salt, showing preferential cytotoxicity during glucose starvation. *Cancer Sci.* **95,** 685–690 (2004).

48. Fallahi-Sichani, M., Honarnejad, S., Heiser, L. M., Gray, J. W. & Sorger, P. K. Metrics other than potency reveal systematic variation in responses to cancer drugs. *Nat. Chem. Biol.* **9,** 708–14 (2013).

49. Fang, M. *et al.* The ER UDPase ENTPD5 promotes protein N-glycosylation, the Warburg effect, and proliferation in the PTEN pathway. *Cell* **143,** 711–724 (2010).

50. Flaherty, K. T. *et al.* Combined BRAF and MEK Inhibition in Melanoma with BRAF V600 Mutations. *N. Engl. J. Med.* **367,** 1694–1703 (2012).

51. Flaherty, K. T. *et al.* Inhibition of Mutated, Activated BRAF in Metastatic Melanoma. *N. Engl. J. Med.* **363,** 809–819 (2010).

52. Frick, P. L., Paudel, B. B., Tyson, D. R. & Quaranta, V. Quantifying heterogeneity and dynamics of clonal fitness in response to perturbation. *J. Cell. Physiol.* **230,** 1403–1412 (2015).

53. Garnett, M. J. *et al.* Systematic identification of genomic markers of drug sensitivity in cancer cells. *Nature* **483,** 570–5 (2012).

54. Gohil, V. M. *et al.* Nutrient-sensitized screening for drugs that shift energy metabolism from mitochondrial respiration to glycolysis. *Nat. Biotechnol.* **28,** 249–255 (2010).

55. Gong, Y. *et al.* Induction of BIM is essential for apoptosis triggered by EGFR kinase inhibitors in mutant EGFR-dependent lung adenocarcinomas. *PLoS Med.* **4,** 1655–1668 (2007).

56. Goutelle, S. *et al.* The Hill equation: A review of its capabilities in pharmacological modelling. *Fundam. Clin. Pharmacol.* **22,** 633–648 (2008).

57. Greaves, M. & Maley, C. C. Clonal evolution in cancer. *Nature* **481,** 306–313 (2012).

58. GREGOIRE, M., MORAIS, R., QUILLIAM, M. A. & GRAVEL, D. On auxotrophy for pyrimidines of respiration-deficient chick embryo cells. *Eur. J. Biochem.* **142,** 49–55 (1984).

59. Haass, N. K. *et al.* Real-time cell cycle imaging during melanoma growth, invasion, and drug response. *Pigment Cell Melanoma Res.* **27,** 764–776 (2014).

60. Haass, N. K. *et al.* The mitogen-activated protein/extracellular signal-regulated kinase kinase inhibitor AZD6244 (ARRY-142886) induces growth arrest in melanoma cells and tumor regression when combined with docetaxel. *Clin. Cancer Res.* **14,** 230–239 (2008).

61. Haferkamp, S. *et al.* Vemurafenib Induces Senescence Features in Melanoma Cells. *J. Invest. Dermatol.* **133,** 1–9 (2013).

62. Halaban, R. *et al.* PLX4032, a selective BRAFV600E kinase inhibitor, activates the ERK pathway and enhances cell migration and proliferation of BRAFWT melanoma cells. *Pigment Cell Melanoma Res.* **23,** 190–200 (2010).

63. Hall, A. *et al.* Dysfunctional oxidative phosphorylation makes malignant melanoma cells addicted to glycolysis driven by the (V600E)BRAF oncogene. *Oncotarget* **4,** 584–99 (2013).

64. Hanahan, D. & Weinberg, R. a. Hallmarks of cancer: the next generation. *Cell* **144,** 646–74 (2011).

65. Haq, R. *et al.* Oncogenic BRAF Regulates Oxidative Metabolism via PGC1α and MITF. *Cancer Cell* **23,** 302–315 (2013).

66. Hardie, D. G. AMP-activated/SNF1 protein kinases: conserved guardians of cellular energy. *Nat. Rev. Mol. Cell Biol.* **8,** 774–785 (2007).

67. Hardie, D. G. The AMP-activated protein kinase pathway - new players upstream and downstream. *J. Cell Sci.* **117,** 5479–5487 (2004).

68. Harris, L. A. *et al.* An unbiased metric of antiproliferative drug effect in vitro. *Nat. Methods* **13,** 1–6 (2016).

69. Hata, A. N. *et al.* Tumor cells can follow distinct evolutionary paths to become resistant to epidermal growth factor receptor inhibition. *Nat. Med.* **22,** 262–269 (2016).

70. Heiser, L. M. *et al.* Integrated analysis of breast cancer cell lines reveals unique signaling pathways. *Genome Biol.* **10,** R31 (2009).

71. Hernandez-Davies, J. E. *et al.* Vemurafenib resistance reprograms melanoma cells towards glutamine dependence. *J. Transl. Med.* **13,** 210 (2015).

72. Hodis, E. *et al.* A landscape of driver mutations in melanoma. *Cell* **150,** 251–263 (2012).

73. Hoek, K. S. *et al.* In vivo switching of human melanoma cells between proliferative and invasive states. *Cancer Res.* **68,** 650–656 (2008).

74. Hosios, A. M. *et al.* Amino Acids Rather than Glucose Account for the Majority of Cell Mass in Proliferating Mammalian Cells. *Dev. Cell* **36,** 540–549 (2016).

75. Howlader, N. *et al. SEER Cancer Statistics Review 1975-2013 National Cancer Institute*. (2016).

76. Hu-Lieskovan, S., Robert, L., Moreno, B. H. & Ribas, A. Combining targeted therapy with immunotherapy in BRAF-mutant melanoma: Promise and challenges. *J. Clin. Oncol.* **32,** 2248–2254 (2014).

77. Hugo, W. *et al.* Non-genomic and Immune Evolution of Melanoma Acquiring MAPKi Resistance. *Cell* **162,** 1271–1285 (2015).

78. Inoue-Yamauchi, A. & Oda, H. Depletion of mitochondrial fission factor DRP1 causes increased apoptosis in human colon cancer cells. *Biochem. Biophys. Res. Commun.* **421,** 81–85 (2012).

79. Intlekofer, A. M. *et al.* L-2-Hydroxyglutarate production arises from noncanonical enzyme function at acidic pH. *Nat. Chem. Biol.* (2017).

80. Johannessen, C. M. *et al.* COT drives resistance to RAF inhibition through MAP kinase pathway reactivation. *Nature* **468,** 968–972 (2010).

81. Johnson, D. B. *et al.* Acquired BRAF inhibitor resistance: A multicenter meta-analysis

of the spectrum and frequencies, clinical behaviour, and phenotypic associations of resistance mechanisms. *Eur. J. Cancer* **51,** 2792–2799 (2015).

82. Kashatus, J. A. *et al.* Erk2 phosphorylation of Drp1 promotes mitochondrial fission and MAPK-driven tumor growth. *Mol. Cell* **57,** 537–552 (2015).

83. Kemper, K. *et al.* BRAF(V600E) Kinase Domain Duplication Identified in Therapy-Refractory Melanoma Patient-Derived Xenografts. *Cell Rep.* **16,** 263–77 (2016).

84. King, M. P. & Attardi, G. Human Cells Lacking mtDNA : Repopulation with Exogenous Mitochondria by Complementation Author (s): Michael P . King and Giuseppe Attardi Published by : American Association for the Advancement of Science Stable URL : http://www.jstor.org/stable/1704589. *Science (80-.).* **246,** 500–503 (1989).

85. King, M. P. & Attardi, G. Isolation of human cell lines lacking mitochondrial DNA. *Methods Enzymol.* **264,** 304–13 (1996).

86. King, Michael P; Attardi, G. Mitochondria-Mediated Transformation of H u m a n p0 Cells. *Methods Enzymol.* **264,** 313–334 (1996).

87. Komurov, K. *et al.* The glucose-deprivation network counteracts lapatinib-induced toxicity in resistant ErbB2-positive breast cancer cells. *Mol. Syst. Biol.* **8,** 1–10 (2012).

88. Konieczkowski, D. J. *et al.* A melanoma cell state distinction influences sensitivity to MAPK pathway inhibitors. *Cancer Discov.* **4,** 816–827 (2014).

89. Kuhn, M. L. *et al.* Structural, kinetic and proteomic characterization of acetyl phosphate-dependent bacterial protein acetylation. *PLoS One* **9,** (2014).

90. Kukat, A. *et al.* Generation of ρ0 cells utilizing a mitochondrially targeted restriction endonuclease and comparative analyses. *Nucleic Acids Res.* **36,** (2008).

91. Larkin, J. *et al.* Combined vemurafenib and cobimetinib in BRAF-mutated melanoma.

N. Engl. J. Med. **371,** 1867–76 (2014).

92. Lee, H., Hanes, J. & Johnson, K. A. Toxicity of Nucleoside Analogues Used to Treat AIDS and the Selectivity of the Mitochondrial DNA Polymerase. *Biochemistry* **42,** 14711–14719 (2003).

93. Lee, J. V. *et al.* Akt-dependent metabolic reprogramming regulates tumor cell Histone acetylation. *Cell Metab.* **20,** 306–319 (2014).

94. Li, B. *et al.* Repurposing the FDA-approved pinworm drug pyrvinium as a novel chemotherapeutic agent for intestinal polyposis. *PLoS One* **9,** 1–9 (2014).

95. Lito, P., Rosen, N. & Solit, D. B. Tumor adaptation and resistance to RAF inhibitors. *Nat. Med.* **19,** 1401–1409 (2013).

96. Livingstone, E., Swann, S., Lilla, C., Schadendorf, D. & Roesch, A. Combining $BRAF^{V600E}$ inhibition with modulators of the mitochondrial bioenergy metabolism to overcome drug resistance in metastatic melanoma. *Exp. Dermatol.* 709–710 (2015).

97. Long, G. V *et al.* Combined BRAF and MEK inhibition versus BRAF inhibition alone in melanoma. *N. Engl. J. Med.* **371,** 1877–88 (2014).

98. Mathur, R. *et al.* Targeting Wnt pathway in mantle cell lymphoma-initiating cells. *J. Hematol. Oncol.* **8,** 63 (2015).

99. McDermott, U., Sharma, S. V. & Settleman, J. High-Throughput Lung Cancer Cell Line Screening for Genotype-Correlated Sensitivity to an EGFR Kinase Inhibitor. *Methods Enzymol.* **438,** 331–341 (2008).

100. Menon, D. R. *et al.* A stress-induced early innate response causes multidrug tolerance in melanoma. *Oncogene* **34,** 4545–4545 (2015).

101. Menzies, A. M. & Long, G. V. Systemic treatment for BRAF-mutant melanoma: Where

do we go next? *Lancet Oncol.* **15,** e371–e381 (2014).

102. Montagut, C. *et al.* Elevated CRAF as a potential mechanism of acquired resistance to BRAF inhibition in melanoma. *Cancer Res.* **68,** 4853–4861 (2008).

103. Nazarian, R. *et al.* Melanomas acquire resistance to B-RAF(V600E) inhibition by RTK or N-RAS upregulation. *Nature* **468,** 973–977 (2010).

104. Niepel, M., Spencer, S. L. & Sorger, P. K. Non-genetic cell-to-cell variability and the consequences for pharmacology. *Curr. Opin. Chem. Biol.* **13,** 556–561 (2009).

105. Ong, S.-E. *et al.* Identifying the proteins to which small-molecule probes and drugs bind in cells. *Proc. Natl. Acad. Sci. U. S. A.* **106,** 4617–22 (2009).

106. Paraiso, K. H. T. *et al.* PTEN loss confers BRAF inhibitor resistance to melanoma cells through the suppression of BIM expression. *Cancer Res.* **71,** 2750–2760 (2011).

107. Parmenter, T. J. *et al.* Response of BRAF-Mutant Melanoma to BRAF Inhibition Is Mediated by a Network of Transcriptional Regulators of Glycolysis. *Cancer Discov.* **4,** 423–433 (2014).

108. Pietrocola, F., Galluzzi, L., Bravo-San Pedro, J. M., Madeo, F. & Kroemer, G. Acetyl coenzyme A: A central metabolite and second messenger. *Cell Metab.* **21,** 805–821 (2015).

109. Poulikakos, P. I., Zhang, C., Bollag, G., Shokat, K. M. & Rosen, N. RAF inhibitors transactivate RAF dimers and ERK signalling in cells with wild-type BRAF. *Nature* **464,** 427–430 (2010).

110. Poulikakos, P. I. *et al.* RAF inhibitor resistance is mediated by dimerization of aberrantly spliced BRAF(V600E). *Nature* **480,** 387–90 (2011).

111. Poulikakos, P. I. & Rosen, N. Mutant BRAF melanomas-dependence and resistance.

Cancer Cell **19,** 11–15 (2011).

112. Quaranta, V. *et al.* trait variability. *Methods* **6879,** (2010).

113. Raj, A. & van Oudenaarden, A. Nature, Nurture, or Chance: Stochastic Gene Expression and Its Consequences. *Cell* **135,** 216–226 (2008).

114. Raj, L. *et al.* Selective killing of cancer cells by a small molecule targeting the stress response to ROS. *Nature* **475,** 231–234 (2011).

115. Ramirez, M. *et al.* Diverse drug-resistance mechanisms can emerge from drug-tolerant cancer persister cells. *Nat. Commun.* 1–8 (2016).

116. Rapp, U. R. *et al.* Structure and biological activity of v-raf, a unique oncogene transduced by a retrovirus (malignant transformation/transduction/molecular cloning). *Biochemistry* **80,** 4218–4222 (1983).

117. Rebecca, V. W., Sondak, V. K. & Smalley, K. S. M. A brief history of melanoma: from mummies to mutations. *Melanoma Res.* **22,** 114–22 (2012).

118. Rees, M. G. *et al.* Correlating chemical sensitivity and basal gene expression reveals mechanism of action. *Nat. Chem. Biol.* **12,** 1–10 (2015).

119. Rehman, J. *et al.* Inhibition of mitochondrial fission prevents cell cycle progression in lung cancer. *FASEB J.* **26,** 2175–86 (2012).

120. Reiss, P. *et al.* Greater and more rapid depletion of mitochondrial DNA in blood of patients treated with dual (zidovudine 1 didanosine or zidovudine 1 zalcitabine) vs . single (zidovudine) nucleoside reverse transcriptase inhibitors. *HIV Med.* **5,** 11–14 (2004).

121. Ribas, A. & Flaherty, K. T. BRAF targeted therapy changes the treatment paradigm in melanoma. *Nat. Rev. Clin. Oncol.* **8,** 426–433 (2011).

122. Rizos, H. *et al.* BRAF Inhibitor Resistance Mechanisms in Metastatic Melanoma: Spectrum and Clinical Impact. *Clin. Cancer Res.* **20,** 1965–1977 (2014).

123. Sakaue-Sawano, A. *et al.* Visualizing Spatiotemporal Dynamics of Multicellular Cell-Cycle Progression. *Cell* **132,** 487–498 (2008).

124. Schaffer, B. E. *et al.* Identification of AMPK Phosphorylation Sites Reveals a Network of Proteins Involved in Cell Invasion and Facilitates Large-Scale Substrate Prediction. *Cell Metab.* **22,** 907–921 (2015).

125. Seashore-Ludlow, B. *et al.* Harnessing connectivity in a large-scale small-molecule sensitivity dataset. *Cancer Discov.* **5,** 1210–1223 (2015).

126. Sharma, S. V. *et al.* A Chromatin-Mediated Reversible Drug-Tolerant State in Cancer Cell Subpopulations. *Cell* **141,** 69–80 (2010).

127. Shaw, R. J. *et al.* The tumor suppressor LKB1 kinase directly activates AMP-activated kinase and regulates apoptosis in response to energy stress. *Proc. Natl. Acad. Sci. U. S. A.* **101,** 3329–3335 (2004).

128. Shen, C. H. *et al.* Phosphorylation of BRAF by AMPK impairs BRAF-KSR1 association and cell proliferation. *Mol. Cell* **52,** 161–172 (2013).

129. Shi, H. *et al.* Melanoma whole-exome sequencing identifies V600EB-RAF amplification-mediated acquired B-RAF inhibitor resistance. *Nat. Commun.* **3,** 724 (2012).

130. Shitara, Y. *et al.* Role of organic cation/carnitine transporter 1 in uptake of phenformin and inhibitory effect on complex i respiration in mitochondria. *Toxicol. Sci.* **132,** 32–42 (2013).

131. Shoemaker, R. H. The NCI60 human tumour cell line anticancer drug screen. *Nat. Rev.*

Cancer **6,** 813–23 (2006).

132. Sieber, M. H., Thomsen, M. B. & Spradling, A. C. Electron Transport Chain Remodeling by GSK3 during Oogenesis Connects Nutrient State to Reproduction. *Cell* **164,** 420–432 (2016).

133. Siegel, R., Ma, J., Zou, Z. & Jemal, A. Cancer statistics, 2014. *CA. Cancer J. Clin.* **64,** 9–29 (2014).

134. Silverman, L. B. *et al.* Improved outcome for children with acute lymphoblastic leukemia: results of Dana-Farber Consortium Protocol 91-01. *Blood* **97,** 1211–1218 (2001).

135. Singh, N., Joshi, R. & Komurov, K. HER2-mTOR signaling – driven breast cancer cells require ER-associated degradation to survive. **8,** 1–14 (2015).

136. Smith, M. P. *et al.* Inhibiting Drivers of Non-mutational Drug Tolerance Is a Salvage Strategy for Targeted Melanoma Article Inhibiting Drivers of Non-mutational Drug Tolerance Is a Salvage Strategy for Targeted Melanoma Therapy. *Cancer Cell* **29,** 270–284 (2016).

137. Sosman, J. A. *et al.* Survival in BRAF V600-mutant advanced melanoma treated with vemurafenib. *N. Engl. J. Med.* **366,** 707–14 (2012).

138. STEPHENSON, R. P. a Modification of Receptor Theory. *Br. J. Pharmacol. Chemother.* **11,** 379–393 (1956).

139. Stratford, E. W. essel *et al.* The tankyrase-specific inhibitor JW74 affects cell cycle progression and induces apoptosis and differentiation in osteosarcoma cell lines. *Cancer Med.* **3,** 36–46 (2014).

140. Sullivan, L. B. *et al.* Supporting Aspartate Biosynthesis Is an Essential Function of

Respiration in Proliferating Cells. *Cell* **162,** 552–563 (2015).

141. Sun, C. *et al.* Reversible and adaptive resistance to BRAF(V600E) inhibition in melanoma. *Nature* **508,** 118–122 (2014).

142. Thorne, C. A. *et al.* Small-molecule inhibition of Wnt signaling through activation of casein kinase 1α. *Nat. Chem. Biol.* **6,** 829–36 (2010).

143. Tomitsuka, E., Kita, K. & Esumi, H. An anticancer agent, pyrvinium pamoate inhibits the NADH-fumarate reductase system-a unique mitochondrial energy metabolism in tumour microenvironments. *J. Biochem.* **152,** 171–183 (2012).

144. Tsai, J. *et al.* Discovery of a selective inhibitor of oncogenic B-Raf kinase with potent antimelanoma activity. **105,** 3041–3046 (2008).

145. Tyson, D. R., Garbett, S. P., Frick, P. L. & Quaranta, V. Fractional proliferation: a method to deconvolve cell population dynamics from single-cell data. *Nat. Methods* **9,** 923–8 (2012).

146. Urteaga, O. & Pack, G. On The Antiquity Of Melanoma. *Cancer* **19,** 607–610 (1966).

147. Van Allen, E. M. *et al.* The genetic landscape of clinical resistance to RAF inhibition in metastatic melanoma. *Cancer Discov.* **4,** 94–109 (2014).

148. Vandamme, N. & Berx, G. Melanoma cells revive an embryonic transcriptional network to dictate phenotypic heterogeneity. *Front. Oncol.* **4,** 352 (2014).

149. Vander Heiden, M. G., Cantley, L. C. & Thompson, C. B. Understanding the Warburg effect: the metabolic requirements of cell proliferation. *Science* **324,** 1029–33 (2009).

150. Vazquez, F. *et al.* PGC1α Expression Defines a Subset of Human Melanoma Tumors with Increased Mitochondrial Capacity and Resistance to Oxidative Stress. *Cancer Cell* **23,** 287–301 (2013).

151. Verduzco, D., Flaherty, K. T. & Smalley, K. S. M. Feeling energetic? New strategies to prevent metabolic reprogramming in melanoma. *Exp. Dermatol.* **24,** 657–658 (2015).

152. Vergani, E. *et al.* Identification of MET and SRC Activation in Melanoma Cell Lines Showing Primary Resistance to PLX4032. *Neoplasia* **13,** 1132–IN17 (2011).

153. Villanueva, J., Vultur, a. & Herlyn, M. Resistance to BRAF Inhibitors: Unraveling Mechanisms and Future Treatment Options. *Cancer Res.* **71,** 7137–7140 (2011).

154. Villanueva, J. *et al.* Acquired Resistance to BRAF Inhibitors Mediated by a RAF Kinase Switch in Melanoma Can Be Overcome by Cotargeting MEK and IGF-1R/PI3K. *Cancer Cell* **18,** 683–695 (2010).

155. Wagle, N. *et al.* Dissecting therapeutic resistance to RAF inhibition in melanoma by tumor genomic profiling. *J. Clin. Oncol.* **29,** 3085–3096 (2011).

156. Wagle, N. *et al.* MAP kinase pathway alterations in BRAF-mutant melanoma patients with acquired resistance to combined RAF/MEK inhibition. *Cancer Discov.* **4,** 61–8 (2014).

157. Walker, U. A. *et al.* Depletion of Mitochondrial DNA in Liver under Antiretroviral Therapy with Didanosine, Stavudine, or Zalcitabine. *Hepatology* **39,** 311–317 (2004).

158. Wang, L., McLeod, H. L. & Weinshilboum, R. M. Genomics and Drug Response. *N Engl J Med.* **364,** 1144–1153 (2011).

159. Wang, W., Karamanlidis, G. & Tian, R. Novel targets for mitochondrial medicine. *Sci. Transl. Med.* **8,** 326rv3-326rv3 (2016).

160. Warburg, O. On the Origin of Cancer Cells. *Science (80-.).* **123,** 309–14 (1956).

161. Welsh, S. J., Rizos, H., Scolyer, R. A. & Long, G. V. Resistance to combination BRAF and MEK inhibition in metastatic melanoma: Where to next? *Eur. J. Cancer* **62,** 76–85

(2016).

162. Wenes, M. *et al.* Macrophage Metabolism Controls Tumor Blood Vessel Morphogenesis and Metastasis. *Cell Metab.* **24,** 701–715 (2016).

163. Whang, Y. M. *et al.* LKB1 deficiency enhances sensitivity to energetic stress induced by erlotinib treatment in non-small-cell lung cancer (NSCLC) cells. *Oncogene* **35,** 856–866 (2016).

164. Whittaker, S. *et al.* Gatekeeper mutations mediate resistance to BRAF-targeted therapies. *Sci Transl Med* **2,** 35ra41 (2010).

165. Whittaker, S. R. *et al.* A genome-scale RNA interference screen implicates NF1 loss in resistance to RAF inhibition. *Cancer Discov.* **3,** 350–362 (2013).

166. Wiley, C. D. *et al.* Mitochondrial Dysfunction Induces Senescence with a Distinct Secretory Phenotype. *Cell Metab.* **23,** 303–314 (2015).

167. Yang, W. *et al.* Genomics of Drug Sensitivity in Cancer (GDSC): A resource for therapeutic biomarker discovery in cancer cells. *Nucleic Acids Res.* **41,** 955–961 (2013).

168. Ye, F. *et al.* Peroxisome Proliferator-Activated Receptor γ (PPARγ) mediates a Ski oncogene-induced shift from glycolysis to oxidative energy metabolism. *J. Biol. Chem.* **286,** 40013–40024 (2011).

169. Zhang, G. *et al.* Targeting mitochondrial biogenesis to overcome drug resistance to MAPK inhibitors. **126,** 1–23 (2016).

170. Zhang, G. E. *et al.* Anti-tumor effects of Mfn2 in gastric cancer. *Int. J. Mol. Sci.* **14,** 13005–13021 (2013).

171. Zhang, H. *et al.* Distinct Metabolic States Can Support Self-Renewal and Lipogenesis

in Human Pluripotent Stem Cells under Different Culture Conditions. *Cell Rep.* **16,** 1536–1547 (2016).

172. Zhao, Y., Butler, E. B. & Tan, M. Targeting cellular metabolism to improve cancer therapeutics. *Cell Death Dis.* **4,** e532 (2013).

173. Zheng, B. *et al.* Oncogenic B-RAF Negatively Regulates the Tumor Suppressor LKB1 to Promote Melanoma Cell Proliferation. *Mol. Cell* **33,** 237–247 (2009).

174. Ziegler, U. & Groscurth, P. Morphological features of cell death. *Cardiovasc. Res.* **19,** 124–128 (2004).

175. Zielonka, J. & Kalyanaraman, B. Hydroethidine- and MitoSOX-derived red fluorescence is not a reliable indicator of intracellular superoxide formation: another inconvenient truth. *Free Radic. Biol. Med.* **48,** 983–1001 (2010).

176. Zuber, J. *et al.* Toolkit for evaluating genes required for proliferation and survival using tetracycline-regulated RNAi. *Nat Biotechnol* **29,** 79–83 (2011).